Impacts of High Penetration of DFIG Wind Turbines on Rotor Angle Stability of Power Systems

Thesis presented for the degree of

Doctor of Philosophy

at the University of Strathclyde

by

Mohamed Faraj Edrah

BSc. (Hons.), MSc. (Distinction)

Supervisor: Professor K. L. Lo

Power System Research Group

Institute of Energy and Environment

Department of Electronic and Electrical Engineering

University of Strathclyde

June 2017

Declaration

This thesis is the result of the author's original research. It has been composed by the author and has not been previously submitted for examination which has led to the award of a degree.

Acknowledgements

First and foremost, all praise is to Allah the Almighty, the only one God, for lighting my way and directing me through each and every success and achievement I have ever reached or may reach. I humbly and sincerely thank Allah, the most gracious and merciful, who gave me the ability and means to accomplish this work.

Many thanks to my supervisor Professor K. L. Lo, Head of the Power Systems Research Group (PSRG) at the University of Strathclyde, Glasgow, for his supervision and valuable guidance throughout my PhD. His encouragement and help contributed greatly in my current achievements.

I wish to extend my gratitude to Dr. Olimpo Anaya-Lara for his technical and moral support during my PhD. Also, I would like to thank the staff and my colleagues at the Department of Electronic and Electrical Engineering at the University of Strathclyde for their valuable discussions during the years of my research.

I would like to acknowledge General Electricity Company of Libya and Ministry of Higher Education and Scientific Research in Libya, for offering me a scholarship to complete my PhD studies.

Last but not least, heartfelt gratitude goes to my parents for their prayers, support and encouragement. I deeply appreciate all the sacrifices and endless support my wife and my children have given throughout my PhD period. I also wish to extend my thanks to my brothers and sisters for their support and encouragement during this research work.

Abstract

This thesis investigates the effects of increased penetration levels of DFIG based wind turbines on rotor angle stability of power systems and how these impacts could be mitigated. The main outcome of this research is the comprehensive assessment of the stability improvements that can be achieved through a novel cost-effective control approach using existing DFIG equipments.

A control strategy for both the rotor-side converter (RSC) and grid-side converter (GSC) of the DFIG is proposed to mitigate DFIGs impacts on the system stability. DFIG-GSC is utilised as a static synchronous compensator (STATCOM) to provide reactive power support during the active crowbar time when controlling of both reactive and active power is lost and a large amount of reactive power is absorbed. In addition, a supplementary power system stabiliser (PSS) is designed taking into account the influence of the crowbar system. To overcome the effects of PSS active power modulation, the PSS is designed to be implemented in the reactive power control loop of DFIG-RSC.

The proposed approaches are examined on IEEE 9-bus and IEEE 39-bus systems under both small and large disturbances. The simulation results show the effectiveness and robustness of both approaches to enhance rotor angle stability. As the levels of wind penetration are increased, the benefit of such a control scheme is that the DFIG-based wind farms are able to take over the synchronous generators responsibility to support power system stability.

As wind power is stochastic and fluctuates with the variation of wind speed, the proposed DFIG PSS should have the capability to damp power system oscillations effectively under non-uniform variable wind speeds across the wind farm. Therefore, the feasibility of the proposed fixed parameters PSS is evaluated using the IEEE 39-bus test system taking into account the non-uniform and variable wind speed profiles. The results confirm the robustness and stabilising effect against various operating modes and under various wind speeds.

Table of Contents

List of Figures

List of Tables

List of Abbreviations

AC	Alternating Current
AVR	Automatic Voltage Regulator
AWEA	American Wind Energy Association
CIGRE	International Council on Large Electric Systems
CO_2	Carbon Dioxide
DC	Direct Current
DFIG	Doubly Fed Induction Generator
d-q	Direct-Quadrature
EWEA	European Wind Energy Association
FMAC	Flux Magnitude and Angle Control
GSC	Grid Side Converter
GWEC	Global Wind Energy Council
Hz	Hertz
IEA	International Energy Agency
IEEE	Institute of Electrical and Electronics Engineers
IGBT	Insulated Gate Bipolar Transistor
lag	lagging
lead	leading
m/s	meter per second
p.f.	Power Factor
p.u.	Per Unit
PCC	Point of Common Coupling
PI	Proportional Integral
PMSG	Permanent Magnetic Synchronous Generator
PSS	Power System Stabiliser
PWM	Pulse Width Modulation
rad/s	radian per second
rpm	revelations per minute
RPS	Renewable Portfolio Standard
RSC	Rotor Side Converter

SCIG	Squirrel Cage Induction Generator
SG	Synchronous Generator
TSI	Transient Stability Index
TSO	Transmission System Operator
TSR	Tip Speed Ratio
UK	United Kingdom
US	United States
VAr	Volt Ampere reactive
V_{DC}	DC Voltage
VSC	Voltage Source Converter
W	Watt
WRIG	Wound Rotor Induction Generator
WSCC	Western System Coordinating Council

List of Symbols

S	Apparent power
P	Active power
Q	Reactive Power
P_s	Stator active power
Q_s	Stator reactive power
P_r	Rotor active power
Q_r	Rotor reactive power
$I_{d,q}$	Current in d-/q-axis
V_{dc}	DC voltage
P_{opt}	Optimal active power
k_{opt}	Parameter obtained from the aerodynamic performance of the wind turbine
S_{agg}	Aggregated rated power
S_i	Rated power of individual wind turbine
n	Number of wind turbines
P_{agg}	Aggregated active power
P_i	Active power of individual wind turbine
$E'_{d,q}$	Transient voltage in d-/q-axis
E_{fd}	Field voltage
$T'_{d0,q0}$	Transient time constant of d-/q-axis
$T''_{d0,q0}$	Sub-transient time constant of d-/q-axis
P_m	Mechanical power
P_e	Electrical power
$X'_{d,q}$	Transient reactance in d- /q-axis
$X''_{d,q}$	Sub-transient reactance in d-/q-axis
X_{ls}	Leakage reactance
δ	Rotor angle
Ψ_{1d}	Flux linkage d-axis damper winding
Ψ_{2q}	Flux linkage q-axis damper winding
E_t	Machine terminal voltage

E_t^{ref}	Machine terminal voltage reference set-point
T_R	Filter time constant (s)
K_A	Regulator gain (p.u.)
T_A	Regulator time constant (s)
T_E	Exciter time constant (s)
K_F	Feedback gain
T_F	Feedback time constant
S_E	Exciter saturation function value (p.u.)
U_{in}	PSS input signal
U_{pss}	PSS output signal
K_{pss}	PSS gain
T_w	Washout filter time constant
$T_{1\text{-}4}$	Lead-lag compensator time constants
φ_{comp}	Required phase angle compensation
m_c	Number of lead-lag blocks
Z_e	Transformer equivalent leakage reactance
n^*	Transformer off-nominal turns ratio
I	Current
Z	Impedance
P_w	Wind turbine output power
v_w	Wind speed
ρ	Air density (kg/m3)
A	Turbine swept area
λ	Tip speed ratio
β	Blade pitch angle
R	Rotor radius
ω_r	Rotational speed of the rotor
ω_s	Synchronous speed of the generator
ω_t	Rotational speed of the turbine
C_p	Power coefficient
V_{ds}	Stator voltage in the d-axis
I_{ds}	Stator current in the d-axis
Ψ_{ds}	Stator flux linkage in the d-axis

V_{qs}	Stator voltage in the q-axis
I_{qs}	Stator current in the q-axis
Ψ_{qs}	Stator flux linkage in the q-axis
V_{dr}	Rotor voltage in the d-axis
I_{dr}	Rotor current in the d-axis
Ψ_{dr}	Rotor flux linkage in the d-axis
V_{qr}	Rotor voltage in the q-axis
I_{qr}	Rotor current in the q-axis
Ψ_{qr}	Rotor flux linkage in the q-axis
R_s	Stator resistance
R_r	Rotor resistance
L_{ls}	Stator leakage inductance
L_{lr}	Rotor leakage inductance
L_m	Magnetising (mutual) inductance
L_s	Self-inductance
I_{sabc}	Three phase stator current
I_{rabc}	Three phase rotor current
V_{rabc}	Three phase rotor voltage
V_{sabc}	Three phase stator voltage
Ψ_{rabc}	Rotor flux linkage
Ψ_{sabc}	Stator flux linkage
r_g	Ac side of GSC resistance
L_g	Ac side of GSC inductance
X_0	State vector
U_0	Input vectors
Δx	Incremental state vector of dimension n
Δu	Incremental input vector of dimension m
A	State or plant matrix of size n×n
B	Control or input matrix of size n×m
Δy	Incremental output vector of dimension p
C	Observation (output) matrix of size p× n
D	Feed-forward matrix of size p×m.
ϕ	Modal transformation matrix

η	Transient stability index
δ_{max}	Maximum angle separation in degrees between any two generators
z	Vector of modal variables
R_i	Open loop residual of the system transfer function
f	Electrical frequency
λ	Eigenvalue
σ	Real component that provides damping
ω	Complex component that gives the frequency of oscillation
ζ	Damping factor
P_{ij}	Participation factor
ϕ_{ji}	The j^{th} entry of the i^{th} right eigenvector
ψ_{ij}	The j^{th} entry of the i^{th} left eigenvector
H	System inertia constant
H_t	Inertia constants of the turbine
H_g	Inertia constants of the generator
T_m	Mechanical torque applied to the turbine
T_e	Electrical torque of the generator
T_{tg}	Internal torque of the model
D_t	Damping coefficients of the turbine
D_g	Damping coefficients of the generator
D_{tg}	Damping coefficient of the shaft
K_{tg}	Shaft stiffness

Chapter 1

Introduction

1.1 Background and Motivation

Traditionally electricity was only generated by converting one of the primary energy sources, such as fossil fuels (oil, natural gas, coal, etc.) or nuclear fission, into electrical power. The primary energy sources are used to generate heat which is used in a steam-cycle to convert the thermal energy into mechanical energy and then to electrical power. However, using fossil fuels or nuclear fission as a primary source of energy have environmental impacts, such as greenhouse effect and nuclear waste disposal [1-3]. Therefore, reducing the emissions has become one of the most important targets agreed under the Kyoto protocol [4]. In order to reduce greenhouse effect and nuclear disposal, more efforts are put in generating electricity from renewable energy sources. Recently, many countries are encouraging the use of renewable clean energy sources due to environmental concern and the push for carbon-free power generation. New policies, such as the Renewable Portfolio Standard (RPS), have been implemented by several countries to encouraging the use of renewable clean energy sources to generate electricity. RPS is a regulation that supports generating electricity from renewable energy sources. It places an obligation on electricity supply companies to produce an increasing proportion of the electricity they supply from renewable sources. RPS mechanisms have been adopted in UK,

Italy, Belgium and USA [5]. Another common name for this concept is renewables obligation in the UK.

Among the renewable energy sources, wind energy is one of the feasible choices which has led to the great expansion of wind power generation during the past decade [6-8]. The total global installed wind at the end of 2015 was capable of meeting 4.3% of electricity demand, up from less than 1% at the end of 2006 [9]. In EU, the total installed grid-connected wind power by the end of 2014 was enough to cover 10.2% of the EU's electricity consumption [10]. Moreover, according to the International Energy Agency (IEA), by the year 2050 between 57 % and 71 % of global electricity demand will be supplied by renewable energy sources "sustainable future" scenario [11]. This growth has been supported by energy policies and wind turbines cost reduction [12]. Worldwide, the installed wind power capacity has reached 433 GW at the end of 2015 with 63GW of new wind power installed during 2015 alone as shown in Figure 1.1 [13].

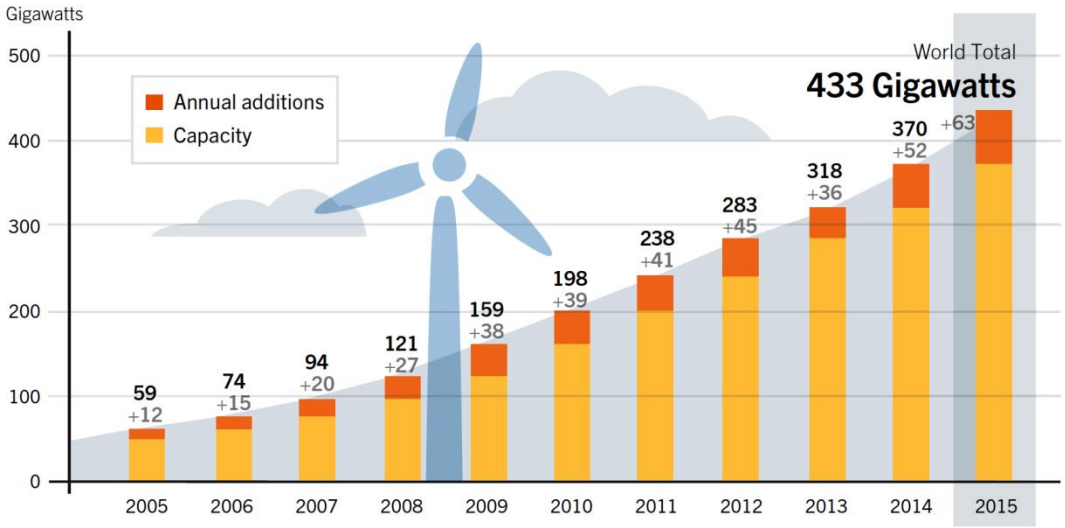

Figure 1.1 Installed wind power global capacity and annual additions, 2005–2015 [13]

At the end of 2015, the UK's wind power total capacity reached 13.6 GW, with 8.5 GW of onshore and 5.1 GW of offshore wind. In 2015, wind power provided 11% of the UK's total electricity supply, breaking the 10% barrier for the first time.

Moreover, in the final quarter 13% of all UK electricity was generated by wind power, and a monthly record of 17% was set in December [14].

The technology of wind energy has improved considerably from fixed speed wind turbines to variable speed wind turbines in the last decades. As variable speed wind turbines have high energy capture efficiency and reduced drive train stresses, they have become the typical type for new wind farm installations [15]. Variable speed wind turbines such as full-scale power converter wind turbine equipped with a direct-drive synchronous generator (SG) and the DFIG have become the two main generator alternatives [16, 17]. The full-scale power converter wind turbines type has the disadvantage of cost mainly due to a power converter rated for the full power [18].

With the increasing penetration of wind power, wind farms begin to influence power systems in a significant manner as wind farms are introduced to replace conventional generation to a certain extent. Due to such increase in wind power, the stability of power systems may be adversely affected as the wind turbines technology are substantially different from conventional power plants [17]. Moreover, wind turbines gradually start to replace the output of conventional power plants and thus many aspects of the power system operation, control, and stability might be affected [19]. Maintaining power system stability during, for example, a short circuit fault will be more important as the levels of wind power is considerably increasing in years to come [20].

The impact of wind power on power system stability can be ignored if the penetration of wind power is very low. However, with high levels of wind power penetration, wind farms may replace large conventional SGs, the dynamic performance of the power system might be affected [21]. Therefore, special requirements are set for wind power integration to avoid any potential negative impacts that wind power can have on the operation and stability of power systems [8, 22]. Wind farms must comply with requirements such as fault ride-through capabilities [23-25], reactive power and voltage control capability[24, 26, 27], and

frequency regulation [24, 28]. Moreover, as the capability to damp power system oscillations is important in power systems, wind farms will be required to contribute to the damping of power system oscillations [19, 29-31].

1.2 Power System Stability Challenges

Power system stability is an essential requirement for secure and reliable operation of power system while minimising the risk of a blackout. Maintaining the stability of power systems during any incident is the main issue of power systems operators, which will be challenged with increasing levels of wind power integrations. Therefore, a comprehensive understanding of power system stability with high penetration of wind generation is crucial for reliable power system analysis and operation, and it is essential to develop methods that mitigate adverse effects of wind power on power system stability.

1.2.1 Power System Stability Issues

Stability of power system is a complex problem. It can be practically divided into groups categorised by their time frame, the size of the disturbance, consequence, and physical character. Power system stability has been defined and classified by the Institute of Electrical and Electronics Engineers (IEEE) and International Council for Large Electric Systems (CIGRE) as follows [32]:

- **Rotor Angle Stability:** This is the ability of SGs in the interconnected power system to remain synchronised after being subjected to a disturbance. For a better understanding of rotor angle stability, it is useful to characterise as follows: small signal stability or (small disturbance rotor angle stability) and transient stability or (large disturbance rotor angle stability).
- **Voltage Stability:** This is the ability of the power system to maintain acceptable voltage levels at all system buses under normal operating conditions, and after being subjected to a disturbance. Voltage instability

may occur as a result of progressive and uncontrollable fall or rise in voltage of some of the system buses.

- **Frequency stability:** This is the ability of the power system to maintain the frequency within its limit after the system is being subjected to disturbance resulting in a significant mismatch between generation and load. Frequency stability depends on the ability of power systems to maintain or restore equilibrium between system generation and load.

This thesis focuses on rotor angle stability. The electromechanical oscillations inherent to power system operation which can lead to wide-spread problems and even system collapse and are of particular interest in this research.

1.2.2 Power System Oscillations

In normal conditions, all interconnected SGs are synchronised with each other and hence rotating at the same speed. In this case, there is a balance between the input mechanical and output electromagnetic torques of each SG in the interconnected system. However, in the event of a disturbance, rotors of synchronous machines may accelerate or decelerate leading to angular position difference between rotors, which can influence the output of SG. The system can sustain rotor angle stability with the help of installed generators controllers that act to reduce this deviation. However, rotor angle stability can be lost if the difference in angular position increases continually leading to large fluctuations in the generator output power, current, and voltage. Growing power system oscillations can lead to system instability and eventually the disconnection of equipment, and possibly can lead to further cascading failures. Ensuring that power system oscillations are well damped is the main problem of modern power systems [32].

1.2.2.1 Consequences of Unstable Power System Oscillations

The first power system oscillation was observed in the Northern American power network in 1964. The oscillation occurred on the tie line during a test to connect the Northwest Power Pool and the Southwest Power Pool [33]. Since then, many power system oscillations incidents have been reported in power systems around the world.

In USA, an outage of the Northern American Western Systems Coordinating Council (WSCC) network on 10 August 1996 was directly due to the power oscillations. A series of events started when a 500 kV line tripped within WECC system led to power oscillation between northern and southern parts of the WSCC which were oscillating against each other. The growing oscillations between the two areas reached an amplitude of 1000 MW, as shown in Figure 1.2, which eventually led to the separation of the WSCC network into four islands. The event affected 7.5 million customers for up to 9 hours and resulted in losing 30 GW of load and 27 GW of generation, and 7.5 million customers were without power [34]. The outage of the WSCC network on 10 August 1996 was directly due to the power oscillations. The blackout could be avoided, and the system could have maintained stability if the power oscillations were sufficiently damped [34-36].

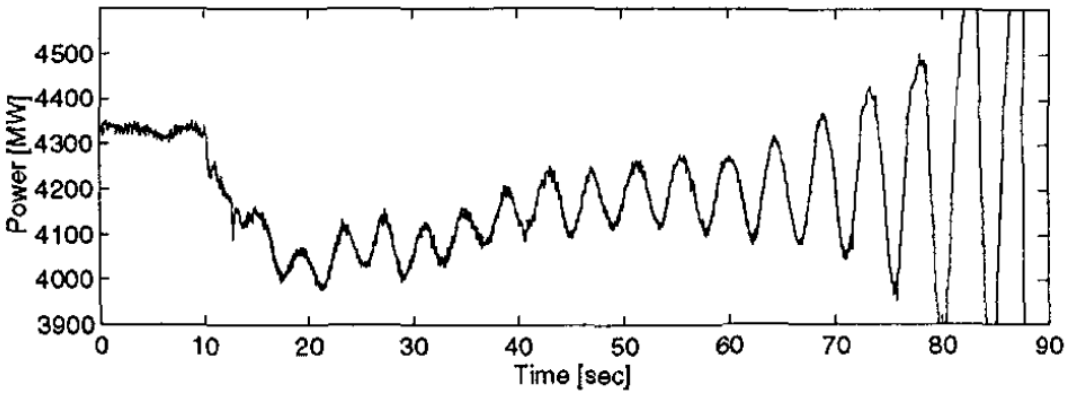

Figure 1.2 Growing power oscillations on California-Oregon AC Intertie that occurred during the 10 August 1996 blackout in the North American Western Interconnected system [34].

WSCC network is one of many examples, with power oscillations causing further issues in a variety of power systems, including [37]:

- Detroit Edison - Ontario Hydro - Hydro Quebec (1960s, 1985)
- Finland-Sweden-Norway-Denmark (1960s)
- Saskatchewan-Manitoba Hydro-Western Ontario (1966)
- Italy-Yugoslavia-Austria (1971-1974)
- Mid-continent area power pool (MAPP) (1971, 1972)
- South East Australia (1975)

- Scotland-England (1978)
- Western Australia (1982, 1983)
- Taiwan (1985)
- Ghana-Ivory Coast (1985)
- Southern Brazil (1975-1980, 1984

1.3 Previous work - State of the Art

The integration of non-synchronous generation units into power systems can have an impact on power system stability. In the literature, considerable research efforts have been dedicated to address the wind power integration issues. With large-scale integration of wind power into power systems, new stability concerns emerged and more attention is paid to understand the effects of wind power on power system rotor angle stability and how their effects can be mitigated [38, 39].

Variable speed wind turbines employing DFIG represent the most popular technology in currently installed wind turbines due to their flexible controllability and relatively low price [16, 17, 40]. DFIG is able to control its own reactive power to operate at a given power factor or to control the generator terminal voltage by using power electronic converters [41]. However, the capability of DFIG voltage control cannot match that of the SG for the reason that its power converters have a limited capacity. Thus, the stability of the power system is affected in the unfortunate event when the voltage control requirement is beyond the capability of the DFIG [42]. This problem can be resolved out by supporting the voltage through a reactive power compensation device such as static synchronous compensator (STATCOM) to provide rapid and smooth reactive compensation and voltage control [43, 44]. However, these devices are expensive, and many utilities hesitate to install them into their grid due to expected high costs [45]. In addition, the size of DFIG converters can be increased to increase the amount of reactive power that can be provided. However, this solution increases the overall cost which is one of the main advantages of DFIG over full power converter wind turbines [18].

In [46], the effect of reactive power supplied by wind generation on rotor angle stability was examined. The study concluded that transient stability could be improved and the oscillations damped more quickly if the terminal voltage of the wind generation is controlled. Moreover, SG rotor angle is directly influenced by reactive power control strategy used by the wind generation. However, [46] does not take into account the influence of the crowbar protection system which can lead to more severe voltage sag [47]. Since keeping the DFIG connected during transient grid faults is a grid code requirement, a number of published papers [48, 49] presented various strategies to ensure the continuous operation of DFIG. In [50], a decoupled fault ride through strategy to improve inertial response and reactive power capability of DFIG is proposed. The result shows that DFIG-GSC can be used to enhance the voltage during a grid fault. The strategy used in [50] prioritises the reactive power control through the GSC over DC voltage control once the terminal voltage drops below a predefined voltage level. Moreover, the rating of the installed GSC is larger than typical rating which is usually at 30% of the nominal generator power [51]. For the full power converter wind turbines, the GSC can also be used as a STATCOM [17, 52]. This can be done at very low wind speeds or during the fault with additional devices to absorb the generated active power. When there is a fault on the AC grid, the grid voltage falls to low levels in the vicinity of the fault location, thereby reducing the power transfer capability from the wind turbines. In contrast, power generated by the wind turbines cannot be ramped down instantaneously. The excess power is accumulated in the DC link leading to DC overvoltage. Chopper controlled resistors are used to dissipate the excess power and thus limit DC voltage rise [53, 54].

The effect of wind power generators on small signal stability depends on the kind of wind generator and their controllers [17]. DFIGs are not synchronously coupled to the power systems as the power electronic converters act as an interface between DFIGs generators and the grid. Therefore, they do not directly engage in power systems electromechanical oscillations nor do they produce new oscillatory modes [29, 55-57]. However, the rapid increment of wind power penetration can lead to the displacement of conventional plant inertia and other topology changes that

have the potential to influence the oscillation modes [55]. Moreover, DFIG wind turbines can affect the overall damping performance when replacing synchronous machines which are equipped with power system stabilisers (PSSs) [58]. Therefore, damping contribution of installed wind turbines is of significant importanc, and this can be achieved by introducing an auxiliary PSS loop into the DFIG controller [29].

Variable speed wind turbines are capable of controlling active and reactive power, and both could be used to improve small signal stability. In recent years, several researchers have examined the capability of DFIGs for damping power oscillations [29-31, 56, 58-60]. In [30, 31, 58-60] an auxiliary DFIG damping controller within the active power controller is proposed. References [30, 31, 59] show that DFIG equipped with PSS within active power control loop can damp the power system oscillation effectively. Consequently, DFIG with PSS can contribute to the oscillation damping much more effectively than the SG with PSS control. However, the control schemes used in [30, 31] are based on flux magnitude and angle control (FMAC) whilst the common control schemes for the commercial DFIG are based on standard decoupled *d-q* vector control mechanism [61]. The use of active power modulation can decrease the damping of the DFIG shaft mode [62]. This increases the stress on the DFIG rotor shaft and decreases the lifespan of the mechanical system. Moreover, reference [63] reported that PSS with active power modulation is adversely influenced by the torque variations due to tower shadow. Additionally, the effectiveness of the PSS with active power modulation can be reduced if the DFIG reactive power is used to control the grid voltage [60].

As DFIGs are able to control real power and reactive power independently, reactive power modulation can be used to regulate the voltage and enhance their capability to damp power oscillations. Only a small number of studies have been published concerning the use of DFIG reactive power for oscillation damping [62, 64, 65]. The results presented in these papers show that DFIGs can effectively damp power system oscillations using an additional control attached to the reactive power control circuit. Also, none of them takes into account the influence of the crowbar system when the control of active and reactive power is lost, and a large amount of

reactive power is absorbed. Moreover, the studies carried out in [62, 64, 65] do not take into account the impact of the stochastic wind speed behaviour on the proposed damping controller.

1.4 Research Aims and Objectives

Throughout the project and in the conducted studies, realistic power systems were analysed with detailed simulation models of a commercially available DFIG based wind turbines to reflect commercial DFIG wind turbine characteristics. The main aims of this research are to investigate and mitigate the impact of increased penetration levels of DFIG based wind turbines on transient and small signal stability of power systems. In order to achieve these aims, the following research objectives have been defined:

- Conduct comprehensive reviews and critically evaluate state of the art research articles in the area of wind power and power system stability to understand the characteristics of various wind turbines, particularly DFIG based wind turbines.
- Build a valid steady-state and dynamic detailed model for DFIG based wind turbines to evaluate the impact of wind generation on rotor angle stability of power systems and investigate the possible contribution of DFIG to damp out power system oscillations.
- Provide a clear understanding of the impacts of replacing conventional SGs with equivalent DFIG wind farms on rotor angle stability of power systems and compare the performance of DFIGs with that of SGs.
- Develop a control strategy by using the available DFIG reactive power to enhance the system stability during the active crowbar time when controlling of both reactive and real power is deactivated and a large amount of reactive power is absorbed.
- Design a PSS to allow DFIG based wind turbines to participate in power systems oscillations damping.

- Examine the capability of DFIG reactive power modulation to damp power system oscillations under different operating conditions within the same wind farm and stochastic wind speed behaviour.

1.5 Original Contributions of the Thesis

The work within this thesis contributes to a number of areas of power systems research, specifically surrounding the effects of high penetration of DFIG wind turbines on the power systems rotor angle stability. The results of the works in this thesis provide a valuable contribution to the following aspects:

- A novel cost-effective control approach is developed to lessen the impacts of DFIG on the rotor angle stability through exploiting the existing DFIG equipment's. A control strategy by utilising the DFIG-GSC to be used as a STATCOM to provide reactive power support during the active crowbar time when controlling of both reactive and real power is deactivated, and a large amount of reactive power is absorbed.
- A PSS was designed to evaluate the capability of DFIGs to damp power system oscillations. To avoid the negative effects of PSS active power modulation, a reactive power modulation PSS using a comprehensive system model is developed taking into account the influence of the crowbar system.
- A nonlinear simulation is used to evaluate the effectiveness of the proposed PSS under different operating conditions within the same wind farm and stochastic wind speed behaviour across two large-scale wind farms.

1.6 Thesis Structure

This thesis consists of seven chapters in total. The six chapters, which follow this introduction, are outlined below:

Chapter 2: Wind Power

This chapter discussed the development of wind power generation and its rapid growth as a result of environmental and economic issues that associated with fossil

fuels. Both global cumulative installed wind capacity and the installed wind power capacity in leading countries have been introduced. Then, a detailed presentation is given on wind turbines technology development and the share of yearly installed wind power for each type. Finally, the power system requirements for wind power integration to avoid any potential negative impacts that can wind power has on the operation and stability of power systems are discussed in this chapter.

Chapter 3: Power System Modelling

This chapter provides the basis for the power system modelling of various components of the power system including DFIG systems. Within this chapter, the mathematical representations of the main electrical power system components are presented including SGs, transmission lines, power transformers and systems loads. Following this, the modelling of DFIGs for power system stability analysis are presented, including wind turbine rotor aerodynamic model, a mechanical model, induction generator model, power converter model, control system model and aggregated DFIG wind farm model. In addition, operating range of DFIG wind turbine, its characteristics, and the maximum power tracking curve for various wind speeds are discussed in this chapter.

Chapter 4: Wind Power and Power System Stability

An extensive analysis of the effects of wind power on the stability of power systems is presented within this chapter. Initially, this chapter details the fundamental concepts of power system stability and its classification. Then, the effects of wind power integration on the three types of power system stability, which are rotor angle stability, frequency stability, and voltage stability, are investigated in this chapter. Finally, two test systems, realistic Western System Coordinating Council and New England 39 bus test system are utilised to show the impact of high penetration of wind power on power system rotor angle stability. Rotor angle stability of power system are analysed with and without wind generation to show the impacts of replacing SGs by equivalent DFIG based wind farms on rotor angle stability.

Chapter 5: Proposed Control Approaches of DFIG

The aim of this chapter is to develop control approaches of DFIG based wind farms to mitigate the impacts of wind power on power systems rotor angle stability as wind penetration levels continue to grow in power systems across the world. In order to continue secure service and power delivery to customers, the developed control technique can be applied to the installed DFIG wind turbines that are a part of power systems today and help maintain system security. This chapter began by presenting power systems modal analysis and how models of nonlinear power systems can be linearised in order to perform small signal stability analysis from which power oscillations damping controller is designed. Residual approach, which has been used for designing PSSs in SGs, is used in this thesis to design DFIG stabiliser controller. Finally, a control approach to utilise the DFIG-PSSs are designed to damp out power system oscillations.

Chapter 6: Enhancement of Rotor Angle Stability by Utilising the DFIG Reactive Power using the Proposed Approaches

This chapter analyse the impacts of replacing conventional SGs with equivalent DFIG wind farms on rotor angle stability of power systems and mitigate these impacts by the proposed control approaches. The effectiveness of the proposed control methods are examined in both standard Western System Coordinating Council and the widely used New England 39-bus test systems. The chapter begins by conducting rotor angle stability on each test system without and with wind generation to show the impacts of replacing a SG by an equivalent DFIG wind turbine on rotor angle stability. Then the integrated DFIG wind turbines are equipped with the proposed control strategies to show how effective they are to improve rotor angle stability of the test system. Moreover, the capability of the proposed conventional fixed parameters PSS to damp power oscillations effectively under non-uniform variable wind speeds across the wind farm is assessed in multi-machines power system with two large wind farms.

Chapter 7: Conclusions and Future Work

In this chapter, the main conclusions of the research are presented, and suggestions are made for the future development and improvement of the presented methods.

1.7 Publications

1.7.1 International Journal Publications

- **Mohamed Edrah**, Kwok L. Lo, and Olimpo Anaya-Lara. "Impacts of high penetration of DFIG wind turbines on rotor angle stability of power systems." IEEE Transactions on Sustainable Energy 6.3 (2015): 759-766.
- **Mohamed Edrah**, Kwok L. Lo, and Olimpo Anaya-Lara. "Reactive power control of DFIG wind turbines for power oscillation damping under a wide range of operating conditions." IET Generation, Transmission & Distribution 10.15 (2016): 3777-3785.
- **Mohamed Edrah**, Kwok L. Lo, and Olimpo Anaya-Lara, "Damping of Power Systems Oscillations through VSC–HVDC Connected Offshore Wind Farms" Under Preparation for Journal Submission (IEEE Transactions on Sustainable Energy).

1.7.2 International Conference Publications

- **Mohamed Edrah**, Kwok L. Lo, Abdussalam Elansari, and Olimpo Anaya-Lara, "Power oscillation damping capabilities of doubly fed wind generators," in Power Engineering Conference (UPEC), 2014 49th International Universities, 2014, pp. 1-6.
- **Mohamed Edrah**, Kwok L. Lo, Olimpo Anaya-Lara, and Abdussalam Elansari, "Impact of DFIG Based Offshore Wind Farms Connected Through VSC-HVDC Link on Power System Stability," in AC and DC Power Transmission, 11th IET International Conference on, 2015, pp. 1-7.
- **Mohamed Edrah**, Kwok L. Lo, Abdussalam Elansari, and Omar .G. Mrehel "Impact of DFIG based Wind Farms on Transient Stability of Power

Systems" in 3rd International Conference on Automation, Control, Engineering and Computer Science (ACECS'16), pp. 1-6.

- **Mohamed Edrah,** Olimpo Anaya-Lara, Ivana Kockar, George Bell, Stevie Adams, and Fraser Macintyre, “Impact of Domestic Frequency Responsive Demand on the Shetland Islands Network Frequency Stability,” accepted to be published in the CIRED 2017 Conference.
- Abdussalam Elansari, Joe Burr, Stephen Finney, and **Mohamed Edrah**, "Optimal location for shunt connected reactive power compensation," in Power Engineering Conference (UPEC), 2014 49th International Universities, 2014, pp. 1-6.
- Abdussalam Elansari, Stephen Finney, Joe Burr, and **Mohamed Edrah**, "Frequency control capability of VSC-HVDC transmission system," in AC and DC Power Transmission, 11th IET International Conference on, 2015, pp. 1-6.

Chapter 2

Wind Power

2.1 Introduction

Traditionally electricity was only generated by converting one of the primary energy sources, such as fossil fuels (oil, natural gas, coal, etc.) or nuclear fission, into electrical power. The primary energy sources are used to generate heat which is used in a steam-cycle to convert the thermal energy into mechanical energy and then to electrical power. However, using fossil fuels or nuclear fission as a primary source of energy have environmental impacts, such as greenhouse effect and nuclear disposal. Moreover, these energy sources are limited sources of energy and also lead to the production of toxic gases in our atmosphere. According to International Energy Agency (IEA), power generation sector, which is the largest emitting sector, is responsible for the largest share of emissions in 2013 with more than 40 % [66]. Therefore, due to environmental and economic issues, which are now becoming dominant issues in our society, more efforts are put in generating electricity from renewable energy sources. Recently, many countries are encouraging the use of renewable clean energy sources to generate electricity by implementing new policies, such as the Renewable Portfolio Standard (RPS) [5]. RPS mechanisms have been adopted in the UK, Italy, Belgium and USA [5]. Another common name for this concept is renewables obligation in the UK. Moreover, under EU action plan, EU

countries will have to follow distinctive paths to meeting their obligations including their legally binding of 2020 renewable energy targets [67].

2.2 Wind Power Generation Development

Among the renewable energy technologies that are being developed, Wind turbine technology is the fastest growing renewable energy technology in the world. Wind power is considered the most promising renewable energy source for the sustainable development of human society. During the last decade, the installed capacity of wind turbines has increased at an astonishing rate, and the wind turbines costs have continued to decrease [68]. This is due to the supportive policies adopted by many countries around the world. Annual installations of wind power in the EU increased from 3.2 GW in 2000 to 11.8 GW in 2014. The capacity of wind power installed in EU in 2014 is counted as almost 44% of all newly installed power capacity [10]. Figure 2.1 Shows the net growth of all installed power capacity in the EU over the period from 2000 to 2014. It is clear that the wind power is dominating the new installed capacity over the past decade. The total installed grid-connected wind power in EU by the end of 2014 was enough to cover 10.2% of the EU's electricity consumption [10].

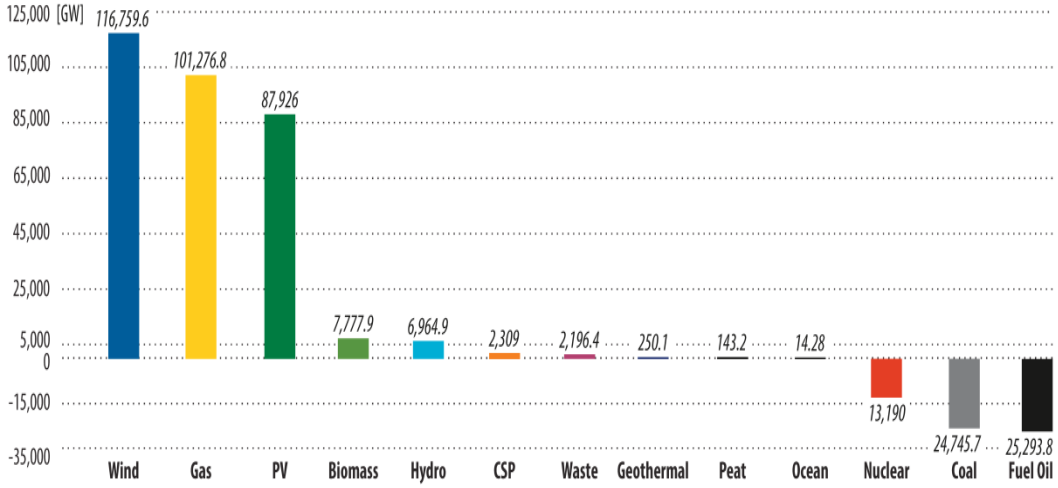

Figure 2.1 Net growth of all installed power capacity in the EU over the period from 2000 to 2014 [10]

Wind power is still the most promising renewable energy source used for electrical power production. The significance of wind power is growing rapidly throughout the world to reduce environmental degradation. According to the Global Wind Energy Council (GWEC), the global cumulative installed wind power capacity worldwide has exceeded 369 GW at the end of 2014 and would reach 712 GW by 2020 [14]. The global installed wind power capacity in a single year reached a new record in 2015 when the total installed wind power capacity was more than 63 GW, which is a sharp rise in comparison to 35.6 GW installed in 2013 as shown in Figure 2.2. The global cumulative installed wind power capacity between 2000 and 2015 is shown in Figure 2.3. The integration of wind power has grown significantly from 17.4 GW in 2000 to more than 432 GW in 2015 [69]. The integration of wind power is expected to continue as more countries have authorised encouraging policies to speed up the wind power development [70]. The continued growth of the use of wind power indicates that wind power would play a significant role in the modern power systems.

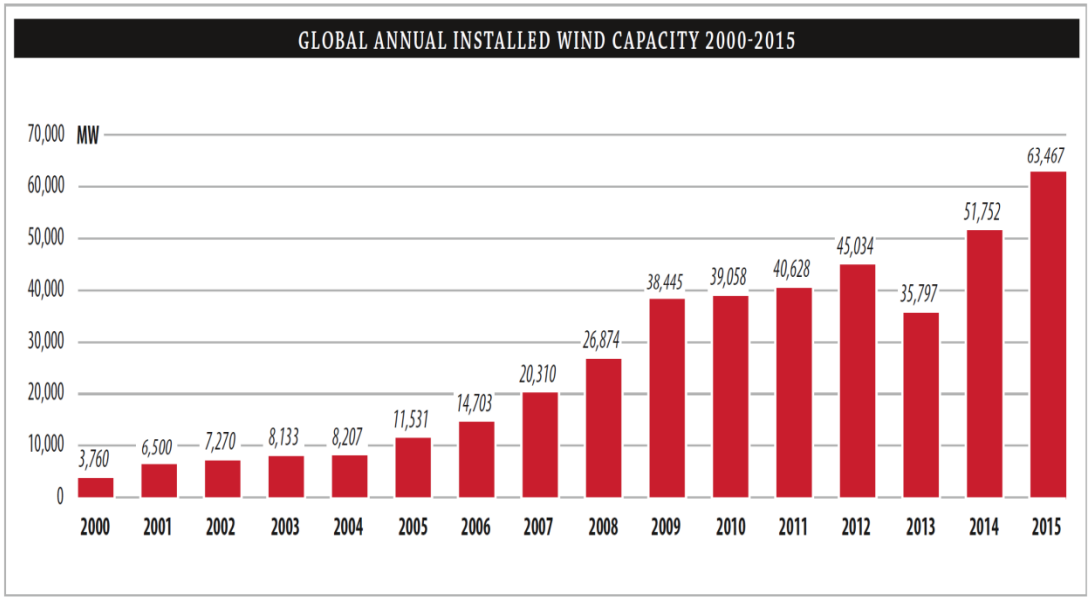

Figure 2.2 Global annual installed wind capacity 2000-2015 [69]

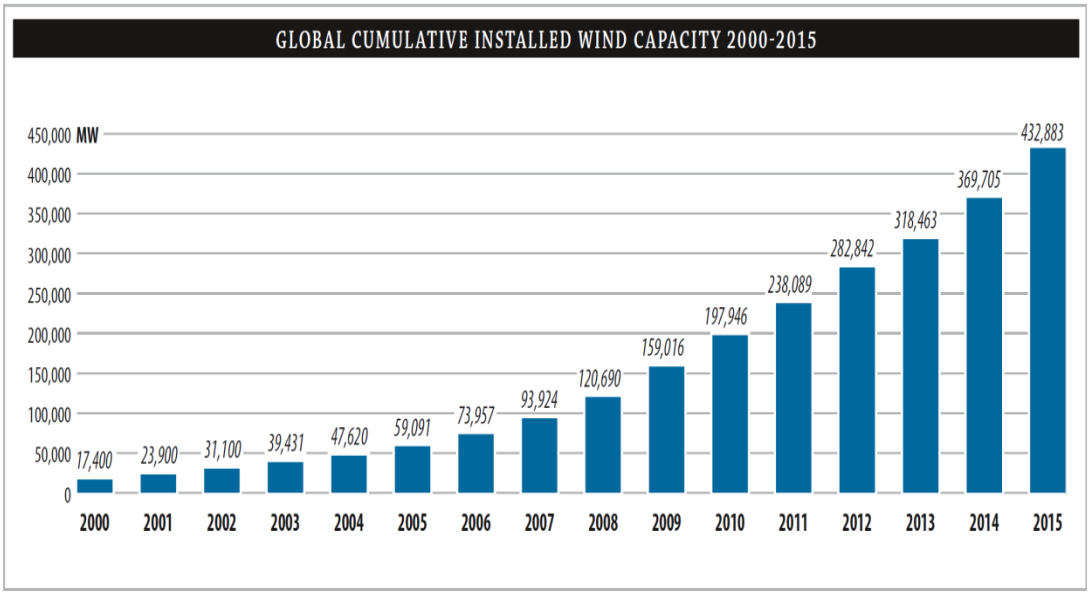

Figure 2.3 Global cumulative installed wind capacity from 2000 to 2015 [69]

2.3 Installed Wind Power Capacity in Leading Countries

There has been a significant growth in interest in wind power generation throughout the world. According to GWEC, Figure 2.4, approximately 311 GW (84 %) of the global wind power capacity are a cumulative capacity of the top ten countries, which are China, the USA, Germany, Spain, India, United Kingdom, Canada, France, Italy and Brazil [4]. The amount of installed wind power in MW for top ten countries is shown in Table 2.1.

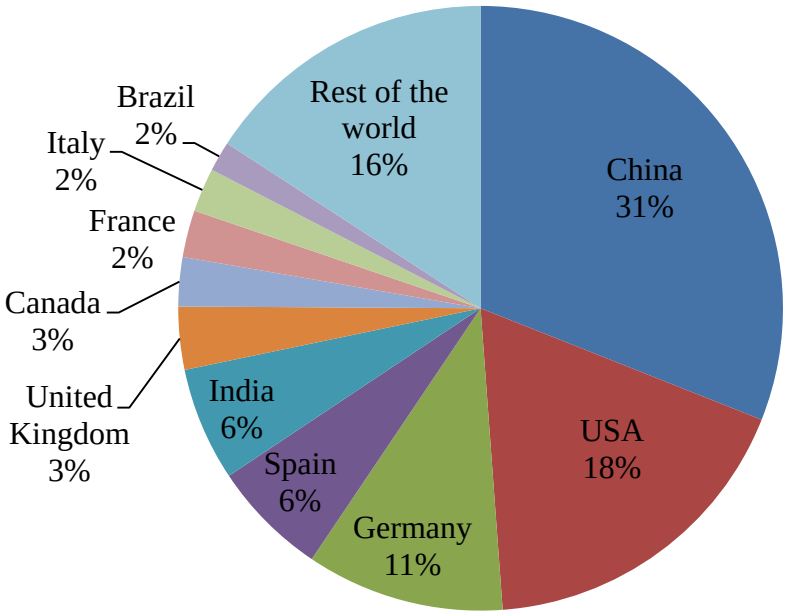

Figure 2.4 Top ten countries cumulative wind power capacity (End of 2014) [10]

Table 2.1 Top ten countries installed cumulative wind power capacity in MW (End of 2014)

Country	Wind power (MW)	Country	Wind power (MW)
China	114,609	France	9,285
USA	65,879	Italy	8,663
Germany	39,165	Brazil	5,939
Spain	22,987	Rest of the	58,473
India	22,465	Total top ten	311,124
United Kingdom	12,440	World total	369,597
Canada	9,694		

2.3.1 China

China began to utilise wind power in the 1970s. However, the use of wind power grow slowly until 2006, when encouraging policies were issued [70]. Currently, wind power growth is led by China since 2010 with more than 23 GW of new wind power installed in 2014 alone, which is the highest annual number for any country ever. It is not surprising that China replaced the US as the biggest wind market, as the total installed capacity has doubled every year from 2006 until 2010. Moreover, the source of wind energy is abundant in China with a usable onshore and offshore wind power capacity of 700 GW to 1,200 GW [71].

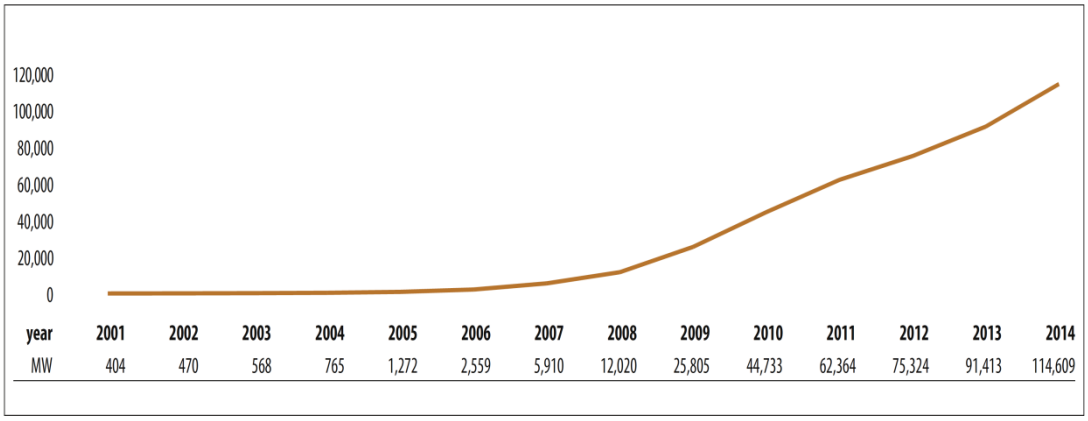

Figure 2.5 Total installed wind power capacity in China from 2001 to 2014 [10]

China in 2014 exceeded the 100 GW (approximately 31 % of global wind power capacity) of cumulative installed wind power capacity, as shown in Figure 2.5, and targets to double this wind power capacity to 200 GW by the end of 2020 [4]. The contribution of generated wind power in China is increased from 1.5% in 2011 to 2.78% in 2014 of the country's total electricity generation.

Recently, new policies have been introduced to force grid companies to give wind and other renewable electricity sources priority access to the grid, as the availability of suitable grid capacity remains the most serious challenge facing the wind industry in China [72].

2.3.2 USA

Currently, the US is the second largest market regarding total installed capacity after China. The newly installed wind power capacity in 2014 was 4,854 MW, which is over four times more than the wind power installed capacity in 2013. The newly installed wind power brings the total cumulative wind power capacity in the USA to 65,879 MW at the end of 2014. This amount of wind power is accounted for 5.23% of total installed generation capacity in the US. Wind power accounted for almost 31% of all new generating capacity installed over the period between 2009 and 2013 [73].

In the past five years, the cost of wind power has dropped remarkably 58% [10]. Generating electricity from wind power at a reasonable price in the US makes it an important choice to be considered by utilities for new generation. The wind energy in the US is growing steeply and could become the mainstream generation technology as shown in Figure 2.6. The wind power vision outlined by US Department of Energy is to double the current contribution of wind power by 2020 and to reach 20% by 2030. By 2050 wind power is expected to provide over the third of the consumed US electricity [10].

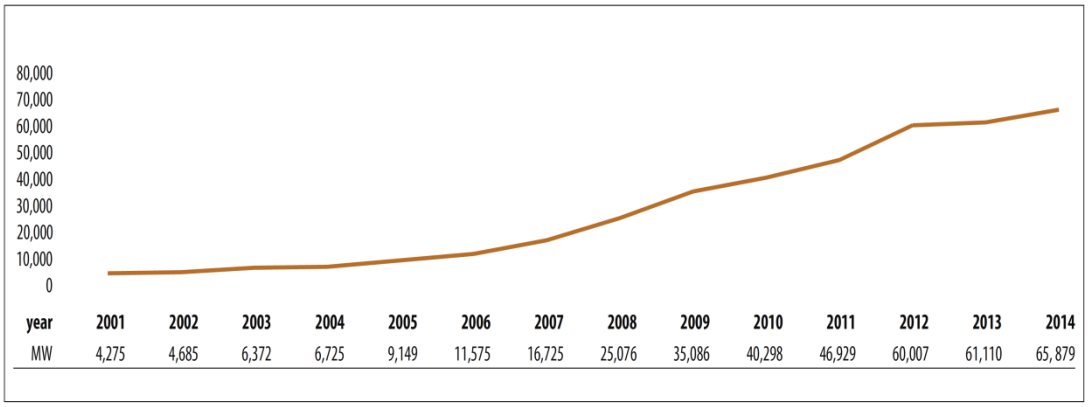

Figure 2.6 Total installed wind power capacity in the USA from 2001 to 2014 [10]

2.3.3 European Union Countries

The use of wind power in Europe grew gradually from the 1980s onwards. Among EU countries, Denmark was the first to invest in wind power leading to a rapid growth of Danish wind power. This followed by a range of support mechanisms by other EU countries to encourage investment in wind power. Nowadays, wind energy and other renewable energy sources in EU have the priority in order to increase energy security and to achieve their commitments under the Kyoto Protocol [74].

During 2014, the newly installed wind power accounted as 12,858 MW across all Europe countries of which 11,375 MW was onshore, and 1,483 MW was offshore. The capacity of newly installed wind energy is more than the new capacity of gas and coal combined in 2014. The newly installed wind power brought the total EU cumulative capacity to almost 128 GW with market growth of 10.5% in 2014. The total installed grid-connected wind power in EU by the end of 2014 was enough to cover 10.2% of the EU's electricity consumption, which is up by 2.2% from the previous year [75]. Over the half of all newly installed wind power in 2014 was in just two countries. The wind power installed in Germany and the United Kingdom in 2014 was approximately 59.5% of the total installed wind power in EU, installing 5,279 MW and 1,736 MW respectively.

In less than ten years, wind energy's contribution to UK electricity needs has grown from less than 1% to 10%, making wind energy the UK's single biggest source of renewable power [76]. According to UK's National Grid, wind power provided 14% of the total UK demand in January 2015 [77]. Moreover, among all EU countries, UK has the largest offshore wind capacity with over 55% (4,494 MW) of all installations worldwide. During 2014, 813 MW of the new installed wind power in the UK was offshore [77]. Between July 2014 and the end of June 2015, an additional 648 MW of onshore and 1,394 MW of offshore wind was installed to increase the total capacity to 13,313 MW as shown in Figure 2.7 [77].

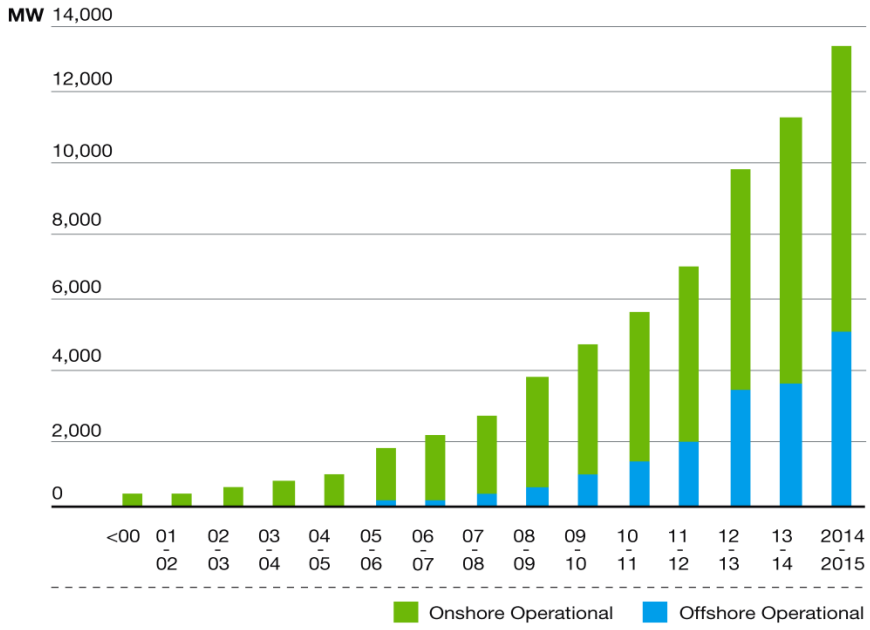

Figure 2.7 Operating capacity of UK wind power (2000-2015) [77]

2.4 Wind Turbine Generator Types

Commercial wind turbines that available for utility size applications can be classified into four major types. These four types can be further divided into fixed and variable speed wind turbines depending on their operational ability. Fixed speed wind turbines were the most common type of wind turbines installed in the early 1990s, and there are still many in operation. In fixed speed wind turbines, the wind turbine's rotor speed is fixed and is determined by the gearbox ratio, the grid frequency, and the generator design. However, variable speed wind turbines are designed to operate over a broad range of wind speeds for maximum aerodynamic efficiency. Currently, variable speed wind turbines have become the dominant types among the installed wind turbines.

2.4.1 Fixed Speed Wind Turbine (Type I)

This is the oldest and simplest wind turbine generation system, which is also known as constant speed wind generator. Type I wind turbine based on a conventional squirrel cage induction generator (SCIG) directly connected to the grid through a step-up transformer, as shown in Figure 2.8. The main components of

Type wind turbines system are turbine aerodynamics, gearbox, induction generator, soft stator, and reactive power compensation device. As this type of wind turbines is connected directly to the grid, no synchronisation device is required. Therefore, the generator rotor has to operate at a constant speed around the frequency of the grid. As a result, the generator operates at almost constant speed with very small slip in the order of 2 % at rated power [78, 79]. Stall or pitch control could be used to control the squirrel cage induction generator. Stall control (passive control) referred to rotor blades that are designed to reduce the aerodynamic torque of the wind when the wind speed is high; whereas pitch control is an active control that can decrease the torque by turning the blade around its axis [80].

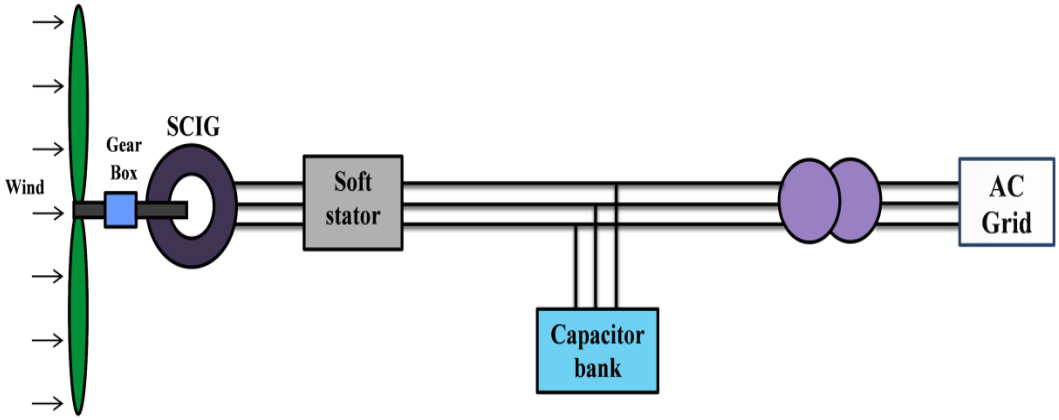

Figure 2.8 The basic configuration of fixed speed wind turbine with SCIG (Type I)

Wind turbines based on SCIG have high starting current due to sudden magnetisation at the instant of coupling to the network. Therefore, they are typically equipped with soft starter mechanism to limit the starting current, which can be up to five to eight times the rated current; and reactive power compensation device such as capacitor banks are needed to help with magnetising current supplied from the grid to the stator winding [81].

Type I wind turbines cannot absorb wind speed fluctuations and thus the fluctuation in the torque will occur. This can lead to larger power fluctuations and gearbox failures due to the mechanical stresses on the turbine drive train. Moreover,

this type always draws varying amounts of reactive power from the grid depending on wind conditions. This is undesirable in most cases, particularly in the case of large turbines and weak grids where both the voltage fluctuations and the line losses may increase. Furthermore, there is no direct control over produced active power or absorbed reactive power. In contrast, this type has a number of advantages such as robustness, easy to install and inexpensive [17].

2.4.2 Limited Variable Speed Wind Turbine (Type II)

This type of wind turbines is similar to the Type I wind turbine. The main difference is that this type uses a wound rotor induction generator (WRIG) with a variable resistance connected to the generator rotor as shown in Figure 2.9. The variable resistance is regulated dynamically by power electronics to control the generator slip to absorb the fluctuations into kinetic energy of the wind turbine shaft to be discharged as heat in the external resistance. This lead to smaller fluctuations in the drive train torque and delivered power. The maximum slip range is approximately 10%, which is limited by the external resistance heat losses [17].

Although the operating speed range is improved in this type in comparison with type I, it has the same drawbacks as the old Type I wind turbine with squirrel cage induction generator.

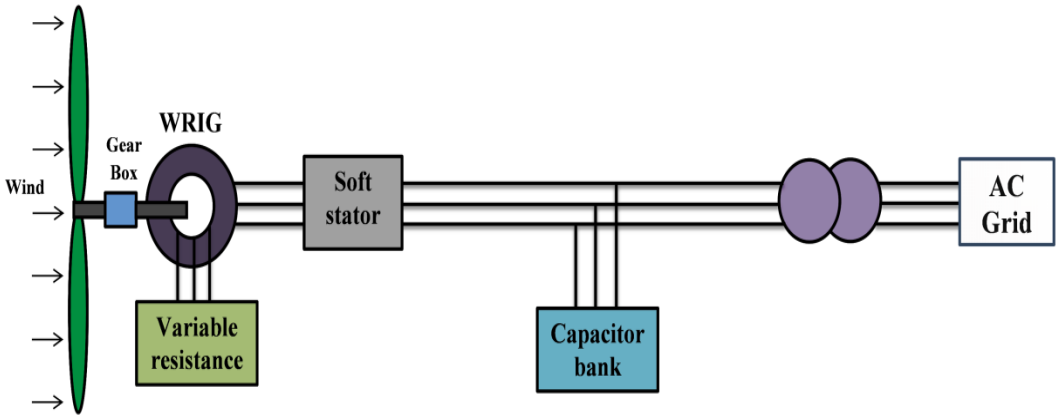

Figure 2.9 The basic configuration of limited variable speed wind turbine with WRIG and variable rotor resistance (Type II)

2.4.3 Doubly Fed Induction Generator Wind Turbine (Type III)

DFIG based wind turbines is a variable speed wind turbine in which the stator windings of the induction generator are directly connected to the grid while the windings of wound rotor are connected to the grid through slip rings and a back-to-back voltage source converter. In a similar way to fixed speed induction generator, the wind turbine is coupled to the DFIG through a gearbox as shown in Figure 2.10. A large number of modern wind turbines are equipped with DFIGs as they can supply active power at a constant voltage and frequency while the rotor speed may be varied. This type does not require a soft starter or a reactive power compensator, as the power converter can provide the magnetisation of the DFIG and control the reactive power independently of the active power. The size of the converter depends on the turbine rating and it is usually around 30% of the turbine rating [17].

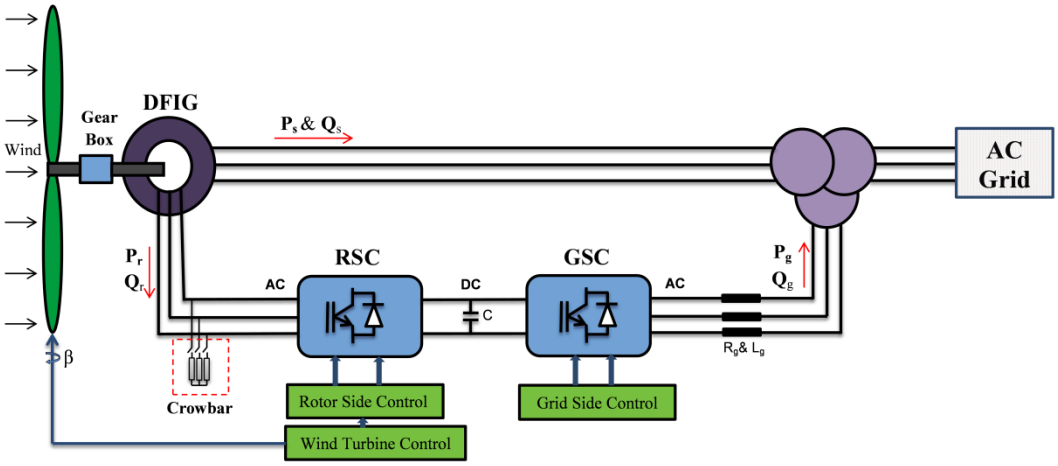

Figure 2.10 Basic configuration of a DFIG based wind turbine (Type IV)

DFIG based wind turbines allow a variable speed operation where the difference between the mechanical and electrical frequency is compensated by the voltage source converter using a current with a variable frequency. The back-to-back power converter consists of two voltage source converters separated by a DC link. The converters are known as rotor side converter (RSC) and grid side converter (GSC). The behaviour of the DFIG during both normal operation conditions and fault is governed by these two converters, which are controlled independently of each other.

The RSC controls the active and reactive power whereas GSC controls the DC link and can be used to regulate the reactive power exchange with the grid.

DFIG base wind turbines have several advantages over fixed speed induction generators. DFIG wind turbines can yield more energy from the wind than fixed speed wind turbines of the same capacity when the wind speed is below its rated value, and they have the capability to control active and reactive power independently by controlling the rotor excitation current. No soft starter or reactive power compensator are required for DFIG. This type has a broad range of speed variation that can be determined by the converter size, which is usually ±30% around synchronous speed. These advantages made wind turbines equipped with DFIGs the most preferred type of wind generation applications. However, the main disadvantage of this kind of wind turbines is that it is very sensitive to grid disturbances. The RSC is exposed to a high overcurrent through the rotor windings, which is caused by a high transient current in stator windings. Therefore, a protection system is needed to protect the power converter and to keep the turbine connected to the grid.

2.4.4 Full-Scale Power Converter Wind Turbine (Type IV)

This type of wind turbine is also a variable speed wind turbine equipped with a fully rated power converter that connects the generator stator to the grid as shown in Figure 2.11. The generator could either be an induction or SG. Synchronous generators can meet different technical requirements in practical wind energy systems. The use of permanent magnet SG (PMSG) in Type IV is advised by many research articles and has been widely used in variable speed wind turbines. In PMSG, the excitation is provided without any energy supply, which allows operation at a high power factor and a high efficiency [17]. PMSC based wind turbines may not include gearbox as the PMSG can be built with a large number of poles and hence rotate at the speed of the turbine blade.

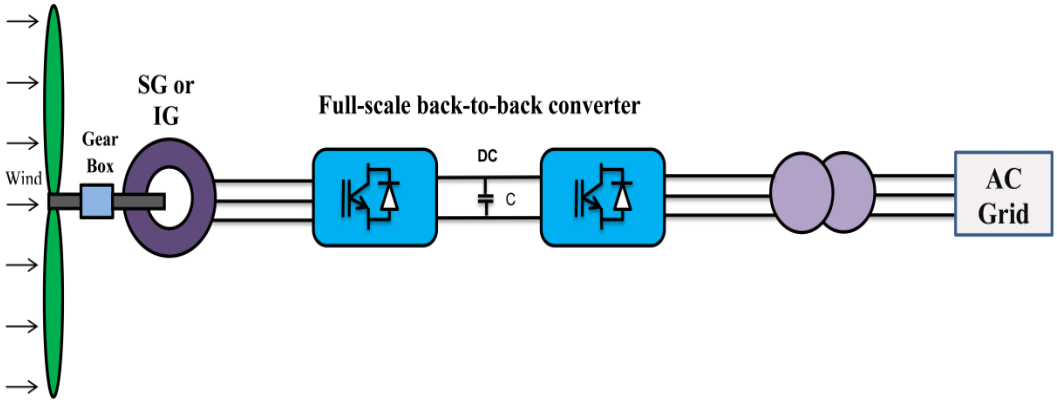

Figure 2.11 Basic configuration of full-scale power converter wind turbine (Type IV)

The power converter of Type IV wind turbine can be arranged in various ways. Generator side converter can be a diode based rectifier or a pulse width modulation voltage source converter while the GSC is usually a pulse width modulation voltage source converter [82]. The power converter of this type of wind turbines enables independent control of both the active and reactive power supplied by the generator to the grid.

Type IV wind turbines have some advantages in comparison to fixed speed wind turbines and DFIG. In this type, the generator is fully decoupled from the grid and hence the grid fault will not be passed to the generator. This is a superior advantage as the grid codes have become more restrictive regarding the immunity of the wind turbines to grid faults. Moreover, as the converter of Type IV wind turbines is scaled to correspond to the rated power of the wind turbine, a wide range of operation speed is provided. Additionally, this type can provide more reactive power than DFIG. However, there are a number of disadvantages including the high cost and losses of full power converter [82].

2.5 Installed Wind Power for Different Wind Turbine Types

In the early 1990s, Type I wind turbines were the most common type of installed wind turbines. However, the yearly installed Type I wind turbines have declined from 70% in 1995 to 39% in 2000 and further reduced to less than 5% in 2009 as

shown in Figure 2.12 [17]. From the figure, it is clear that the advantages of variable speed wind turbines make them dominate the market from the last decade. The yearly installed power of limited variable speed wind turbine has also declined in favour of variable speed wind turbines after 1997 to reach its lowest level in 2005. In contrast, DFIG based wind turbine installed power has increased to more than 60% of the yearly installed power over the period between 1995 and 2009. DFIG based wind turbine was first introduced in 1996 and in just five years it started to dominate the market. As the global cumulative installed wind capacity reached 120 GW at the end of 2008 [69], the installed DFIG capacity worldwide at the end of 2008 was approximately 82 GW. Unlike previous wind turbines types, the yearly installed power of Type IV wind turbines has no dramatic change over the years between 1995 and 2009. However, grid requirement, which makes variable speed wind turbines favoured over fixed speed wind turbines, Type IV wind turbines will have a strong increasing share of the market. Nevertheless, due to the advantages of DFIG wind turbines such as costs, weight, and size, they will remain competitive with respect to Type IV wind turbines [17].

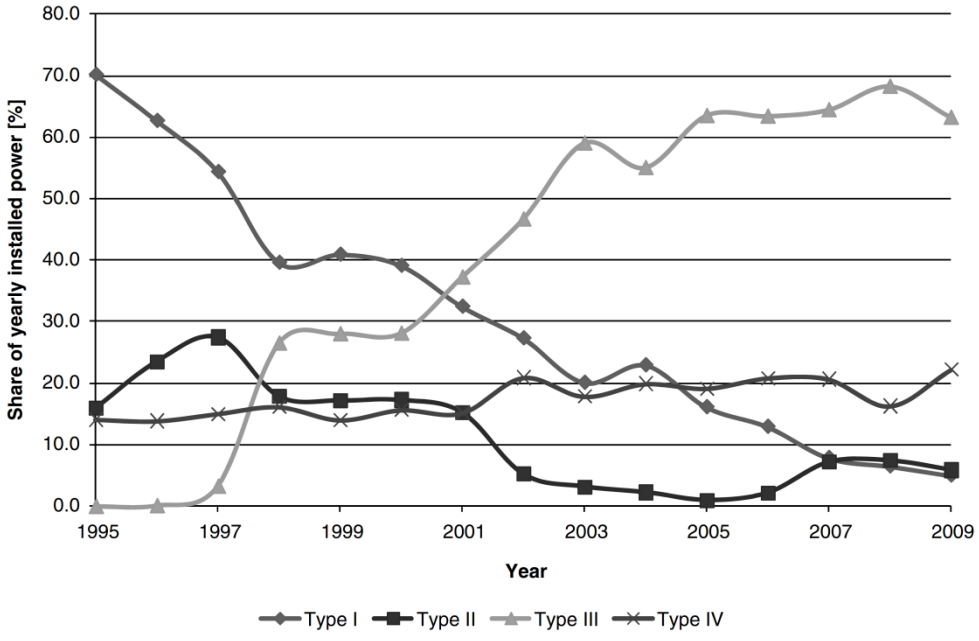

Figure 2.12 Share of yearly installed wind power for different wind turbine types [17]

2.6 Requirements for Wind Power Integration

Rules for wind power integration are usually developed by the transmission system operator (TSO) to support the system needs. In general, the power system requirements for wind power integration depend mainly on the wind power penetration level and the power system configuration. In the past, there were no requirements for wind power integration into a grid as the levels of wind power penetration were very small in comparison to the total installed conventional generation. When the penetration of wind power is low, the impact of installing additional wind power on the power system will be very small and could be ignored. Reference [17] defined the penetration of wind is high if more than 15% of gross electricity consumption is covered by wind power and it is low if less than 5% of total demand is supplied by wind power.

Recently, the installation of wind turbines into power systems has increased dramatically and thus the levels of wind power penetration are getting higher. With high penetration levels of wind power, the synchronous power system operation and stability can be affected. Moreover, currently, large wind farms are being connected to the grid and thus may have a significant impact on power systems. Therefore, special requirements are set for wind power integration to avoid any potential negative impacts that wind power has on the operation and stability of power systems. The most important technical requirements are as follows:

- Frequency and voltage tolerance
- Reactive power and voltage control capability
- Frequency regulation
- Fault ride-through capabilities

And future technical requirements may include:

- Inertial response
- Power system stabiliser

2.6.1 Frequency and Voltage Tolerance

Requirements for wind power integration are similar to requirements that apply to the connection of large conventional power plants. In a similar way, the requirements for wind turbines addresses the performance of the entire wind farm at the point of connection rather than addressing individual wind turbines in a wind farm. Wind farms are required to operate continuously to provide energy into the power system over the range of frequency and voltage and not to trip during system disturbances. Figure 2.13 shows the typical shape of voltage and frequency requirements for a wind farm. The value of voltage and frequency can vary from country to country [83].

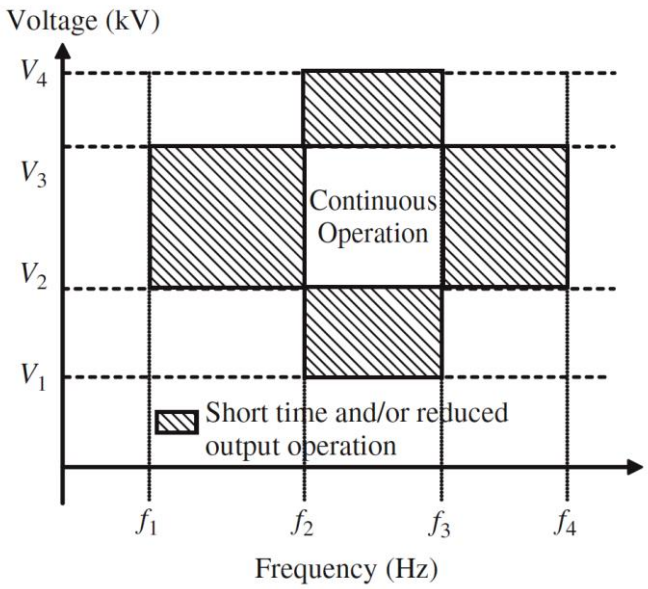

Figure 2.13 Typical shape of voltage and frequency requirements for a wind farm [83]

In the UK, the voltage for 400 kV level normally remains within the limit ±5% of the nominal value during normal conditions and could be between ±10% for no longer than 15 minutes unless abnormal conditions are observed. Voltages on the 275 kV and 132 kV levels normally remain between ±10% of the nominal value during normal operation conditions and within limits ±6% of the nominal value for voltage levels less than132 kV [24]. For system frequency, wind farms have to maintain

constant active power output continuously when the system frequency varies between 50.5 Hz and 49.5 Hz [24].

2.6.2 Reactive Power and Voltage Control Capability

The voltages at transmission level are determined mainly by the flows of reactive power. In a similar way to conventional power plants, wind farms have to regulate the voltage at the connection point at a certain limit or to exchange a certain amount of reactive power with the transmission network. In the UK Grid Code, the reactive power requirement of the wind farm is defined as shown in Figure 2.14.

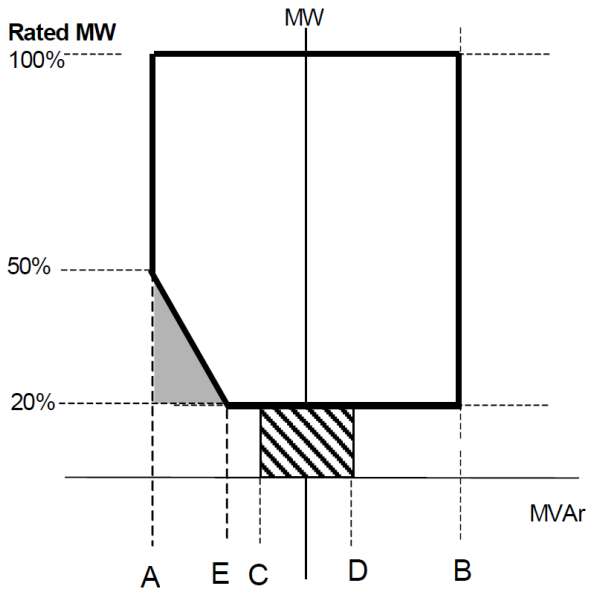

Figure 2.14 Typical reactive power requirement of a grid connected wind farm in UK [24].

Wind farms should operate anywhere within the specified area as instructed by the transmission system operator as follows:

- Point A is equivalent (in MVAr) to: 0.95 leading power factor at rated MW output.
- Point B is equivalent (in MVAr) to: 0.95 lagging power factor at rated MW output.
- Point C is equivalent (in MVAr) to: −5% of rated MW output.

- Point D is equivalent (in MVAr) to: +5% of rated MW output.
- Point E is equivalent (in MVAr) to: −12% of rated MW output.

Wind farms connected to voltage levels of 132 kV, 275 kV, and 400 kV, must be able to supply rated active power at any point between the limits 0.95 power factor leading and 0.95 power factor lagging. With all plant in service, the reactive power limits will apply for any active power output above 20% of the rated output active power for lagging power factor. However, the reactive power limits will reduce linearly below 50% of active power [24].

2.6.3 Frequency Regulation

Due to the dynamic nature of electrical power systems and the large variation of load demand, the mismatch between the generation and demand may cause the system frequency to increase or decrease. The system frequency usually varies in small quantities, which depend on the net difference between generation and demand as the active power balance in the power system is strongly coupled to the frequency. Over a certain range of frequency, power systems are able to operate continuously in a normal manner. Wind farms have to maintain constant active power output continuously when the system frequency varies between 50.5 Hz and 49.5 Hz. However, the system frequency could rise to 52 Hz or fall to 47.5 Hz in exceptional conditions. Wind farms are required to operate continuously in the specified frequency range, and the active power output of the wind farm should not be reduced by more than 5% of the system frequency changes within a range 49.5 Hz to 47 Hz. Moreover, wind farms are required to operate for a period of at least 20 seconds when the frequency drops below 47.5 Hz [24].

2.6.4 Fault Ride-Through Capabilities

Traditionally, wind turbines are allowed to trip once the voltage at their terminals reduces to a specified level. However, with the rapid increase of wind power penetration, a higher spinning reserve is required to prevent the risk of a blackout. Since the capability of any power system to return to the normal operation condition after clearing faults is a very important issue, fault ride-through capability for wind

turbines connected to transmission system is essential. It is an obligation for wind farms to remain connected during close-up solid three-phase short circuit fault or any unbalanced short-circuit fault. Wind farms should withstand a drop to zero volts and remain connected during any network fault with a clearance time of up to 140 ms. Wind turbine generators are able to trip only when the voltage is sufficiently low for a long time. Following fault clearance, recovery of the voltage at the terminals of the wind farm to 90% should not take longer than 180 s [24].

2.6.5 Inertial Response

Conventional SGs rotate at synchronous speed, and therefore, provide a substantial synchronously rotating inertia. Any small deviations in system frequency cause a change in their rotational speed and associated exchange of energy with the system as required. This inertial response is provided instantaneously by SGs without any control system. In contrast, wind turbine generators cannot contribute to the system inertia as their electromagnetic torque is partly or fully decoupled from the power system frequency via power electronic converters. Therefore, in the event of large generator trip, wind turbines will not provide any additional energy instantaneously as SGs do [84]

With the rapid increase of wind power penetration, wind turbines are gradually displacing conventional generators, and thus there will be less spinning inertia. In this case, the entire power system will become more vulnerable to unexpected frequency changes such as sudden change in large loads or loss of generator. Therefore, to enhance the system security and stability, it is feasible that future requirements for wind power integration will require wind turbine generators to provide inertial response [85].

The lack of inertial response to system frequency changes can be overcome by equipping variable speed wind turbines with additional control loops. Several papers are published regarding wind turbines inertial response [86-88].

2.6.6 Power System Stabiliser

Power system stabiliser based on shaft speed is used successfully in traditional SGs to provide power damping during and after large disturbances. The function of PSS is to add a damping torque component to the generator rotor oscillation by controlling its excitation. With the increase of wind penetration, damping provided by conventional SGs may be inadequate, and thus, wind turbines contribution toward power system oscillations damping becomes essential. To deal with power oscillations issues, wind turbines requires not only fault ride-through capability but also power oscillations damping capability [19].

DFIG wind turbines are not synchronously connected to the grid. Hence, they do not directly participate in power system electromechanical oscillations [56]. However, wind power variation can reduce the damping of electromechanical oscillations [29]. Moreover, with the rapid increase of wind power penetration, DFIG wind turbines can affect the damping performance when replacing synchronous machines, which are equipped with a PSS [58]. Therefore, the damping contribution of installed wind turbines is significantly required, and this can be achieved by introducing an auxiliary PSS loop into the DFIG controller [29]. Several researchers have examined the capability of variable speed wind turbines to provide a damping effect for power system oscillations [30, 31, 60].

Since introducing a damping torque by variable speed wind turbines to damp power system oscillation is achievable, future requirements for wind power integration will require wind turbine generators to provide a damping effect to enhance the interconnected power systems security and stability.

2.7 Summary

This chapter has discussed the rapid growth of wind power generation as a result of environmental and economic issues that associated with fossil fuels. The global cumulative installed wind power capacity worldwide has exceeded 432 GW at the end of 2015 and would reach 712 GW by 2020. Wind power growth is led by China

since 2010 with more than 23 GW of new wind power installed in 2014 alone, which is the highest annual number for any country ever. In the past, fixed speed wind turbines were the most common type of installed wind turbines. However, currently, variable speed wind turbines such as doubly fed induction generator wind turbine and Type IV wind turbine are dominating the market. This is due to the advantages of variable speed wind turbines over fixed speed wind turbines as they can control active and reactive power independently over a broad range of wind speeds. As the penetration of wind power continues to increase, special requirements are set for wind power integration to avoid any potential negative impacts that wind power may have on the operation and stability of power systems, such as frequency and voltage tolerance, reactive power and voltage control capability, frequency regulation, fault ride-through capabilities, inertial response, and power system stabiliser.

Chapter 3

Power System Modelling

3.1 Introduction

This chapter provides a brief overview of the main power system components that have been modelled including DFIG systems, which have been used throughout the research to provide the simulation results presented later. Within this chapter, the mathematical representations of the main electrical power system components are presented including SGs, transmission lines, power transformers and systems loads. Following this, the modelling of DFIGs for power system stability analysis are presented, including wind turbine rotor aerodynamic model, mechanical model, induction generator model, power converter model, control system model and aggregated DFIG wind farm model.

3.2 Synchronous Generators

Synchronous machines are one of the oldest and most important components in power systems. They form the largest source of electricity generator in power systems. As maintaining SGs in synchronism is crucial to system stability, their characteristics and accurate modelling are very important to the study of power system stability. SGs can be modelled with varying levels of complexity depending on the nature of the study [89, 90]. In dynamic studies, the SGs are generally

represented using the sixth order degrees of complexity model. The sixth order model is preferred for representing the round rotor in stability studies, and it is employed in this research. Detailed model of synchronous machines can be found in [89] and [91]. The synchronous machine is described by the following six equations [91]:

$$\frac{d}{dt}E_d^{'} = \frac{1}{T_{qo}^{'}}\left[-E_d^{'} + (\mathrm{X}_q - \mathrm{X}_q^{'})\left\{I_q - \frac{\mathrm{X}_q^{'} - \mathrm{X}_q^{''}}{(\mathrm{X}_q^{'} - \mathrm{X}_{lk,s}^{'})^2}(\psi_{2q} + (\mathrm{X}_q^{'} - \mathrm{X}_{lk,s}^{'})I_q + E_d^{'}\right\}\right] \tag{3.1}$$

$$\frac{d}{dt}E_q^{'} = \frac{1}{T_{do}^{'}}\left[\begin{array}{l} -E_q^{'} + (\mathrm{X}_d - \mathrm{X}_d^{'})\left\{I_d - \frac{\mathrm{X}_d^{'} - \mathrm{X}_d^{''}}{(\mathrm{X}_d^{'} - \mathrm{X}_{lk,s}^{'})^2}(\psi_{2d} + (\mathrm{X}_d^{'} - \mathrm{X}_{lk,s}^{'})I_d + E_q^{'}\right\} \\ +E_{fd} \end{array}\right] \tag{3.2}$$

$$\frac{d}{dt}\psi_{1d} = \frac{1}{T_{do}^{''}}\left[-\psi_{1d} + E_q^{'} - (\mathrm{X}_d^{'} - \mathrm{X}_{lk,s}^{'})I_d\right] \tag{3.3}$$

$$\frac{d}{dt}\psi_{2q} = \frac{1}{T_{qo}^{''}}\left[-\psi_{2q} + E_d^{'} - (\mathrm{X}_q^{'} - \mathrm{X}_{lk,s}^{'})I_q\right] \tag{3.4}$$

$$\frac{d}{dt}\Delta\omega_r = \frac{1}{2H}\left[P_m - P_e - D\Delta\omega_r\right] \tag{3.5}$$

$$\frac{d}{dt}\delta = (\omega_r - \omega_s) = \Delta\omega_r \tag{3.6}$$

where $E_{d,q}^{'}$ Transient voltage in d-/q-axis

E_{fd} Field voltage

H Inertia constant

$I_{d,q}$ Current in d-/q-axis

$T_{do,qo}^{'}$ Transient time constant of d-/q-axis

$T_{do,qo}^{''}$ Subtransient time constant of d-/q-axis

P_m	Mechanical power
P_e	Electrical power
$X'_{d,q}$	Transient reactance in d- /q-axis
$X''_{d,q}$	Subtransient reactance in d-/q-axis
X_{ls}	Leakage reactance
δ	Rotor angle
ψ_{1d}	Flux linkage d-axis damper winding
ψ_{2q}	Flux linkage q-axis damper winding
ω_r	Rotor speed
ω_s	Synchronous rotor speed: 2πf

3.2.1 Generator Excitation Systems

The generator excitation system supplies the generator with DC field current to provide a satisfactory performance of the generator. By controlling the field current, the excitation system can maintain the machine terminal voltage E_t as the output varies and thus be able to contribute towards maintaining power system stability. This can be done by an automatic voltage regulator (AVR) which provides an automatic adjustment of the field current of the SG by regulating the field voltage E_{fd} in order to reach the generator stator terminal voltage reference set-point E_t^{ref} .In the case of a disturbance, the AVR has to act fast enough to enhance the transient stability of power system [89, 91].

SGs can be equipped with a PSS in order to reduce rotor speed variations following system disturbances. The common used input signal for PSS are generator rotor speed deviation [89]. Figure 3.1 shows the functional relationship between the SG, excitation system, and the power system stabiliser.

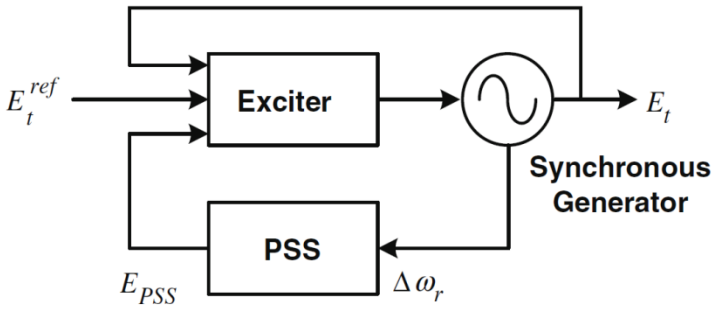

Figure 3.1 Block diagram of typical SG excitation system PSS.

Reference [92] provides comprehensive details for many excitation systems which can be found in practice. The excitation systems used within this thesis is IEEE Type 1 excitation system which is shown in Figure 3.2 [92]. This type of excitation systems represents a majority of excitation systems and is widely used in dynamic studies.

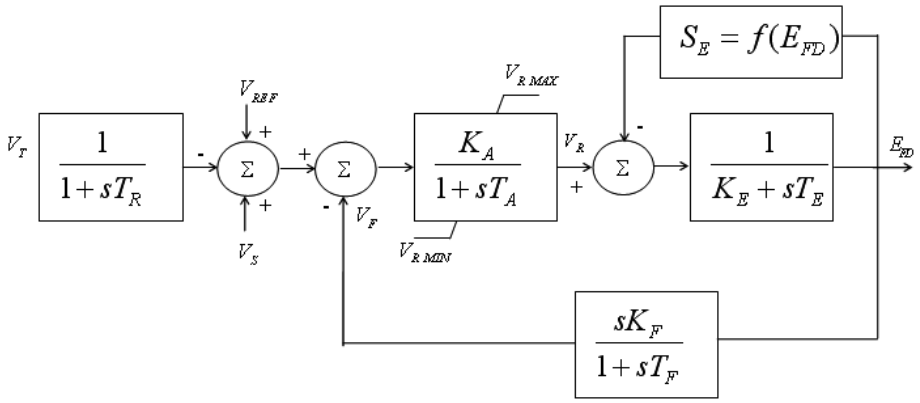

Figure 3.2 The basic schematic of IEEE Type 1 Excitation system.

The first block represents the voltage setting circuit where the T_R is the filter time constant (s). The second block represents the automatic voltage regulator with minimum/maximum voltage regulator outputs limits where K_A is the regulator gain (pu), and T_A is regulator time constant (s). The third block represents the self-exciter where K_E is exciter constant related to the self-excited field (p.u.), and T_E is the exciter time constant (s). The lowest derivative stabilising loop represents the

feedback loop where K_F (p.u.) and T_F (s) are the feedback gain and time constant respectively. The top feedback loop represents the exciter saturation function value S_E (p.u.) at the corresponding exciter voltage.

The dynamics of the exciter is represented by differential equations as follows [93]:

$$\frac{dE_{fd}}{dt} = \frac{1}{T_E}\left\{-(K_E + S_E(E_{fd})E_{fd}) + V_R\right\} \tag{3.7}$$

$$\frac{dR_f}{dt} = \frac{1}{T_f}(-R_f + \frac{K_F}{T_F}E_{fd}) \tag{3.8}$$

$$\frac{dV_R}{dt} = \frac{1}{T_A}\left\{-V_R + K_A R_F - \frac{K_A K_F}{T_F}E_{fd} + K_A(V_{ref\_}V_{t)}\right\} \tag{3.9}$$

3.2.2 Power System Stabilisers

Power system stabilisers are used to damp power system oscillations. The output signal of a PSS is sent to the excitation system in order to add damping to generator rotor oscillations and improve power system dynamic performance.

An example of a PSS is shown in Figure 3.3 where U_{in} is the input signal (the rotor speed deviation signal is used in this research for SG PSS), and U_{pss} is the output signal of PSS. The amount of damping is determined by the PSS gain K_{pss}. Washout block is a high pass filter that allows a selected input frequency range and expected to act only during the transient period. The dynamic phase compensator can provide a lead or lag phase compensation to ensure the introduced electrical damping torque component is in phase with the rotor speed variation. The limiter is used to prevent the output signal from exceeding control limits.

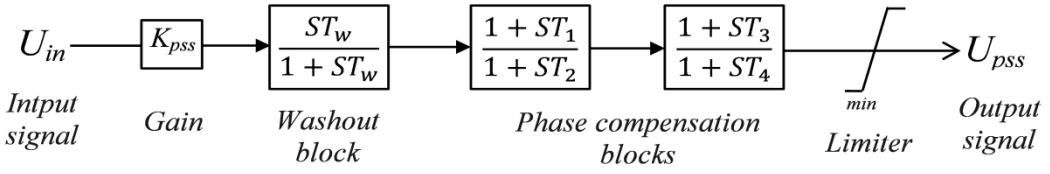

Figure 3.3 Block diagram of a PSS

3.3 AC Transmission Lines

Generated electrical power is transmitted to consumers through overhead transmission lines and cables. All transmission lines in a power system can be characterised by four parameters which are series resistance and inductance due to the conductor resistivity and surrounding magnetic field respectively, shunt conductance due to the leakage current between the phase and the ground, and shunt capacitance due to the electrical field between conductors. In transmission lines, the effect of shunt conductance is very small and usually neglected. Transmission lines are usually modelled using the well-known π equivalent circuit as shown in Figure 3.1 [89]. This model was used for modelling AC transmission lines in this research.

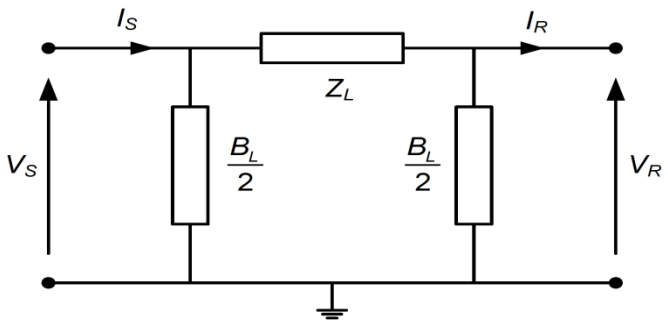

Figure 3.4 Equivalent π circuit of a transmission line

3.4 Transformers

Transformers are used because of their capability to either step up or step down the voltage across the power system. In addition, tap changers are often used to

control the voltage by changing the transformer turns ratio. In this thesis, two winding transformers are used to step up or step down the voltage between SGs and consumption level respectively, whereas three winding transformers are used for DFIG based wind turbines for three different voltage levels with different ratings. For power flow and stability studies, the representation of the transformer as a π model is shown in Figure 3.5 and is widely used. The π equivalent circuit with parameters expressed in terms of transformer off-nominal turns ratio n^* where $C = 1/n^*$ and transformer equivalent leakage reactance Z_e where ($y_e = 1/Z_e$). The detailed description of π model for two and three winding transformers is well documented in [89].

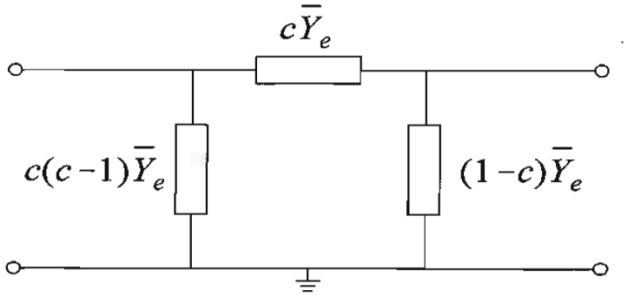

Figure 3.5 Two winding transformer π model [89]

3.5 Loads

Load plays an important role in power system stability as the stability of power system relies on the continuous balance between the generated and consumed power. As the typical power system has a large number of diverse load components, the way in which power system loads are modelled can have a significant effect on the power system stability results [94]. For power system stability studies, the variations of loads active and reactive power with changes in voltage magnitude and frequency have to be modelled [95]. In this thesis, the load model is represented using the active and reactive load components at each bus by a combination of constant impedance (Z), constant current (I), and constant power (P) components, as shown in the following formula [96, 97]:

$$P = P_0\left[P_1\left(\frac{V}{V_0}\right)^2 + P_2\left(\frac{V}{V_0}\right) + P_3\right] \tag{3.10}$$

$$Q = Q_0\left[Q_1\left(\frac{V}{V_0}\right)^2 + Q_2\left(\frac{V}{V_0}\right) + Q_3\right] \tag{3.11}$$

Where P_0, Q_0 are the initial values of active and reactive power at an initial value of voltage V_0, coefficients P_1 to P_3 and Q_1 to Q_3 are the fraction of the constant power, constant current and constant impedance components in the active and reactive power loads respectively.

3.6 Modelling of DFIG

Induction machines can work as generators when they are converting mechanical input power to electrical output power at speeds greater than their synchronous speeds. DFIGs operate on the same principles as conventional induction machines but with the support of additional external power electronic circuits to improve the wind turbine operation. The basic structure of a DFIG based wind turbine is shown in Figure 2.10.

The DFIG based wind turbine consists of a wound rotor induction generator and back to back converter connecting rotor slip rings to the grid. The wind turbine is connected to the induction generator through a mechanical shaft system. A gearbox is linking high and low-speed shafts in the shaft system. The induction generator stator is directly connected to the grid whereas the rotor is fed through back to back (AC-DC-AC) voltage source converter. The crowbar is used, during grid faults, to protect the RSC from over current in the rotor circuit.

The operation of the DFIG wind turbine is regulated by a control system, which consists of electrical control and mechanical controls. The electrical control of DFIG is achieved by controlling RSC and GSC within the back to back converter of DFIG based wind turbine. The power flow between the rotor circuit and the grid is

controlled both in magnitude and in the direction in order to generate electrical power over a wide speed range. The mechanical control is achieved by controlling the pitch angle of the wind turbine blades.

3.6.1 Aerodynamic Model

Wind turbine power production depends on the interaction between the rotor and the wind. A simple model, which was developed by Betz (1926), can be used to determine the power from an ideal turbine rotor [98]. Pressure and speed variation in an ideal model of a wind turbine is shown in Figure 3.6 [99]. *S* is the area swept by the turbine blade with the air cross-section upwind from the rotor designated as S_1, and downwind as S_2. The speed of the wind *V* passing through the turbine rotor is considered uniform with V_1 as upwind speed, and V_2 as downwind speed at a distance from the rotor. Extraction of mechanical energy by the rotor occurs by reducing the kinetic energy of the air stream from upwind to downwind, or simply applying a braking action on the wind [99].

The power as the rate of change in kinetic energy from upstream to downstream is given by [99]:

$$P_{\mathrm{w}} = \frac{\Delta E}{\Delta t} = \frac{1}{2}\,\rho\,\mathrm{S}(V_1^{\,2} - V_2^{\,2}) \tag{3.12}$$

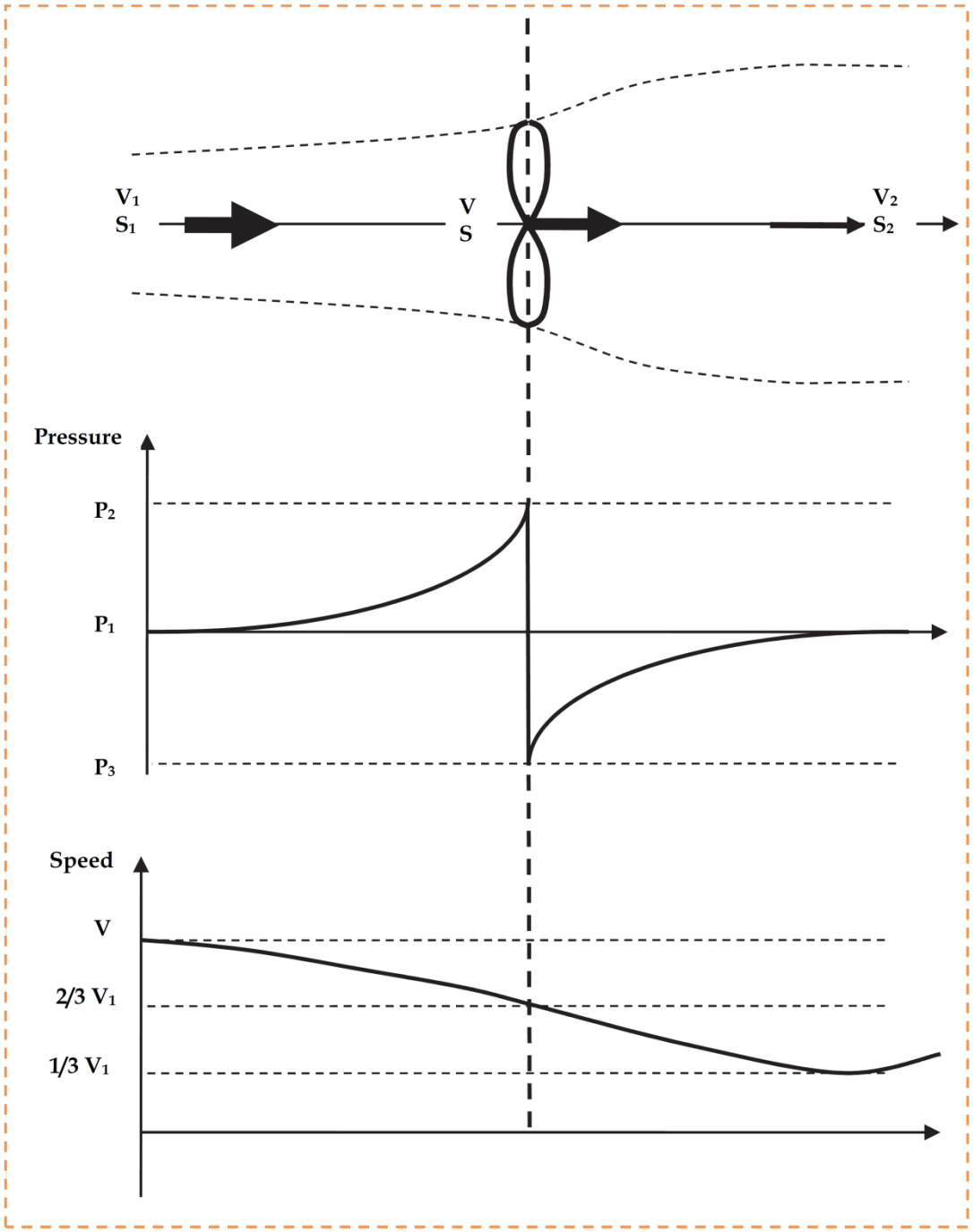

Figure 3.6 Pressure and speed variation in an ideal model of a wind turbine [99].

Wind kinetic energy is converted to mechanical energy by the wind turbine to drive an electrical generator through the turbine shaft system. Mechanical power of a wind turbine is the power of an air mass that flows vertically in area *A* at a speed *V* and is given by the expression:

$$P_w = \frac{1}{2} \rho A V^3 \quad (3.13)$$

Where P_w is the extracted power from the wind turbine (w), ρ is the air density (kg/m^3), $A = \pi R^2$ is the area swept by the rotor blades (m^2), R is the wind turbine rotor radius (m), and V is the average wind speed passing through the A surface (m/s).

The extracted energy from the wind can be modelled by the aerodynamic model which is based on the coefficient of power. The wind energy cannot be completely extracted by the wind turbine as the air mass would be stopped completely in the intercepting rotor area. The theoretical maximum mechanical power that can be extracted from the wind kinetic energy is limited (Betz's limit) to 59.3% [68]. Hence, even if power extraction without any losses were possible, only 59% of the wind power could be utilized by a wind turbine. Mechanical power that a rotor extracts from the wind is given by [68]:

$$P_m = P_w \; C_p(\lambda, \beta) = \frac{1}{2} \rho A \, v^3 C_p(\lambda, \beta) \quad (3.14)$$

Mechanical torque on aerodynamic rotor shaft can be determined using turbine rotational speed ω_t

$$T_m = \frac{P_m}{\omega_t} \quad (3.15)$$

The performance coefficient C_p depends on pitch angle β and tip speed ratio λ which is defined as the ratio of rotor tip speed to free wind speed and can be calculated from the following expression [78].

$$\lambda = \frac{\omega_t R}{v} \quad (3.16)$$

Where, ω_t is the mechanical speed of the turbine, R is the rotor radius, and v is the incoming wind speed.

The power coefficient C_p is a function of the tip speed ratio λ and the pitch angle β.The relation between C_p, tip speed ratio λ and blade pitch angle β is shown in Figure 3.7 [100].

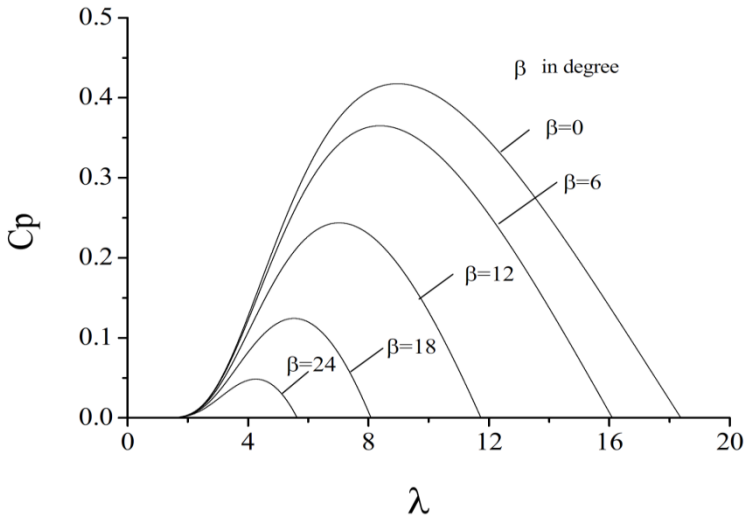

Figure 3.7 Power coefficient C_p as a function of tip speed ratio λ [100]

The following equation can be used to approximate the power coefficient curve [100], [101].

$$C_p = \frac{1}{2}(\lambda - 0.022\beta^2 - 5.6)e^{-0.17\lambda} \tag{3.17}$$

Figure 3.8 shows the aerodynamic model of DFIG wind turbine used in this research.

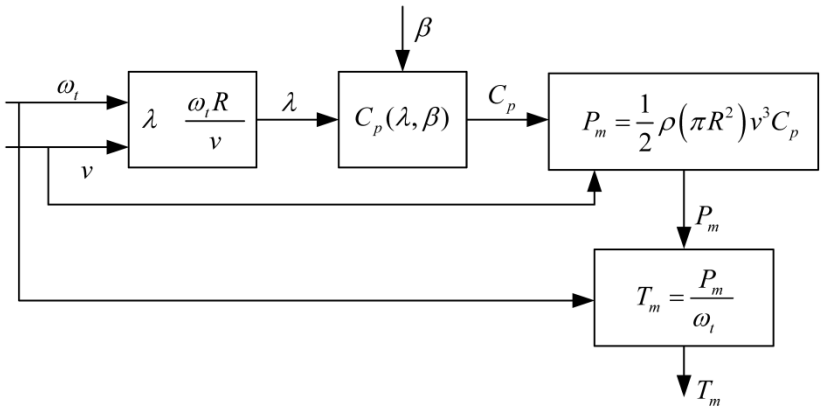

Figure 3.8 General structure of DFIG wind turbine aerodynamic model

3.6.2 Drive Train Model

The drive train model, which is also known as the shaft model, contains turbine rotor, gearbox, low and high-speed shafts, and the induction generator rotor. The wind turbine rotor (aerodynamic model) is connected to the generator through a gearbox to increase the speed of the shaft rotation. The drive train can be represented either by a six-mass drive train model, two-mass model or by a single lumped-mass model [101-103]. The lumped-mass model is too simple, as the dynamics of a wind turbine and wind generator are lumped together and work as a single rotating mass. Stability analysis based on the one-mass shaft model may give significant errors as the shaft flexibility is neglected. For large wind turbines, the shaft flexibility is noticeable and therefore cannot be neglected [101, 104]. The six-mass model system has six inertias, which are the three blades' inertias, hub inertia, gearbox inertia and generator inertia. The six-mass drive train model is very complicated leading to a significant increase in simulations time due to complex and lengthy mathematical computation with small time-steps [101]. A comparison between the three types of drive train models for stability studies has been conducted in [100]. The study shows that unequal blade torque sharing has no effect on the transient stability of wind turbines. Therefore, the two-mass reduced order drive train models can be used, where it is assumed that the turbine torque is equal to the sum of the torques acting on the three blades. The effect of inertia constant, spring and damping constants on two-mass and six-mass models have been compared in [100]. The study shows that

two-mass model has almost the same transient characteristics of the six-mass model for transient stability analysis.

As the two-mass model can provide satisfactory results, it is implemented in this thesis. In this model, two masses, which are the large turbine mass (lumped inertia of the turbine, part of the gearbox and the low speed shaft) and the generator mass (generator rotor mass, high speed shaft along with its disc brake and the rest of the gearbox), are connected together by a shaft with certain damping and stiffness coefficient values [105]. The two-mass model of DFIG based wind turbine is shown in Figure 3.9 [106].

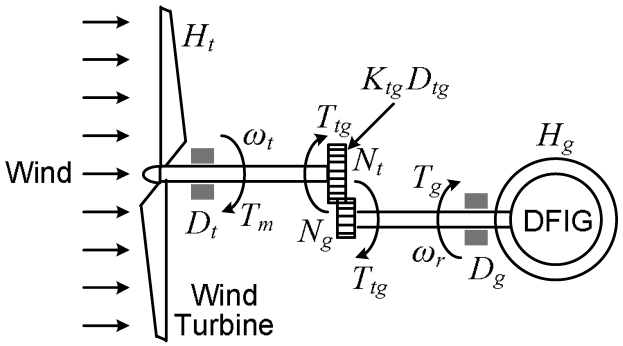

Figure 3.9 Two-mass model of DFIG wind turbine model drive train [106]

The electromechanical dynamic equations are then given by

$$2H_t \frac{d}{dt}\omega_t = T_m - D_t\omega_t - D_{tg}(\omega_t - \omega_r) - T_{tg} \tag{3.18}$$

$$2H_g \frac{d}{dt}\omega_r = T_{tg} - D_{tg}(\omega_t - \omega_r) - D_g\omega_r - T_e \tag{3.19}$$

$$\frac{d}{dt}T_{tg} = K_{tg}(\omega_t - \omega_r) \tag{3.20}$$

In which

H_t = the inertia constants of the turbine (s)

H_g = the inertia constants of the generator (s)

ω_t = the turbine rotor speed (rad/s)

ω_r = the generator rotor speed (rad/s)

T_m = mechanical torque applied to the turbine (p.u.)

T_e = electrical torque of the generator (p.u.)

T_{tg} = internal torque of the model (p.u.)

D_t = the damping coefficients of the turbine (p.u. torgue/(rad/s))

D_g = the damping coefficients of the generator (p.u. torgue/(rad/s))

D_{tg} =the damping coefficient of the shaft between the two masses (p.u .torgue/(rad/s))

K_{tg} = the shaft stiffness (p.u. torgue/(rad/s))

3.6.3 Generator Model

The generator that used in this study is a wound rotor induction machine. The doubly fed induction generator mathematical equations are the same as those of the induction generator. The main difference is that the rotor voltage is not zero because the rotor windings are not shorted. The induction generator stator and rotor equations can be written as follows [107]:

$$v_{sabc} = R_s i_{sabc} + \frac{d\psi_{sabc}}{dt} \tag{3.21}$$

$$v_{rabc} = R_r i_{rabc} + \frac{d\psi_{rabc}}{dt} \tag{3.22}$$

where v_{sabc}, v_{rabc} are respectively the stator and rotor voltages, R_s, R_r are stator and rotor resistances respectively, i_{sabc}, i_{rabc} are respectively the stator and rotor currents, ψ_{sabc}, ψ_{rabc} are respectively the stator and rotor flux linkage.

Applying synchronous reference frame transformation rotating by angular speed ω_s to the above equations, the differential equations of the DFIG induction machine in *d*-*q* are [106-108]:

$$v_{ds} = R_s i_{ds} - \omega_s \psi_{qs} + \frac{d\psi_{ds}}{dt} \tag{3.23}$$

$$v_{qs} = R_s i_{qs} + \omega_s \psi_{ds} + \frac{d\psi_{qs}}{dt} \tag{3.24}$$

$$v_{dr} = R_r i_{dr} - (\omega_s - \omega_r)\psi_{qr} + \frac{d\psi_{dr}}{dt} \tag{3.25}$$

$$v_{qr} = R_r i_{qr} + (\omega_s - \omega_r)\psi_{dr} + \frac{d\psi_{qr}}{dt} \tag{3.26}$$

where $v_{qs}, i_{qs}, \psi_{qs}$ are respectively the stator voltage, current and flux linkage in the *q*-axis, and $v_{qr}, i_{qr}, \psi_{qr}$ are respectively the rotor voltage, current and flux linkage in the *q*-axis. $v_{ds}, _s\, i_{ds}, \psi_{ds}$ are respectively the stator voltage, current and flux linkage in the *d*-axis, and likewise $v_{dr}, i_{dr}, \psi_{dr}$ are respectively the rotor voltage, current and flux linkage in the *d*-axis. ω_s and ω_r are rotational speed of the synchronous reference frame and the rotor speed.

Flux linkage equations in *d*-*q* axis:

$$\psi_{ds} = L_{ls} i_{ds} + L_m (i_{ds} + i_{dr}) = L_s i_{ds} + L_m i_{dr} \tag{3.27}$$

$$\psi_{qs} = L_{ls} i_{ds} + L_m (i_{qs} + i_{qr}) = L_s i_{qs} + L_m i_{qr} \tag{3.28}$$

$$\psi_{dr} = L_{lr} i_{dr} + L_m (i_{ds} + i_{dr}) = L_r i_{dr} + L_m i_{ds} \tag{3.29}$$

$$\psi_{qr} = L_{lr} i_{dr} + L_m (i_{qs} + i_{qr}) = L_r i_{qr} + L_m i_{qs} \tag{3.30}$$

where the stator L_s and rotor L_r inductance are respectively defined by:

$$L_s = L_{ls} + L_m, \quad and \quad L_r = L_{lr} + L_m \tag{3.31}$$

In which L_m is the mutual inductance and L_{ls}, L_{lr} are the stator and rotor leakage inductance respectively.

The equivalent circuit of the DFIG model is shown in Figure 3.10

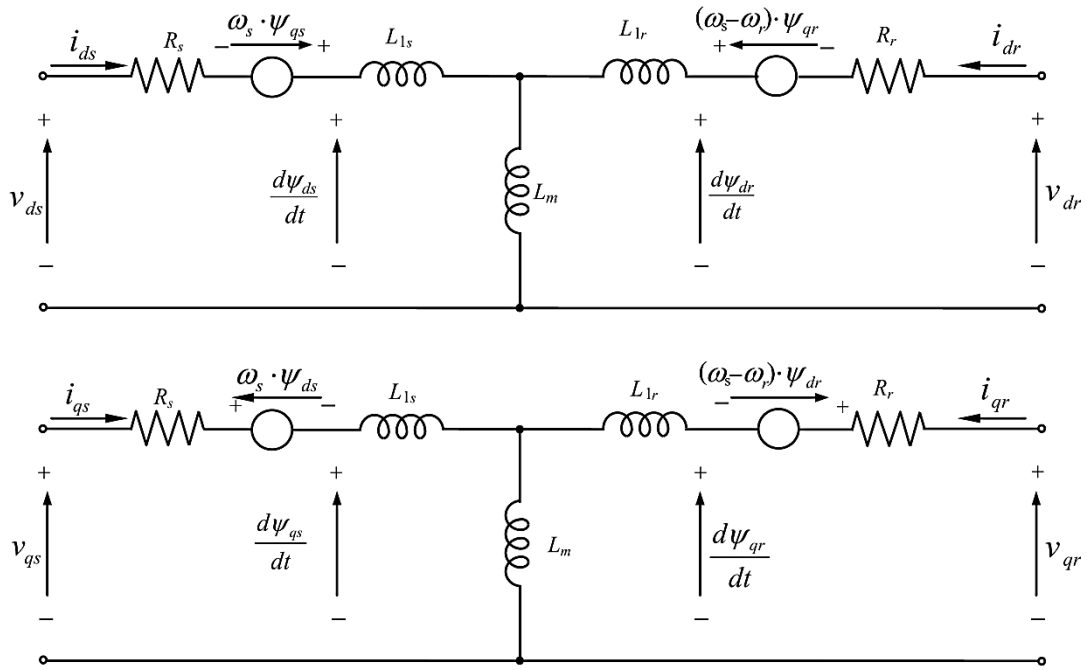

Figure 3.10 Equivalent circuit of DFIG

The difference between mechanical and electrical torque results in a change of generator speed that can be calculated using the generator equation of motion:

$$\frac{d\omega}{dt} = \frac{1}{2H}(T_m - T_e) \tag{3.32}$$

$$T_e = \psi_{ds} i_{qs} - \psi_{qs} i_{ds} = \psi_{qr} i_{dr} - \psi_{dr} i_{qr} = L_m (i_{qs} i_{dr} - i_{ds} i_{qr}) \tag{3.33}$$

where ω is the rotational angular speed of the shaft, H is the inertia constant (s), T_m is the mechanical torque, and T_e is the electromagnetic torque developed by the induction generator.

The equations of active and reactive power are:

$$P_s = \frac{3}{2}(\upsilon_{ds} i_{ds} + \upsilon_{qs} i_{qs}) \tag{3.34}$$

$$Q_s = \frac{3}{2}(\upsilon_{qs} i_{ds} - \upsilon_{ds} i_{qs}) \tag{3.35}$$

$$P_r = \frac{3}{2}(\upsilon_{dr} i_{dr} + \upsilon_{qr} i_{qr}) \tag{3.36}$$

$$Q_r = \frac{3}{2}(\upsilon_{qr} i_{dr} - \upsilon_{dr} i_{qr}) \tag{3.37}$$

The total active and reactive powers exchanged by the DFIG with the electrical network are the sum of the stator and rotor powers:

$$P_{total} = P_s + P_r = \frac{3}{2}(\upsilon_{ds} i_{ds} + \upsilon_{qs} i_{qs} + \upsilon_{dr} i_{dr} + \upsilon_{qr} i_{qr}) \tag{3.38}$$

$$Q_{total} = Q_s + Q_r = \frac{3}{2}(\upsilon_{qs} i_{ds} - \upsilon_{ds} i_{qs} + \upsilon_{qr} i_{dr} - \upsilon_{dr} i_{qr}) \tag{3.39}$$

In the previous equations, the converter efficiency has to be taken into account for the active power supplied by the DFIG into an electrical network. The total reactive power Q_{total} is not necessarily to be the exact amount fed into the grid because converters can generate or consume reactive power which thus affects the total amount of reactive power fed into the grid.

More details about the modelling of induction machines can be found in [89, 109, 110].

3.6.4 Power Converters Model

Power converters play a significant role in DFIG wind turbines as they allow the DFIG to operate at variable speeds. Since the converter can supply the rotor circuit with variable frequency current to compensate the difference between the mechanical and electrical frequency, the DFIG has the ability to operate over a broad range of variable speeds. The performance of DFIG wind turbine during both normal operation and fault conditions is governed by the power converter and its controllers. The back-to-back power converter has two voltage source converters, which are known as RSC and GSC. The rotor side and grid side converters are separated by a DC link so that they can be controlled independently of each other as shown in Figure 2.10. The power converter of DFIG wind turbines is rated about 30% of turbine‘s rated power. Therefore, in comparison with the Type IV wind turbines the DFIG converters are smaller in size, cost less and lead to lower losses. In power system stability studies, the switching dynamics of the converter is usually neglected when modelling power converters [111].

3.6.5 Rotor Side Converter

The RSC can be modelled as a current controlled voltage source converter. The most common method to control the rotor current is by utilising PWM modulation [51, 112]. The control of DFIG stator active power P_s and reactive power Q_s is achieved by controlling the rotor current i_{rabc} in the stator flux oriented reference frame [76]. The rotor current i_{rabc} are transferred to *d-q* current component i_{dr} and i_{qr} in the stator flux oriented reference frame.

In the stator flux oriented reference frame, the ψ_s (stator flux linkage) is aligned to the *d*-axis. Therefore, the stator flux linkage in *d-q* will be ($\psi_s = \psi_{ds}$) and ($\psi_{qs} = 0$) [106].

Equation (3.28) can be rewritten as:

$$i_{qs} = -\frac{L_m}{L_s} i_{qr} \tag{3.40}$$

From equations(3.23), (3.24) and (3.27)

$$i_{ds} = \frac{L_m}{L_s}\left(\frac{v_{qs} - R_s i_{qs}}{\omega_s L_m} - i_{dr}\right) = \frac{L_m}{L_s}(i_{ms} - i_{dr}) \tag{3.41}$$

where

$$i_{ms} = \frac{v_{qs} - R_s i_{qs}}{\omega_s L_m} \tag{3.42}$$

In this case, equations (3.34) and (3.35) can be rewritten as:

$$P_s = -\frac{3}{2}\left(\omega_s \frac{L_m^2}{L_s} i_{ms} i_{qr}\right) \tag{3.43}$$

$$Q_s = \frac{3}{2}\left(\omega_s \frac{L_m^2}{L_s} i_{ms}(i_{ms} - i_{dr})\right) \tag{3.44}$$

By substituting equations (3.29), (3.30), (3.40) and (3.41) into (3.25) and (3.26)

$$v_{dr} = R_r i_{dr} + \sigma L_r \frac{d}{dt} i_{dr} - (\omega_s - \omega_r)\sigma L_r i_{qr} \tag{3.45}$$

$$v_{qr} = R_r i_{qr} + \sigma L_r \frac{d}{dt} i_{qr} + (\omega_s - \omega_r)\left[\sigma L_r i_{dr} + \frac{L_m^2}{L_s} i_{ms}\right] \tag{3.46}$$

In which $$\sigma = 1 - \frac{L_m^2}{L_s L_r} \tag{3.47}$$

Equations (3.43) and (3.44) show that DFIG stator active and reactive power (P_s and Q_s) can be controlled independently by the *d-q* axes rotor current i_{qr} and i_{dr} respectively. The reference values of rotor current i_{qr} and i_{dr} can be determined directly from P_s and Q_s by the outer power control loops.

By rewriting the equations (3.45) and (3.46)

$$\upsilon_{dr} = \upsilon_{dr1} - \upsilon_{dr2} \tag{3.48}$$

$$\upsilon_{qr} = \upsilon_{qr1} + \upsilon_{qr2} \tag{3.49}$$

where

$$\upsilon_{dr1} = R_r i_{dr} + \sigma L_r \frac{d}{dt} i_{dr} \tag{3.50}$$

$$\upsilon_{qr1} = R_r i_{qr} + \sigma L_r \frac{d}{dt} i_{qr} \tag{3.51}$$

$$\upsilon_{dr2} = (\omega_s - \omega_r)\sigma L_r i_{qr} \tag{3.52}$$

$$\upsilon_{qr2} = (\omega_s - \omega_r)[\sigma L_r i_{dr} + \frac{L_m^2}{L_s} i_{ms}] \tag{3.53}$$

The rotor current i_{dr} and i_{qr} of equations (3.50) and (3.51) in term of υ_{dr1} and υ_{qr1} can be written as:

$$\frac{d}{dt} i_{dr} = -\frac{R_r i_{dr}}{\sigma L_r} + \frac{1}{\sigma L_r} \upsilon_{dr1} \tag{3.54}$$

$$\frac{d}{dt}i_{qr} = -\frac{R_r i_{dr}}{\sigma L_r} + \frac{1}{\sigma L_r} v_{qr1} \tag{3.55}$$

Equations (3.54) and (3.55) indicate that i_{dr} and i_{qr} respond respectively to v_{dr1} and v_{qr1} respectively. Therefore, a proportional-integral (PI) controller can be designed as follows:

$$v_{dr1} = (k_{pr} + \frac{k_{ir}}{s})(i_{dr}^{*} - i_{dr}) \tag{3.56}$$

$$v_{qr1} = (k_{pr} + \frac{k_{ir}}{s})(i_{qr}^{*} - i_{qr}) \tag{3.57}$$

Substituting equations (3.56) and (3.57) into (3.48) and (3.49)

$$v_{dr} = (k_{pr} + \frac{k_{ir}}{s})(i_{dr}^{*} - i_{dr}) - s\omega_s(\sigma L_r i_{qr}) \tag{3.58}$$

$$v_{qr} = (k_{pr} + \frac{k_{ir}}{s})(i_{qr}^{*} - i_{qr}) + s\omega_s(\sigma L_r i_{dr} + \frac{L_m^2}{L_s} i_{ms}) \tag{3.59}$$

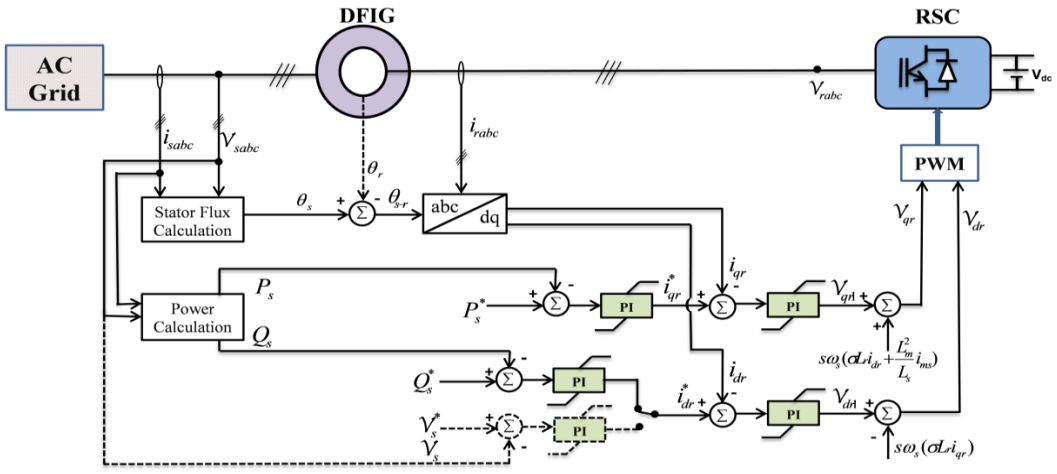

Figure 3.11 Overall vector control scheme of the DFIG-RSC, voltage control strategy (dashed black lines).

Figure 3.11 shows the overall vector control scheme of the DFIG-RSC. The reference signals i^*_{dr} and i^*_{qr} in the outer control loops are generated by controlling the stator reactive and active power respectively. Then, the error signals are generated by deducting the current signals i_{dr} and i_{qr} from reference signals i^*_{dr} and i^*_{qr} respectively. The generated error signals are formed into two voltage signals v_{dr1} and v_{qr1} by the inner control loops using two PI controllers. Finally, the output of the inner current loops (v_{dr1} and v_{qr1}) are compensated by the corresponding cross-coupling terms (v_{dr2} and v_{qr2}) to form the *d–q* voltage signals (v_{dr} and v_{qr}) respectively. These signals are then connected to pulse width modulation (PWM) to create signals for the IGBT gate control [76, 106].

3.6.6 Grid Side Converter

The GSC can also be modelled as a current controlled voltage source converter. The main objective of GSC is to control the voltage of DC link to maintain it within a certain limit. However, it also regulates the reactive power that GSC exchanges with the grid to support the grid during a fault [111].

Following the same procedure as in RSC, the *d-q* equations of GSC can be obtained by the following feedback loops and PI controller:

$$v_{dg} = (k_{pg} + \frac{k_{ig}}{s})(i^*_{dg} - i_{dg}) - \omega_s L_g i_{qg} + v_s \tag{3.60}$$

$$v_{qg} = (k_{pg} + \frac{k_{ig}}{s})(i^*_{qg} - i_{qg}) + \omega_s L_g i_{qg} \tag{3.61}$$

In which i^*_{dg} and i^*_{qg} are the outer control loops reference signals in *d-q* axes, i_{dg} and i_{qg} are measured current signals *in d-q* axes and $(k_{pg} + \frac{k_{ig}}{s})$ is the PI controller.

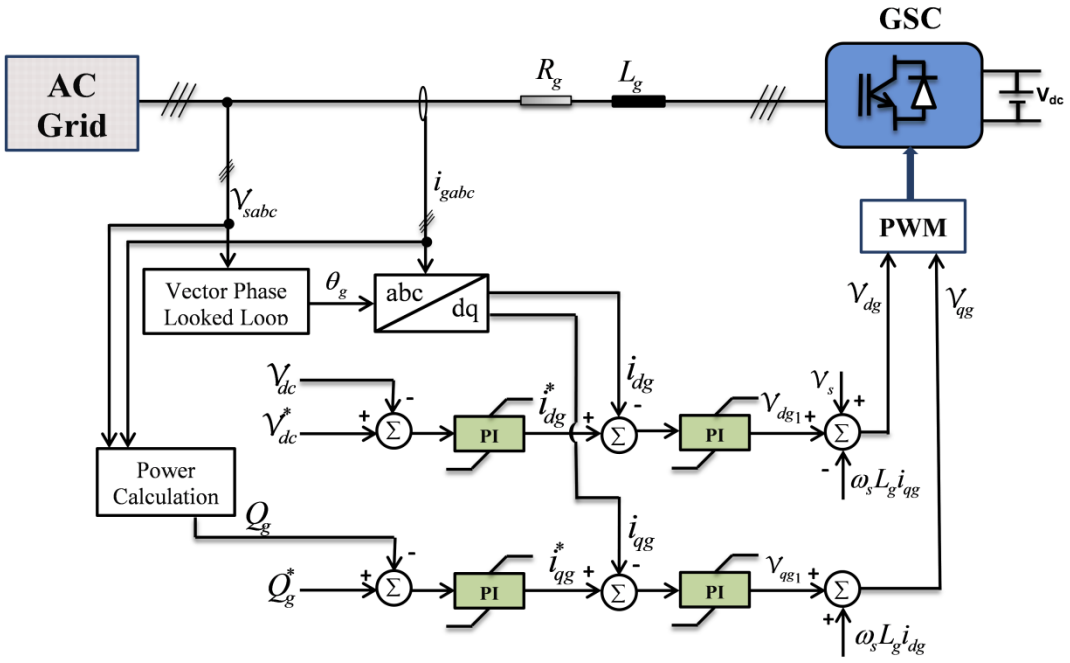

Figure 3.12 Overall vector control scheme of the DFIG-GSC.

The overall vector control scheme of the GSC is shown in Figure 3.12, in which the stator current i_{gabc} in the synchronously rotating reference frame is used to control the DC voltage (v_{dc}) and the reactive power Q_g that can be exchanged between the grid and the GSC. The grid current i_{gabc} are transferred to *d-q* current component i_{dg} and i_{qg} by applying the synchronously rotating reference frame. In a similar way to the RSC, the GSC has two control loops which are outer control and inner control loops [76, 113]. The outer control loops of DFIG-GSC regulates the voltage of the dc link and the reactive power that exchanged between the grid and the GSC to generate reference signals i^*_{dg} and i^*_{qg} of the *dq* axes current components respectively. These signals are compared to measured current signals i_{dg} and i_{qg} in the *dq*-axes to form two voltage signals by the inner control loops. These voltage signals are compensated by the corresponding cross-coupling voltage in *dq* axes to form the *dq* voltage signals v_{dg} and v_{qg} respectively. These signals are then connected to pulse width modulation (PWM) to create signals for the IGBT gate control to drive the GSC.

3.6.7 Protection System Model

Modern DFIG wind turbines are also equipped with a protection device called crowbar circuit. Due to the direct connection between the DFIG stator windings and the grid, any fault electrically close to the wind turbine can cause the stator current to rise. Consequently, this disturbance is transmitted to the rotor circuit resulting in high rotor currents and voltages due to electromagnetic coupling between the stator and the rotor circuits. Since the capacity of the RSC is relatively small when compared to the rated capacity of the generator unit, in this situation, semiconductor switches inside power electronic converters could be damaged. Therefore, the power converter should be protected from the rotor over currents to prevent potential damage. The action performed by the crowbar circuit is to protect the RSC from over current and also to protect the DC link from overvoltage in the case of a grid fault [108]. During the active crowbar time, the rotor is short-circuited and hence the DFIG operates as an induction generator with no control over active and reactive power [50].

The crowbar system consists of an external resistance connected to the rotor windings in the case of grid fault to limit rotor current as shown in Figure 3.13. The value of the resistance used in the crowbar is usually ranged between 1 to 10 times the rotor resistance [114]. A low crowbar resistance can lead to a higher electrical torque, over currents and hence low rotor voltages. However, high values for the crowbar resistor will result in a lower electrical torque and rotor currents but higher rotor voltages [115].

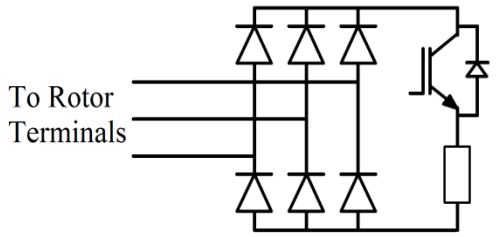

Figure 3.13 Schematic diagram of the crowbar circuit

In this work, a crowbar circuit was implemented in the DFIG model to protect the converter. The converter is deactivated, and the rotor windings of the DFIG are

short-circuited upon the detection of rotor current magnitude above the current protection limit. Since the current rating of an IGBT is typically 100% higher than the continuous current rating, the instantaneous rotor current should be limited below 2 p.u., while the converter dc-link voltage is also maintained below the device's voltage rating [116]. Therefore, the DFIG rotor current is set to 1.8 p.u. in this thesis.

3.6.8 Pitch Angle Controller

The mechanical system of DFIG wind turbine is controlled by blade pitching. The pitch angle controller is used to reduce the mechanical power extracted from the wind and prevents the turbine from overspeeding. Therefore, turbine blade pitch control is only activated at high wind speeds or during a grid fault to limit the acceleration of the turbine. Figure 3.14 shows the wind turbine blade pitch control, where ω_r is the rotating speed of the DFIG [117]. The reference pitch angle is provided by the speed controller for comparison with the actual pitch angle to generate an error signal. The generated signal is passed through a delay time constant and limitation for both the pitch angle (0 to 30 degrees) and its rate of change. Since the pitch actuation system cannot respond instantly, a rate limiter is added (±10 degrees /second) to obtain a realistic response. The pitch angle rate of change limitation decides how fast the aerodynamic power can be changed [118].

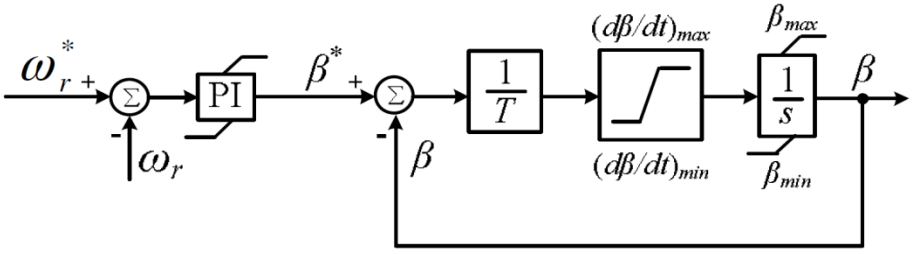

Figure 3.14 Pitch angle controller.

If the wind turbine is required to generate its maximum power during low-speed wind, the ω_r is set at its reference values. Therefore, the blade pitch control is deactivated in this situation. However, if the wind turbine is required to generate a constant amount of power less than its maximum power rating (an active power

curtailment is demanded due to external requests from grid operator or wind plant control), the pitch control loop need to be activated [106]. More about the design of the pitch angle controller, which is well documented in the literature, can be found in [106, 117, 118].

3.6.9 Operating Range of DFIG

In general, wind turbines can only operate within a certain range of wind speed between two thresholds which are known as the cut-in and cut-out. The wind turbine will be halted if the rotor is below cut-in speed or above the cut-out speed. The imposed minimum speed limit is to prevent the wind turbine from spinning at speeds matching the resonant frequency of the tower and to avoid RSC voltage saturation caused by sliding of rotor voltage. The imposed maximum speed limit is to ensure the safety of the turbine components during high wind speeds. In modern wind turbines, the cut-in wind speed is about 4 m/s, and the cut-out wind speed is about 25 m/s [119].

Figure 3.15 shows the DFIG wind turbine characteristics and the maximum power tracking curve for various wind speeds. Within the restricted speed limit, there is a particular rotor speed at which the maximum power occurs at any given wind speed. Therefore, the speed of generator rotor is controlled to extract the maximum possible power from the wind. To achieve this, the active power is set to follow the curve of maximum power tracking characteristics. This can be done by measuring the value of rotor speed and then the corresponding active power set point is chosen from rotor speed generator power characteristic. Both the measured rotor speed and the corresponding active power set point are used to derive the torque set point. The required torque is reached by calculating the current reference signal as there is a direct relation between electric torque and rotor current. The current reference signal is controlled by the RSC [82, 107]. The curve of optimal power P_{opt} extracted from the wind is defined by the following relationship [51].

$$P_{opt} = k_{opt}\omega^3 \tag{3.62}$$

where k_{opt} is a parameter obtained from the aerodynamic performance of the wind turbine.

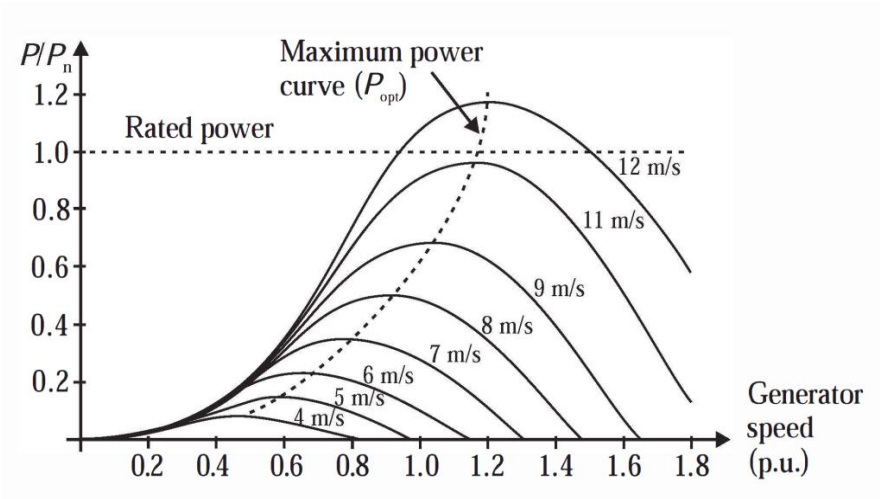

Figure 3.15 DFIG wind turbine maximum power tracking curve [82].

The DFIG wind turbine maximum power tracking curve can be further divided into several regions depending on the control strategy used and is shown in Figure 3.16. The optimal mechanical power that can be extracted for various wind speeds is shown in Figure 3.16a while the optimal extracted active power in term of the generator rotor speed for different wind speeds is shown in Figure 3.16b [82].

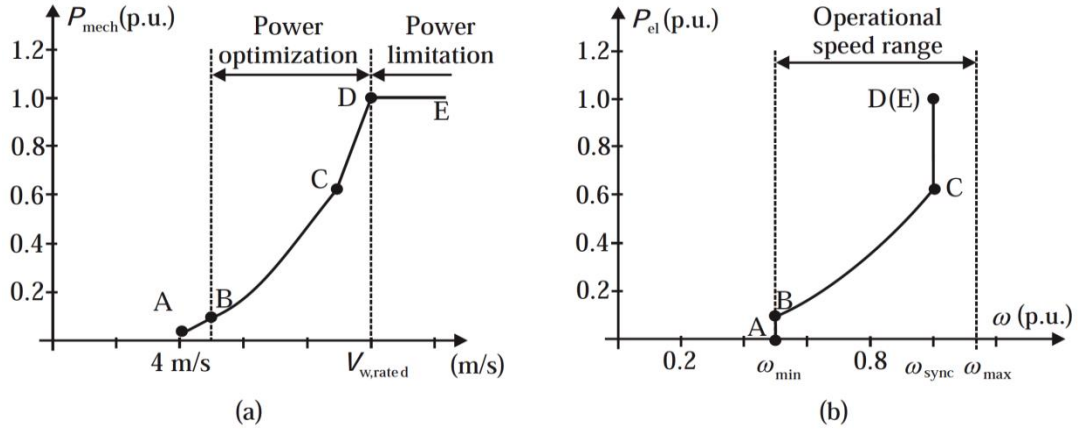

Figure 3.16 DFIG wind turbine maximum power tracking curve, (a) mechanical power that can be extracted versus wind speed, (b) active power versus generator rotor speed for various wind speeds [82].

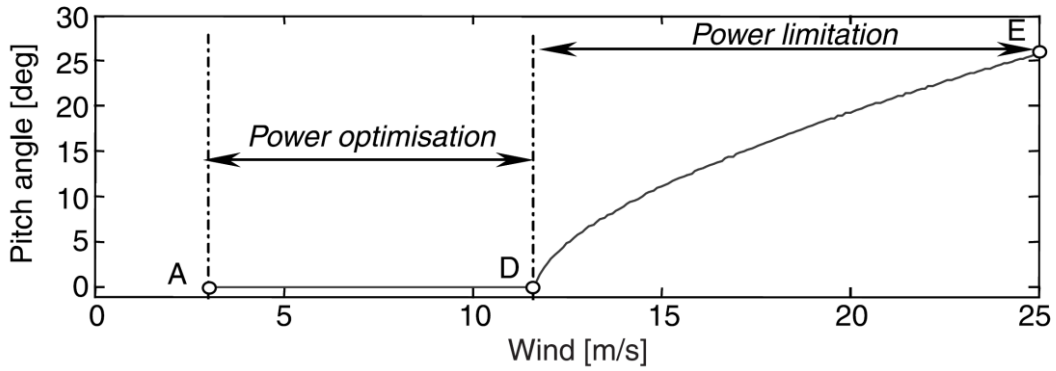

Figure 3.17 DFIG based wind turbine pitch angle active region [120]

The wind turbine operates at almost constant minimum rotor speed above its cut-in wind speed in the region (A-B). However, during low to medium wind speeds region (B-C), the turbine operates at different rotor speeds to follow the optimal power curve for maximum power extracting. As the rated power of the wind turbine is not reached in this region, the pitch angle is still deactivated as can be seen in Figure 3.17 and the control of the generator speed is provided by the rotor-side converter. When the generator reaches the synchronous speed at wind speeds lower than the rated wind speed, the generator is maintained around the rated speed as shown in Figure 3.16 region (C-D). In this region, the rotor speed may increase above the synchronous speed for not more than 15–20% above the synchronous speed due to power converter limitations [121]. Once again, as the rated power of the wind turbine is not reached in this region, the pitch angle is still deactivated, and the control of the generator speed is provided by the RSC. However, when the wind speed increases beyond the rating value as shown in Figure 3.16 region (D-E), the pitch angle control is activated to reduce the aerodynamic torque and keep it at a constant value. As the RSC is no longer able to maintain the torque under control in this region, the pitch angle control will be in service until the cut-out speed is reached [82].

As stated above, for low wind speed region, the pitch controller is deactivated where the angle is saturated at 0 degrees and an optimum power-speed curve is followed. In this thesis, the optimal active power is based on predefined power and

rotor speed lookup table. This table provides the optimal power that can be extracted from wind for a certain wind speed. This optimum power will be passed to the outer power control loop in the RSC as a power command.

In general, DFIG has three different operation modes which can be categorised according to the rotor speed when compared to the synchronous speed and the direction of the power flow passing the power converter. The three operations modes are known as super-synchronous, synchronous, and sub-synchronous operations as shown in Figure 3.18 [82].

During low wind speeds, the rotor speed of DFIG is lower than the synchronous speed (sub-synchronous operation mode) and the rotor absorbs power from the grid through the power converter. The slip in the sub-synchronous operation mode is positive. However, during high wind speeds, the rotor speed of DFIG is greater than the synchronous speed (super-synchronous operation mode), and rotor supplies power to the grid through the power converter. For the super-synchronous operation mode, the slip becomes negative. When the rotor of DFIG is rotating at the synchronous speed, there is no power flowing through the power converter. When the generator operates at the synchronous speed, the generator slip is almost zero. The slip is defined as [120]:

$$S = \frac{\omega_s - \omega_r}{\omega_s} \tag{3.63}$$

where ω_s and ω_r are the synchronous speed and generator rotor speed in rpm, respectively.

Assuming that all stator and rotor circuit losses are neglected, the power flow through the power converter can be expressed as a function of stator power and slip as follows:

$$P_{rotor} \approx -S\ P_{stator} \tag{3.64}$$

The delivered stator power can be expressed as a function of the grid power as follows:

$$P_{stator} = \frac{P_{grid}}{1-S} \tag{3.65}$$

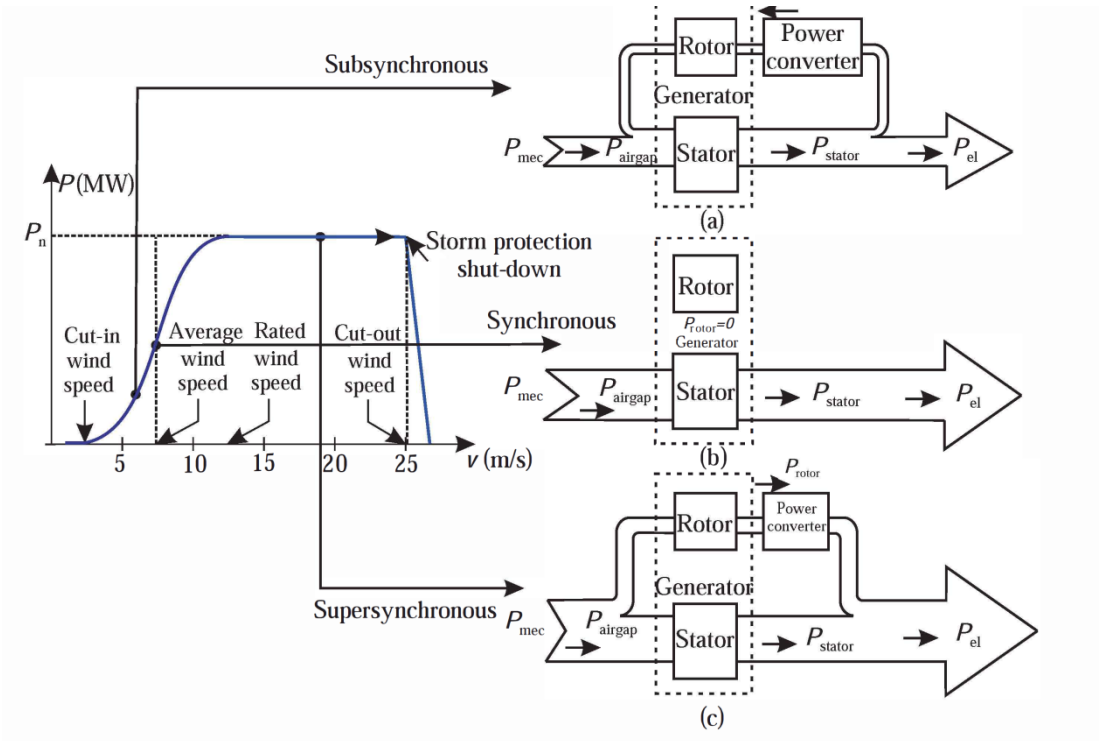

Figure 3.18 DFIG operation modes [82]

3.6.10 Aggregation of DFIG Wind Turbines

A wind farm may consist of a large number of individual DFIG wind turbines. Representing each DFIG wind turbine of the wind farm with a detailed model in the simulation tool increases system complexity and simulation time. This is due to the excessive number of equations to be computed. The simulation time and the complexity of the wind farms can be reduced using an equivalent model instead of presenting a detailed model of each wind turbine. In order to represent DFIG wind farm without the complexity of representing the complete wind farm model, reduced

equivalent model of wind turbines have been used [122-124]. An aggregation method can be applied to reduce a large number of wind turbines and to make the system simpler.

Depending on the incoming wind speed and the size of the wind farm, the entire wind farm can be aggregated to one or several groups of equivalent wind turbines. The simplest and most used aggregation method is based on presenting the whole wind farm as a single large wind turbine [124]. This method considers all the wind turbines of the wind farm facing the same incoming wind speed and all wind turbines within the wind farm are of the same type. Therefore, the output power and rating of the equivalent unit is a sum of the individual wind turbines as follows [124-126]:

$$S_{agg} = \sum_{i=1}^{n} S_i = nS_i \tag{3.66}$$

$$P_{agg} = \sum_{i=1}^{n} P_i \tag{3.67}$$

where S_{agg} aggregated rated power, S_i rated power of individual wind turbine, n number of wind turbines, P_{agg} aggregated active power, P_i active power of individual wind turbine.

The equivalent generator mechanical torque is n times the torque of an individual wind turbine when the values are in p.u.

$$T_{Magg} = \sum_{i=1}^{n} T_{Mi} = nT_{Mi} \tag{3.68}$$

$$H_{agg} = H_{Tagg} + H_{Gagg} = \rho \sum_{i=1}^{n} (H_{Ti} + H_{Gi}) \tag{3.69}$$

$$\text{where} \qquad \rho = \frac{S_{Gi}}{S_{Gagg}} \tag{3.70}$$

In the case of similar n DFIG rated capacity

$$\rho = \frac{S_{Gi}}{S_{Gagg}} = \frac{1}{n} \tag{3.71}$$

Therefore $$H_{agg} = H_{Tagg} + H_{Gagg} = \frac{1}{n}\sum_{i=1}^{n} (H_{Ti} + H_{Gi}) \tag{3.72}$$

The equivalent wind turbine includes the same model as an individual wind turbine for the generation system (induction generator and frequency converter), the control scheme and the controllers (rotor speed, reactive power, and pitch angle controller) and the protection system.

$$R_{agg} = \frac{1}{n}\sum_{i=1}^{n} R_i \tag{3.73}$$

$$X_{agg} = 1/(\frac{1}{n}\sum_{i=1}^{n} (1/X_i)) \tag{3.74}$$

The capacitance of the DC

$$C_{agg} = \sum_{i=1}^{n} C_i \tag{3.75}$$

PI controllers

$$K_{agg} = \frac{1}{n}\sum_{i=1}^{n} K_i \tag{3.76}$$

The transformer connecting the equivalent turbine to the grid is also scaled appropriately to allow power transfer of the aggregate generator.

This aggregation method assumed that all wind turbines within the wind farm are receiving the same wind speed and thus operating at the same operating point to produce the same power. However, in practice, the powers produced by wind turbines are different depending on wind speed variation and their location inside the wind farm due to the weak effect. Therefore, a multi-machine equivalent method can be used when the turbines within the wind farm are facing different wind speeds [127]. The multi-machine equivalent method will be used later in Chapter 6.

In this thesis, two different aggregation methods (single equivalent and multi-machine equivalent) are used depending on the size of the represented wind farm. For small DFIG based wind farms, the whole wind farm is represented as a single equivalent wind farm using the above aggregation method. For large-scale wind farms, both the single and multi-machine equivalent methods are used. Different wind speeds are taken into account when representing the entire wind farm by the multi-machine equivalent methods.

3.7 Summary

This chapter illustrates the modelling of the various components of a power system with the help of mathematical equations and diagrams. The well documented conventional SGs, excitation system, and PSS are briefly mentioned in this chapter. Moreover, the important components of the power system such as AC transmission lines, transformers and loads are also briefly introduced in this chapter. Furthermore, the general structure of the DFIG base wind turbine has been briefly discussed together with their control systems. The process of how the wind energy is extracted and converted to mechanical energy by the wind turbine using the aerodynamic model is included. It has been discussed that representing the mechanical system of DFIG based wind turbines by two-mass shaft system is appropriate to be implemented in the thesis for investigating power system stability with high penetration of DFIG wind power. The differential equations of the DFIG induction machine in *d-q* with an illustrated diagram are mentioned in this chapter. The control methods of DFIG rotor and grid side converter using the common control schemes

for the commercial DFIG, which are based on standard decoupled *d-q* vector control mechanism, are mentioned in this chapter. In practice, the DFIG wind turbines are equipped with protection system known as crowbar system which is used in this thesis. A conventional pitch controller is discussed, as well as the operating range of DFIG and maximum power tracking curve.

Chapter 4

Wind Power and Power System Stability

4.1 Introduction

Among the renewable energy technologies that are being developed, wind power is one of the most important sources of alternative power generation. With the continuous increase of wind power integration into power systems, the overall power system performance can be influenced, and thus power system stability becomes a very important subject. Therefore, investigation into the effects of wind power integration on existing conventional power plants and power system stability is becoming an increasingly important issue in order to identify potential impacts and to develop measures to lessen those impacts.

As power systems are highly nonlinear and involve complicated electromagnetic and electromechanical phenomena, Power system stability can be practically divided into three main categories for the purpose of clarification. The three distinct classifications of stability are rotor angle stability, frequency stability, and voltage stability. The impacts of wind power on the three main stability classifications are argued within this chapter to gain a greater understanding of how wind power especially DFIG wind turbines, which are gradually replacing conventional SGs in existing power systems, can affect power system stability. This will be followed by three case studies conducted on realistic power systems to show the impacts of

replacing SGs by equivalent DFIG based wind farms on rotor angle stability of these power systems. The first case is a base case without wind power, in which all generators are considered to be conventional SGs. The results of the base case are compared later with cases where wind power is included. In the second case SGs are replaced by equivalent wind farms equipped with DFIG. The wind farms ratings are the same as the SGs rating, and they produce the same amount of active and reactive power that was generated by the replaced SGs. The last case is conducted to show the effect of reactive power generated by DFIG on the rotor angle stability of power system.

4.2 Power System Stability

Electrical power systems are the largest and most complicated man-made dynamic systems ever created. They are highly nonlinear and involve complicated electromagnetic and electromechanical phenomena. The size and complexity of power systems made the power system stability phenomenon an extremely important and challenging issue. In modern power systems, more new technologies are being connected to electrical power systems due to a variety of factors such as the need for greenhouse gases reduction, fossil fuel price rise, and the increased sustainability demand. Among these new technologies, wind power is one of the fastest growing technologies worldwide. With the large penetration of wind power into power systems, power system stability became a vital concern. Therefore, understanding the impacts of wind power penetration on conventional power plants and power system stability are becoming increasingly important issues.

According to [32] power system stability is defined as "*Power system stability is the ability of an electric power system, for a given initial operating condition, to regain a state of operating equilibrium after being subjected to a physical disturbance, with most system variables bounded so that practically the entire system remains intact*".

Power system instability can be presented in several different ways depending on the operation conditions and configuration of the power system. As electrical power

systems are highly nonlinear systems, they tend to operate continuously under small disturbances such as changes in the loads or generators. Under these small disturbances, power systems must have the capability to respond to these changes without any adverse effect and adapt to new situations. Moreover, since most of power systems are large in size (cover a large geographical area), they are likely to expose to large disturbances, such as short circuits, due to the sudden loss of their main components. In these conditions, protection system has to act to isolate the faulty component from the network leading to change in power system structure. Depending on the strength of the system, it might lose its stability for a particular large disturbance and remain stable for another. However, the power system is expected to remain stable by reaching a new operating condition or returns to the original operating condition [128].

4.3 Classification of Power System Stability

Stability of power system is a complex problem depending on several factors. Power system stability can be practically divided into groups categorised by their time frame, the size of the disturbance, consequence, physical character. Accordingly, concerning the time frame, stability can be classified to short term and long term stability. For the size of the disturbance, stability can be divided into mall disturbance and large disturbance stability; where the first one can be examined by linearization of the system dynamic equations while the second involves the use of nonlinear simulation [129].

Power systems instability can occur in different ways depending on the network configuration and the power system operation condition. As most of the used generators are SGs, the stability of any power system is largely influenced by the dynamics of generator rotor angles and power angle relationships. Moreover, power system instability may occur as a result of voltage collapse due to the lack of reactive power or an appropriate voltage control. Voltage collapse can also occur in large load areas with induction motor loads as they consume a large amount of reactive

power. Additionally, power systems instability can occur in the form of frequency due to the lack of balance between load and generation.

In general, power system stability problems can be classified into three main categories for the purpose of clarification. The three distinct classifications of stability are rotor angle stability, frequency stability, and voltage stability. These types are further broken down into small disturbance or a large disturbance, and the short term or long term as shown in Figure 4.1 [32].

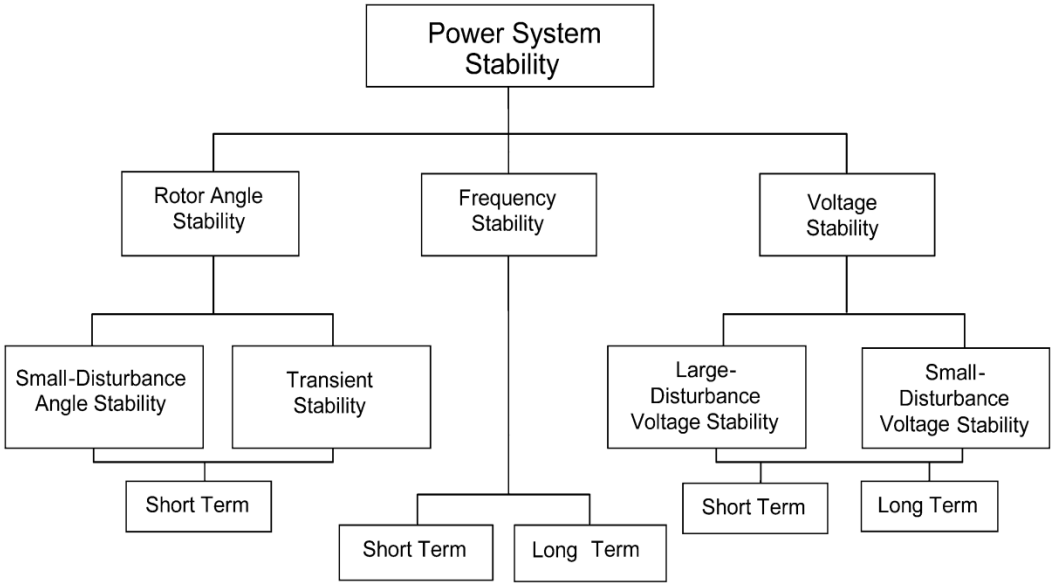

Figure 4.1 Classification of power system stability [32]

4.3.1 Rotor Angle Stability

It is the ability of SGs in the interconnected power system to remain synchronised after being subjected to a disturbance. In normal conditions, all interconnected SGs are synchronised with each other and hence rotating at the same speed. In this case, there is a balance between the input mechanical and output electromagnetic torques of each SG in the interconnected system. However, in the event of a disturbance, rotors of synchronous machines may accelerate or decelerate leading to angular position difference between rotors, which can influence the output of SGs. In this case, the system can sustain rotor angle stability if the difference in

angular position decreases until the synchronous speed is reached again. However, rotor angle stability can be lost if the difference in angular position increases continually. In this case, the generator will lose synchronism with the rest of generators leading to large fluctuations in the generator output power, current, and voltage. Loss of synchronism can also take place between groups of machines, with synchronism maintained inside each group after separating from each other. Therefore, the power system stability for any particular condition is determined by whether or not the deviations in angular positions of the rotors result in sufficient restoring torques [89].

For a better understanding of rotor angle stability, it is useful to characterise as following: small signal stability or (small disturbance rotor angle stability) and transient stability or (large disturbance rotor angle stability). Both small signal stability and transient stability are categorised as short-term phenomena.

4.3.1.1 Small signal stability

It is the ability of the power system to remain synchronised after being subjected to a small disturbance. The equations of the power system in small signal stability can be linearized for purposes of analysis as disturbances are considered small, for instance, small changes in load, which are frequently encountered in normal operation conditions. Small signal stability depends on some factors including the initial operating state of the system, system strength, and type of generator excitation controls used.

Instability can occur due to the lack of synchronising torque (increase in rotor angle through a non-oscillatory mode) or the lack of damping torque (increase in the amplitude of rotor oscillations). Small signal stability in today's practical power systems is usually associated with the increase oscillations amplitude as a lack of damping torque [32].

The time of interest for small signal stability is between 10 and 20 seconds after the disturbance.

4.3.1.2 Transient stability

It is the ability of the power system to remain synchronised after being subjected to a severe disturbance, for example, a short circuit on a transmission line. Transient stability depends on both severity of the disturbance and the initial operating state of the system. Steady state operation condition after severe disturbance is usually different from pre-disturbance operation condition as a result of system alteration [32].

Transient instability can occur in the form of a periodic angular separation due to insufficient synchronising torque, which known as first swing instability. However, transient instability can occur as a result of rotor angle oscillations in the form of inter-area and local oscillations. These oscillations can cause a large excursion of rotor angle beyond the first swing [89].

The time domain for transient angle stability studies is normally under 5 second and can be extended to 10-20 second for large power systems.

4.3.2 Voltage stability

It is the ability of the power system to maintain the voltage levels at all nodes of the system at acceptable limit under normal operating conditions, and after being subjected to a disturbance. Voltage instability may occur as a result of progressive and uncontrollable fall or rise in voltage of some the system nodes. In general, voltage instability is a local phenomenon. However, widespread impact such as cascading outages and voltage collapse of the entire power system can occur as a result of voltage instability [32, 89].

Severe voltage drop can also be associated with rotor angle instability as rotor angles going out of step. When the rotor angles of two synchronous machines groups approach or exceed 180° as a result of the gradual loss of synchronism, voltages at middle points in the network close to the electrical centre will experience rapid drop. In this case, the rapid oscillation between high and low values of voltages

near the electrical centre will occur as a result of repeated rotor angle separation between the two groups [130].

In a similar way to rotor angle stability, voltage stability can be classified into following categories:

- Large disturbance voltage stability in which the system has to maintain steady voltages following severe disturbances such as power system fault, loss of large generator or circuit contingencies. Voltage stability may be either a short-term or a long-term phenomenon. Thus, the time frame of this kind of study can vary from few seconds to minutes to capture the performance of power system equipment's [89].
- Small disturbance voltage stability in which the system has to maintain steady voltages following small disturbances such as changes in system load. To investigate small disturbance voltage stability, the system equations can be linearized with appropriate assumptions computation. However, nonlinear effects such as tap changer controls, dead-bands, and time delays are not taken into account with linearized method [131]. The time frame of this kind of study is the same as the large disturbance voltage stability time frame.

4.3.3 Frequency stability

It is the ability of the power system to maintain the frequency within its limit after the system being subjected to disturbance resulting in a significant mismatch between generation and load. Frequency stability depends on the ability of power systems to maintain or restore equilibrium between system generation and load [32].

Severe system disturbances generally result in a considerable fluctuation in frequency, power flows, voltage, and other system variables. In general, frequency stability problems are associated with inadequate responses from system components, poor coordination of control and protection equipment, or inadequate generation reserve. The time frame of frequency stability studies is varying from a

fraction of seconds to several minutes. The small time corresponding to the response of under frequency load shedding relays, generator controls, and protections devices response time. Whereas the large time is corresponding to the response of prime mover energy supply systems and load voltage regulators [89, 130].

4.4 Wind Power and Power System Stability

In ordinary power systems, large synchronous machines are extensively used to produce the required power. These machines are well known, reliable and have complex control systems that allow the system to maintain high levels of stability. As the dynamic behaviour of any power system is largely determined by the dynamic behaviour of its interconnected generators, the integration of wind power turbines into these systems can affect the dynamic behaviour of power systems.

With the rapid increase in penetration of wind power in power systems, wind turbines are being installed as a group in larger farms. The production capabilities of these large wind farms are approaching those of conventional power plants. As a result, wind turbines gradually start to replace the output of these conventional power plants and thus many aspects of the power system operation, control, and stability might be affected [132]. The impact of wind power on power system stability can be ignored if the penetration of wind power is very low. However, with high levels of wind power penetration, wind farms may replace large conventional SGs, the dynamic performance of the power system might be affected [21].

As wind power becomes a more common source of generation in power systems, the increasing of wind power penetration seems to continue, and its impact on power system stability will be significant. These impacts have to be mitigated as wind power turbines should be able to contribute to network support and operation in order to keep the entire power system in stable condition [31].

The impact of increased wind penetration on the three types of power system stability (rotor angle stability, voltage stability, and frequency stability) will be considered separately and discussed.

4.4.1 Impact of Wind Power on Rotor Angle Stability

The ability of power systems to return the balance between electromagnetic and mechanical torques is determined by the rotor angle stability of each SG. However, with the increase of wind power penetration into power systems, systems experience a change in their dynamic characteristics as the technology of wind turbines are different from synchronous machines.

4.4.1.1 Impact on Small Signal Stability

Small signal stability problem normally takes place due to inadequate damping torque, and as a consequence, the amplitude of rotor oscillations will increase [89]. The dynamic response of wind power generators is different from the dynamic response of large SGs. Therefore, following the increasing of wind power penetrations levels in power systems, the impact of wind power on system oscillations will increase as well. The effect of wind power on power system small signal stability depends largely on the technology installed on wind turbine [133]. Since the productions of wind farms are approaching the productions of larger conventional SGs, wind farms should make a contribution to the stabilisation of power systems. Therefore, the capability of wind farms should be examined carefully.

In recent years, the influence of wind power on power system oscillation has been addressed in the literature. [134] concluded that wind turbines do not participate in electromechanical oscillations as wind power generators are not synchronously coupled to the power systems. However, the effect of the wind power generators on small signal stability depends on the kind of wind generator and their controllers. In [132, 134, 135] the impact of wind turbines on power system oscillations are presented. They find that fixed speed wind generators do not have a significant effect on inter-area oscillations damping; however, they can improve the damping of inter-area oscillations slightly. Moreover, fixed speed wind turbines can improve the damping of inter-area oscillations better than DFIG wind turbines whereas DFIG wind turbines are slightly better than full-scale power converter wind turbines for inter-area oscillation damping.

A small two area power system used in [136] to study a number of operating scenarios for DFIG based wind turbine and find that the DFIG base wind turbines tend to improve the damping of power system oscillations for most of the scenarios. However, an adverse impact is found for certain scenarios. A study is carried out in [137] to analyse the impact of DFIG wind turbines on power system oscillations in the large five-area system. The study concluded that the effect on a particular oscillatory mode highly depends on the replaced SGs. A significant impact could occur when replacing SGs that are used to stabilise certain modes.

In contrast, as variable speed wind turbines can control active and reactive power independently, they have the capability to contribute to power oscillation damping and hence improve small signal stability. To improve the oscillations damping of power systems with high penetration of DFIG based wind farms, an auxiliary damping control loop for DFIG is used. Eigenvalue analysis and time domain simulation were used in [31] to study the capability of DFIG to damp power oscillations. The results indicate that damping of network oscillation can be significantly enhanced by a proper designed DFIG-PSS. The proposed PSS can work over the full operational slip without degradation the system voltage. In the above study, the adopted PSS is similar to the PSS of the SGs, and it was attached to the active power control loop of the DFIG-RSC. In [138], a two area system with a large wind farm is analysed by a time domain simulator. An axillary damping control loop is added to the DFIG-RSC to improve the damping of inter-area oscillations in high wind power penetration. The paper concluded that the active power modulation of DFIG based wind farm is an efficient method for damping oscillations in power systems. Moreover, [139] stated that DFIG is able to improve power oscillations better than other types of wind generators even in weak systems.

4.4.1.2 Impact on Transient Stability

In asynchronous generators, the electrical torque falls below the level of mechanical torque in the event of a disturbance, which will cause the rotor to accelerate and increases the angular position of the rotor flux vector. The natural characteristics of synchronous machines drive the electrical torque back toward the

level that matches the mechanical torque, which is known as synchronising torque. However, in severe disturbance such as during a nearby fault, the SG speed will increase rapidly due to loss of synchronism [140]. In the case of the wind power generators, the electrical torque also falls below the level of mechanical torque in the event of a disturbance, which gives rise to variations in the speed and the position of the rotor. However, synchronising torque does not exist due to the asynchronous operation [141].

In the past, the wind turbines generators are usually allowed to be disconnected from the grid in the event of large disturbance to be protected from high transient current, rotor over-speed, mechanical stresses, and voltage dips. The ability of wind turbines to withstand network disturbance are very limited in comparison to conventional SGs. With the massive integration of wind power generators in the grid, they are required to ride through grid disturbances and support the grid voltage during and immediately after the grid disturbances [142].

The impact of wind power on power system transient stability has been addressed by several researchers. The authors of [42] studied the effects of wind power on power system stability, and they find that higher installation of wind power can affect the transient stability of power systems. This is due to the fact that transient stability of any power system mainly depends on the installed generators technologies. As the dynamic characteristics of wind turbines are different from that of the SGs, high penetration levels of wind power will bring new challenges to power systems transient stability. Reference [143] compared the effect of fixed speed wind turbines and DFIG wind turbines on power system transient stability. The results indicate that although fixed speed wind turbines contribute positively to system oscillation damping, their contribution to the transient stability is very weak due to voltage stability issues. However, DFIG based wind turbines can enhance the transient stability in term of voltage recovery after a disturbance.

The impact of wind generators on transient stability depends on the location of the disturbance. During fault period, voltage sags at DFIG terminal lead to a high

current in RSC. Since the converter rating is only (25- 30) % of the generator rating, the high current can damage the converter. For this reason, the converter systems have to be disconnected; the rotor windings are short-circuited by crowbar protection system and hence the generator could trip out. In this case, the DFIG will act as a fixed speed induction generator and hence the real and reactive power cannot be controlled [144]. However, [145] argued that by using dynamic reactive power compensation, a continuous operation of DFIG can be achieved during a fault condition. Moreover, by using a fast control system, DFIG can effectively ride through a grid fault and thus has no problem with transient stability. The same author claims that DFIG could be superior over SGs to improve transient stability during severe disturbances. However, further research reveals that transient stability of power systems could be either reduced or enhanced when some SGs are replaced by DFIG wind turbines [146].

In [46], the effect of reactive power supplied by wind generation on power system transient stability is examined. The study concluded that transient stability could be improved and the oscillations damping quickly if the terminal voltage of the wind generation controlled to achieve 1.0 p.u. Furthermore, the SG rotor angle is directly influenced by reactive power control strategy used by the wind generation.

4.4.2 Impact of Wind Power on Voltage Stability

Generally, induction generators are absorbing reactive power from the grid, and they will absorb more reactive power when the voltage drops. Reactive power consumption will increase as the rotor continues to accelerate if the voltage continues to drop below the nominal level, and hence, the generator can become unstable.

Several studies have been conducted to study the impact of wind power on voltage stability of power systems. The authors of [145] studied the impact of a wind farm on steady state and transient voltage stability. They found that connecting fixed speed wind turbines to the grid deteriorates both kinds of voltage stability. However, the study concluded that DFIG wind turbines have better voltage recovery than the fixed speed wind turbines since the former can regulate reactive power independently

from the generated active power [147]. In addition, a comparison between the two variable speed wind turbines has been made by [148]. The results show that full-scale power converter wind turbines can improve voltage stability better than DFIG wind turbines, as this kind of turbines have the capability to supply a large amount of reactive power. The studies carried out by [145] and [147] show that the effect of a wind turbine on small disturbance voltage stability is insignificant when the generated active power is low from wind farms. However, injecting more wind power could lead to a voltage collapse in the event of a small disturbance.

A wind farm sizing method for a weak power system is proposed by [149]; the authors found that large wind power penetration has an adverse impact on power system voltage stability. However, placing a voltage support device at the weakest system bus can resolve this problem. Reference [150] concluded that voltage stability margin could be improved by choosing an appropriate location and size for the renewable generation.

The author of [148] reviewed the fault ride through strategies for different wind turbine systems. The author concluded that the main task of fault ride through strategies for fixed speed wind turbines was to prevent rotor over speeding phenomena. On the contrary, DFIG wind turbines and full-scale power converter wind turbines have better fault ride-through capability, and also, they can control reactive power to support grid voltage for a quick voltage recovery. In addition, the impact of wind power on voltage stability is also influenced by the voltage level that wind turbines are connected to. Connecting wind turbines to distribution and sub-transmission systems have a negative effect on voltage stability more than connected them to transmission systems. This is due to the fact that reactive power support is typecally limited in low and medium voltage levels [151].

4.4.3 Impact of Wind Power on Frequency Stability

The increase of wind power penetration in electricity grid reduces the power system inertia, which directly affects frequency change rate following disturbances. Replacing conventional SGs by a fixed speed wind turbines has a small impact on

the system frequency after losing generation or load in the power system. Fixed speed wind turbines provide an inertia response to system frequency changes as the rotational speed and system frequency are coupled. The inertia response of this type of wind turbines is smaller and also slower than SGs because of their slip (1-2) %. However, replacing conventional SGs by a DFIG wind turbines lead to a significant change in system frequency for the reason that DFIG wind turbines provide negligible inertial response [152, 153].

DFIG wind turbine could be sensitive to system frequency by adopting frequency control methods to release the kinetic energy stored in the rotating masses. In the same way, according to [154], DFIG wind turbines could response to frequency variation and provide a frequency regulation. However, providing frequency response capability from wind farms would increase the balancing costs as the output only a proportion of the available wind power. The alternative to spilling wind to provide frequency response capability is using wind farm level energy storage [155].

4.5 Analysis of the Impact of DFIG Wind Turbines on Power System Small Signal Stability

The small signal stability problem usually occurs as a result of inadequate damping of one of the system rotor oscillations. The small signal stability analysis can detect system modes, which are produced by electromechanical interactions between power system SGs. Since DFIG wind turbines are not synchronously coupled to the power systems, wind turbines do not participate in electromechanical oscillations. The methodology of small signal stability analysis is described in the following steps:

- Run small signal stability analysis in the frequency range of 0.1 to 2 Hz.
- Identify main modes that have low damping factor (less than 10%).
- Determine the dominant machines with their main state variables and their participation factor in the main mode.

- Analyse the mode shape corresponding to the rotor speed state variable to identify generators oscillating against each other.
- Repeat the previous steps for different scenarios.

To investigate the effect of grid connected DFIG base wind turbines on the small signal stability of power system, SGs are replaced by equivalent wind farms equipped with DFIG. The wind farms rating are the same as SGs rating, and they produce the same amount of active and reactive power that are generated by the replaced SGs. The topology operation condition of the test system with wind farm has to be the same with one without wind farm.

4.5.1 Small Signal Stability Analysis of the IEEE 9-bus System with Integration of DFIG Wind Turbines

The IEEE 9-bus test system is used to study the impact of DFIG wind turbine on power system small signal stability as shown in Figure 4.2. The system consists of three SGs with three fixed-tap step-up transformers, six transmission lines and three loads totalling 315 MW and 115 MVAr. The three SGs are equipped with an IEEE type 1 exciter. However, the three generators were not equipped with PSS for more straightforward assessment. The synchronous machines G1 and G2 are equipped with turbine governor type TGOV1. The static and dynamic data of the test system can be found in [156]. The three loads were modelled as nonlinear ZIP loads (33% constant impedance *Z*, 33% constant current *I*, and 33% constant power *P*) [97].

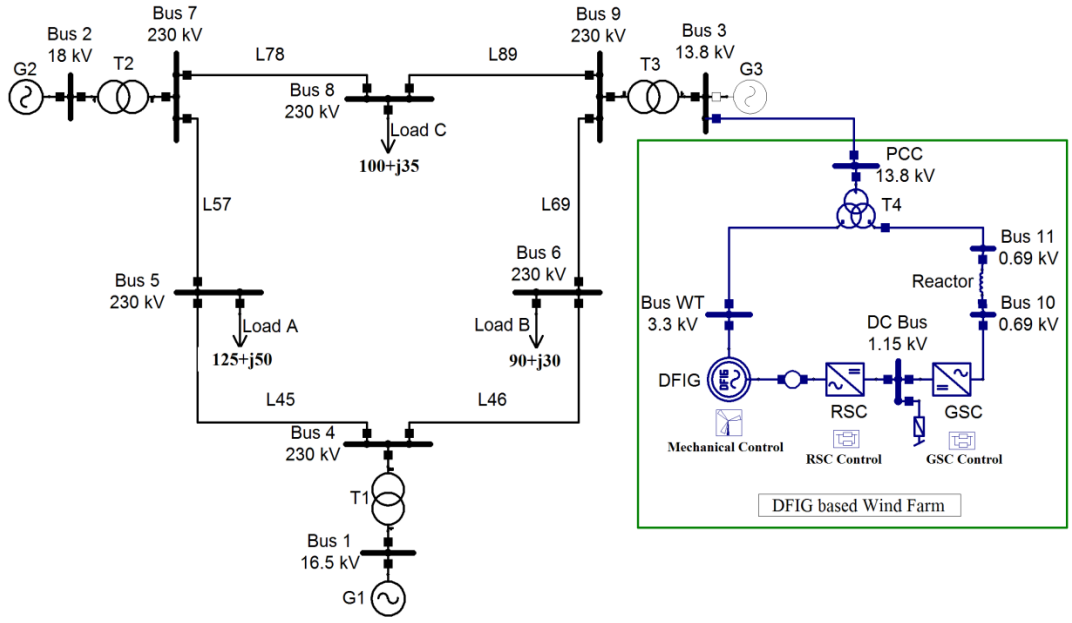

Figure 4.2 Single line diagram of the IEEE 9-bus test system with DFIG based wind farm.

To investigate the effect of DFIG based wind farm on the power system small signal stability, a DFIG wind farm is connected to the test system. Both the test system and wind farm are modelled in details as described in Chapter 3 by using NEPLAN software [157]. NEPLAN is a power system simulation package with a user-friendly graphical interface that allows the user to perform study cases very efficiently. It allows wind turbines and their control schemes to be modelled in detail. NEPLAN dynamic simulator offers also excellent functionalities to develop user-defined models. In this thesis, both small signal stability and transient stability are examined using the NEPLAN software.

A wind farm may consist of a large number, between (10 -100s), of individual DFIG wind turbines. Representing each wind turbine of the wind farm in the simulation tool increases system complexity and simulation time. Therefore, the aggregation method described in Chapter 3 is applied to reduce a large number of wind turbines and to make the system simpler. The DFIG wind turbine that represents the single machine equivalent DFIG based wind farm is shown in Figure 4.2. The 85 MW wind farm was aggregated from 17 turbines of 5 MW each to achieve an equivalent generated power to replace SG G3. Hence, the generated

power from DFIG wind farm is accounted for 27% of the consumed total power of the test system.

The analysis is carried out for three different cases:

- **Case 1:** SG case, this is a base case scenario in which all generators are considered to be conventional SGs with G3 operate at a fixed unity power factor.
- **Case 2:** G3 is replaced by DFIG based wind farm operating at fixed unity power factor (no reactive power injected into the system from DFIG).
- **Case 3:** G3 is replaced by DFIG based wind farm controlled its terminal voltage at 1 p.u. (the reactive power is controlled to achieve a specified voltage value at terminal bus).

4.5.1.1 Results and Discussion

A detailed small signal stability study on the test system was conducted on the rotor angle of the three SGs for the three cases. The rotor angle oscillations in the frequency range of 0.1 to 2 Hz are monitored. The dominant eigenvalue and their frequency, damping factor, main machine and the participation factor for each main state variables for each case are shown in Table 4.1. The results indicate that the system is stable in the three cases, and there is a critical mode with less than 10% damping factor for each case.

Table 4.1 Main electromechanical modes of Case 1 (SG case), Case 2 (G3 is replaced by DFIG based wind farm operating at fixed unity power factor), Case 3 (G3 is replaced by DFIG based wind farm controlled its terminal voltage at 1 p.u.).

Cases	**Case 1**	**Case 2**	**Case 3**
Eigenvalue $\lambda = \sigma + j\omega$ (p.u.)	-0.265 ±j7.615	-0.297±j7.778	-0.306 ± 7.734
Frequency f (Hz)	1.212	1.238	1.231
Damping Factor ζ (%)	3.5	3.8	3.9
Dominant Variable	ρ, ω	ρ, ω	ρ, ω
Dominant Machine	G2	G2	G2

Participation Factor (%)	35.8, 37.5	40.3, 42.1	40.2, 42.3

As can be seen in Table 4.1, the main modes of each of the three cases are dominated by rotor angle ρ and speed ω of generator G2. The frequency of each mode is relatively unchanged in the three cases. However, the rotor angle oscillation of case 2 is slightly more stable than case 1 as the damping factor of the main mode is improved from 3.5% to 3.8% when the SG is replaced by an equivalent wind farm. This improvement is further enhanced when the voltage at the connection point is regulated by the wind farm.

Although G2 is dominating the main oscillatory modes for each case, its contribution to the oscillatory modes after the SG is replaced by the wind farm is higher. The participation factor of G2 increased from 35.8% in the first case to more than 40% when the G3 is replaced by equivalent DFIG based wind farm.

For more detailed analysis, mode shape that is corresponding to the rotor speed state variable for the three cases is examined. In the first scenario, the results indicate that the three SGs of the test system are participating in the mode, where G1 is oscillating against the other two (G2 and G3). However, when G3 is replaced by DFIG based wind farm, the wind farm does not contribute to the main mode. The dominant mode after the synchronous machine is replaced by the wind farm gets the contribution from G1 and G2, which are oscillating against each other.

The results of small signal stability analysis of the IEEE 9-bus system with integration of DFIG based wind turbines show that replacing the SG with a DFIG based wind farm has no negative impacts on the small signal stability of power systems. The results indicate that DFIG based wind turbines do not participate in electromechanical oscillations, and hence, power system small signal stability is likely to be improved by DFIG based wind turbines installation. DFIG base wind turbines tend to improve the damping of power system oscillations for the examined cases.

4.5.2 Small Signal Stability Analysis of the IEEE 39-bus System with Integration of DFIG Wind Turbines

The widely used New England 10-machine 39-bus system has been chosen as the test system to be used to study the impact of DFIG based wind turbines on power system small signal stability as shown in Figure 4.3 [158]. The system consists of 10 synchronous machines in which G1 is an equivalent external generator, 12 transformers, 46 transmission lines and 19 loads modelled as nonlinear ZIP loads (33% constant impedance Z, 33% constant current I and 33% constant power P) [97]. Every synchronous machine is equipped with (TGOV1) turbine governor and (IEEEX1) exciter. However, only SGs G5, G7, G9 are equipped with (STAB1) PSS.

To investigate the impact of DFIG based wind turbines on power system small signal stability, two large-scale DFIG wind farms were installed in the test system to replace two large synchronous machines G7 and G9 equipped with PSS. The generated power from the two wind farms accounts for 22.6% of the total consumed power of the test system.

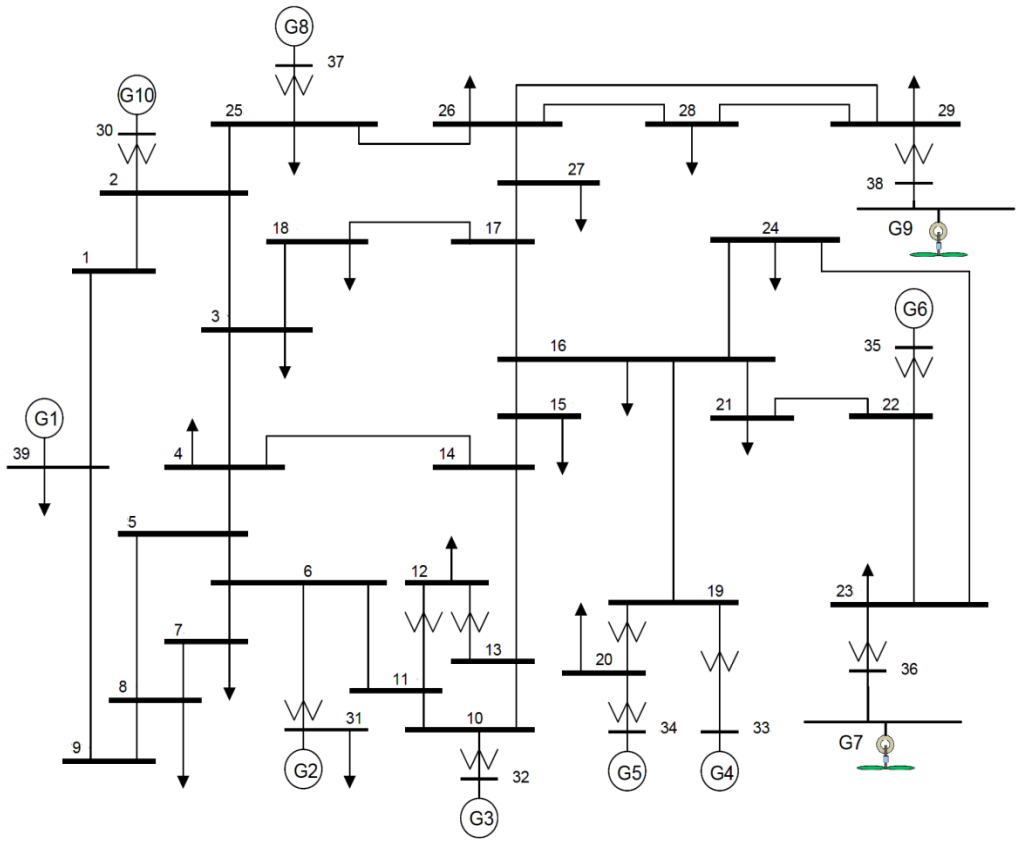

Figure 4.3 Single line diagram of the IEEE 39-bus test system with two DFIG based wind farms.

The analysis is carried out for three different cases:

- **Case 1:** SG case, this is a base case scenario in which all generators are considered to be conventional SGs without any PSS.
- **Case 2:** SG case with PSS, SGs G5, G7, G9 are equipped with (STAB1) PSS.
- **Case 3:** SGs G7 and G9, which are equipped with PSS, are replaced by DFIG wind farms which control their terminal voltage at 1 p.u. (the reactive power is controlled to achieve a specified voltage value at the terminal bus).

4.5.2.1 Results and Discussion

A detailed small signal stability study on the test system was conducted for the three cases. The main eigenvalues with damping factors of less than 10% for each

case presented in Table 4.2. It is clear that the test system without any PSS is unstable as there are two oscillatory modes have positive real parts with negative damping factors. Negative damping factors indicate that there are two growing oscillatory modes, which lead to system instability. The mode shape analysis of the first mode shows that there are two groups of generators swinging against each other. The first group consists of three generators, which are G8, G9, and G10. This group is dominated by machine G9 with a participation factor of 53.1 %. The second group consists of the rest of generators, which are dominated by G5 with a participation factor of 21.3 %. Moreover, the mode shape analysis of the second unstable mode shows that the second unstable mode is excited mainly by G1 (the equivalent of a large number of generators), and the rest of the SGs in the test system, which are swinging against each other. The rest of the electromechanical modes are stable modes with low damping factors. The mode dominated by G5 has a low damping factor of 0.4% oscillating at a low frequency of 0.909 Hz.

However, in the second case, in which SGs G5, G7, and G9 are equipped with PSSs, the system is stable as the unstable modes are damped by the selected PSSs. The number of oscillatory modes with damping factors less than 10% is decreased from eight in the first case to four in the second case. Critical modes dominated by G1, G5, G6, G7 and G9 in the base case are damped out in this case by the selected PSSs. Moreover, the damping factor of modes dominated by G3, G4 and G8 increased from 2.1%, 4.7% and 8% to 2.2%, 8.7% and 8.5% respectively. However, there is a new local mode dominated by G4 with a damping factor of 8.7% presenting in this case.

Table 4.2 Main electromechanical modes of Case 1 (SG case without any PSS), Case 2 (G5, G7, G9 is equipped with PSS), Case 3 (G7 and G9 are replaced by DFIG based wind farms controlled their terminal voltage at 1 p.u.).

Case	**Eigenvalue $\lambda = \sigma + j\omega$ (p.u.)**	**Damping Factor ζ (%)**	**Frequency f (Hz)**	**Dominant Machine**
1	0.135±j5.63	-2.4	0.896	G9
	0.047±j3.70	-1.3	0.589	G1

	-0.024±j5.71	0.4	0.909	G5
	-0.146±j6.82	2.1	1.086	G3
	-0.171±j6.29	2.7	1.002	G6
	-0.37±j7.84	4.7	1.247	G4
	-0.414±j8.07	5.1	1.284	G7
	-0.64±j7.97	8.0	1.269	G8
2	-0.151± j 6.83	2.2	1.086	G3
	-0.264± j 6.16	4.3	0.98	G2
	-0.654 ±j 7.53	8.7	1.199	G4
	-0.683 ± j7.99	8.5	1.272	G8
3	-0.149± j6.85	2.2	1.091	G3
	-0.19± j3.89	4.9	0.619	G1
	-0.354± j6.22	5.7	0.99	G2
	-0.52± j7.821	6.6	1.245	G4
	-0.625± j6.87	9.1	1.094	G6
	-0.717± j7.93	9	1.262	G8

To show the impact of replacing large synchronous machines equipped with PSS by an equivalent DFIG based wind farm, G7, and G9 that equipped with PSS are replaced by two equivalent DFIG based wind farms. The results show that the system is stable as shown in Table 4.2. The two wind farms installed did not participate in electromechanical oscillations, and therefore, the unstable oscillatory modes in the first case that mainly excited by G9 do not exist in this case. Moreover, there are less oscillatory modes than in the base case.

Critical modes dominated by G5, G7, and G9 in the base case are damped out in this case as the mode dominated by G5 is damped by the G5 PSS and modes dominated by G7 and G9 are damped as a result of replacing these two synchronous machines with equivalent DFIG base wind farms. Moreover, the integration of the two wind farms has a positive effect on the damping of the other modes. The

unstable mode in the base case that dominated by G1 is shifted to the stable region, and the damping factor increased from -1.3% to 4.9%. The damping ratio associated with the mode dominated by G6 is increased from 2.7% to 9.1% as a result of replacing G7 by an equivalent wind farm. In addition, the damping factor of modes dominated by G3, G4, and G8 in the base case is improved from 2.1%, 4.7% and 8% to 2.2%, 6.6% and 9% in case3 when the SGs G7 and G9 are replaced by equivalent DFIG based wind farms.

The small signal stability results indicate that replacing large-scale SGs by equivalent DFIG based wind farms improves the damping of power system oscillations. However, replacing large-scale SGs equipped with PSSs by an equivalent DFIG based wind farms can have a negative impact on the damping of power system oscillations as can be seen in Table 4.2. In a comparison of case 2 with case 3 (replacing G7 and G9 that are equipped with PSSs by equivalent DFIG based wind farm), case 2 is more stable than case 3 as there are additional two critical modes in the wind farm case. These two modes are dominated by G1 and G6 with a damping factor of 4.9% and 9.1% respectively.

These results reveal that replacing synchronous machines fitted with PSSs by equivalent DFIG based wind farm have negative impacts on the small signal rotor angle stability of power systems. However, if the replaced synchronous machines are not fitted with PSSs, the impacts on small signal rotor angle stability of power system will be positive as the installed DFIG based wind farms will not participate in electromechanical oscillations.

4.6 Analysis of the Impact of DFIG Wind Turbines on Power System Transient Stability

The main objective of examining the impact of DFIG wind turbines on power system transient stability is to determine the capability of a power system to maintain synchronism when subjected to a large disturbance. This has to be done through a

nonlinear time domain simulation by using appropriate models for the various power system components.

To conduct a transient stability analysis, the system has to be exposed to a large disturbance such as a three-phase short circuit fault. The location of the disturbance has to be chosen carefully for transient stability study. It may be selected according to the result of a small signal stability study. Modes with low damping factors can be aggravated by a large disturbance. Therefore, the fault has to be near the machine that has the highest participation factor in the specified mode.

When the synchronous machines electrical torque falls below mechanical torque during a fault, the rotor will accelerate leading to a higher rotor angle position. However, for DFIG, the torque-angle characteristic does not exist due to its asynchronous operation. Hence, the dynamic response of a DFIG to system disturbances is different from that of a SG [141].

The synchronous machines rotor angle measured with respect to a synchronously rotating reference is considered as one of the parameters to test the stability of the system. The power system is said to be unstable if the differences of rotor angle of any SG in relation to other SGs increase indefinitely.

In this thesis, the rotor angle of the interconnected SGs will be used to assess the stability of power system. Transient stability can be measured by transient stability index (TSI) which is defined as follows [159]:

$$\eta = \frac{360° - \delta_{max}}{360° + \delta_{max}} \times 100 \qquad \text{where} \qquad -100 < \eta < 100 \tag{4.1}$$

Where: η and δ_{max} are the transient stability index symbol and the maximum angle separation (in degree) between any two generators in the system at the same time in the post fault condition respectively.

The transient stability index can vary from -100 to +100. The power system is considered as a stable system if the value of transient stability index is greater than zero.

Moreover, the transient stability can be assessed by observing post-fault conditions. Different generator variables can be evaluated after the fault to identify whether the power system is in stable condition or not. The variables that can be monitored are:

- Generator rotor angle: if the generators rotor angle drops out of phase, the generators are in a high possibility to lose the synchronism. As a result, the power system will be in unstable condition.
- Active power: the power system is in unstable condition if there are increasing undamped oscillations after the fault.
- Terminal voltage: the system is treated as being stable as long as the terminal voltage of the generator recovers quickly.
- Reactive power: absorbing a large amount of reactive power by the grid after the fault is a sign of transient instability. This could be due to voltage collapse of the power system.

4.6.1 Transient Stability Analysis of the IEEE 9-bus System with Integration of DFIG Wind Turbines

The IEEE 9-bus test system is used to study the impact of DFIG wind turbine on power system transient stability as described in Section 4.5.1.

The analysis is carried out for three different cases, which are similar to the cases used to study small signal rotor angle stability:

- **Case 1:** SG case, this is a base case scenario in which all generators are considered to be conventional SGs with G3 operate at a fixed unity power factor.

- **Case 2:** G3 is replaced by a DFIG based wind farm operating at fixed unity power factor (no reactive power injected into the system from DFIG).
- **Case 3:** G3 is replaced by a DFIG based wind farm controlled its terminal voltage at 1 p.u. (the reactive power is controlled to achieve a specified voltage value at terminal bus).

The result of small signal stability study shows G2 has the highest participation factor. Therefore, the location of the disturbance has to be near G2. A 3-phase to ground fault with duration of 150 ms was imposed near Bus 7 on line 5-7. The fault was cleared by opening both sides of the faulted line simultaneously.

4.6.1.1 Results and Discussion

In order to assess the effect of DFIG based wind farm on transient stability of the test system, rotor angle of each generator is observed, from which the transient stability index is calculated. Active and reactive power output of each generator are monitored. Moreover, the terminal voltage of the replaced SG (Bus 3) is monitored. The angle of the largest SG G1, which is the slack generator, was taken as a reference angle.

In Figure 4.4, rotor angle oscillation of the G2 relevant to G1 can be seen for the three cases. At 0.1 s the rotor angle of G2 starts to accelerate as a result of the 3-phase to ground fault that imposed near Bus 7, but it remains in stable condition as the rotor angle did not drop out of phase. The figure shows that rotor angle variation of G2, when a wind farm of an equivalent size replaced SG G3, has a larger rotor angular swing than that in the base case. However, the rotor angular swing is improved when the DFIG based wind farm controls its terminal voltage at 1 p.u. This indicates that controlling the reactive power of the wind farm to achieve a predefined voltage value can improve rotor angle stability.

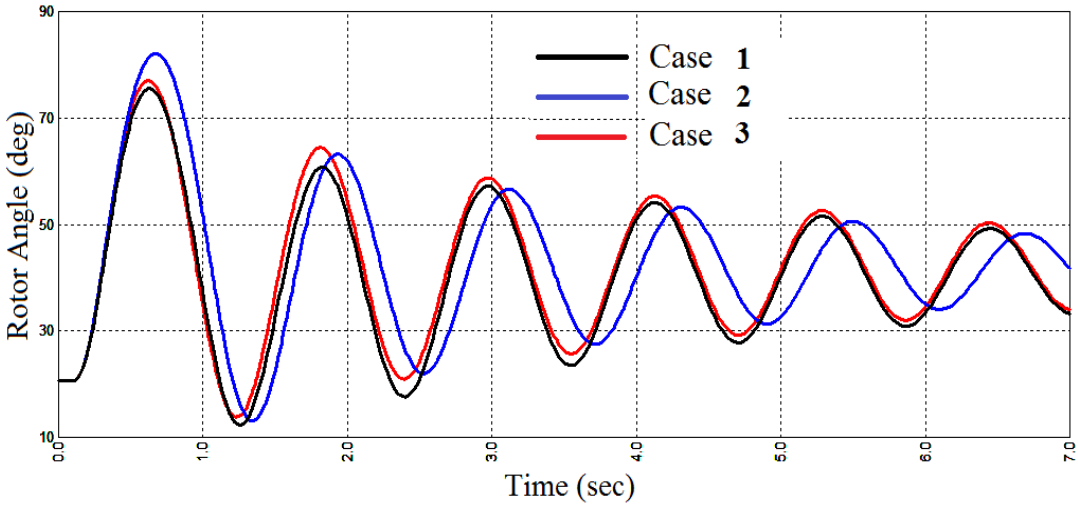

Figure 4.4 Rotor angle of G2 for case 1 (SG case), case 2 (G3 is replaced by DFIG based wind farm operating at fixed unity power factor), case 3 (G3 is replaced by DFIG based wind farm controlled its terminal voltage at 1 p.u.).

Moreover, Table 4.3 shows that the stability of the test system is reduced after SG G3 is replaced by an equivalent wind farm operating at a unity power factor, as the transient stability index is decreased from 65.3 in the first case to 62.87 in the second case. Controlling the terminal voltage of DFIG wind turbine improves the transient stability index from 62.87 to 64.77. These results support the results obtained by small signal stability analysis.

Table 4.3 Transient stability index of cases 1-3

TSI	**Case 1**	**Case 2**	**Case 3**
η	65.3	62.87	64.77

The terminal voltage of G3 falls to 0.7 p.u. during the fault period and then recovered quickly to its normal value after the fault is cleared as indicated in Figure 4.5. However, in the case of the wind farm (both cases 1 and 2), the terminal voltage of DFIG falls to 0.4 p.u. during the fault period and then recovers to approximately 0.8 p.u. after fault clearance when the crowbar is still active. After the crowbar circuit is deactivated and the DFIG start to control active and reactive power, the terminal voltage of wind farm in scenario C recovers more quickly to its

predefined value after the crowbar is deactivated. This is due to the reactive power that is injected into the grid to maintain the terminal voltage of the wind farm at its nominal value.

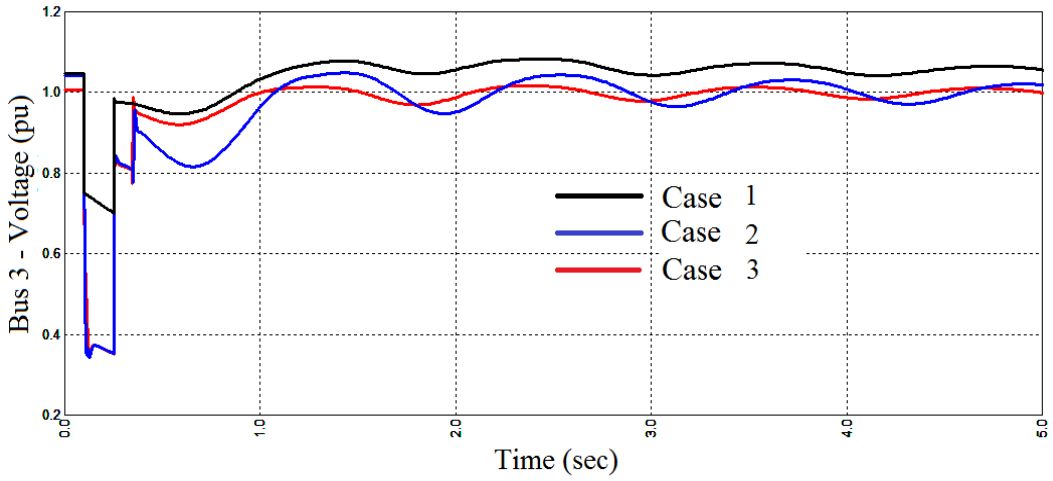

Figure 4.5 Simulation results of the terminal voltage (Bus 3) for the three cases

The reason behind the large fall in voltage in cases 2 and 3 is the lack of reactive power support from DFIG during the fault as shown in Figure 4.6 (a). SGs have the ability to inject reactive power over the whole fault period while DFIG based wind farm act as an induction generator and hence absorb reactive power leads to further voltage drop. After the fault and during the active crowbar time the induction generator absorbs a large amount of reactive power, this clarifies why the terminal voltage of the wind farm does not recover to its normal voltage after the fault clearance.

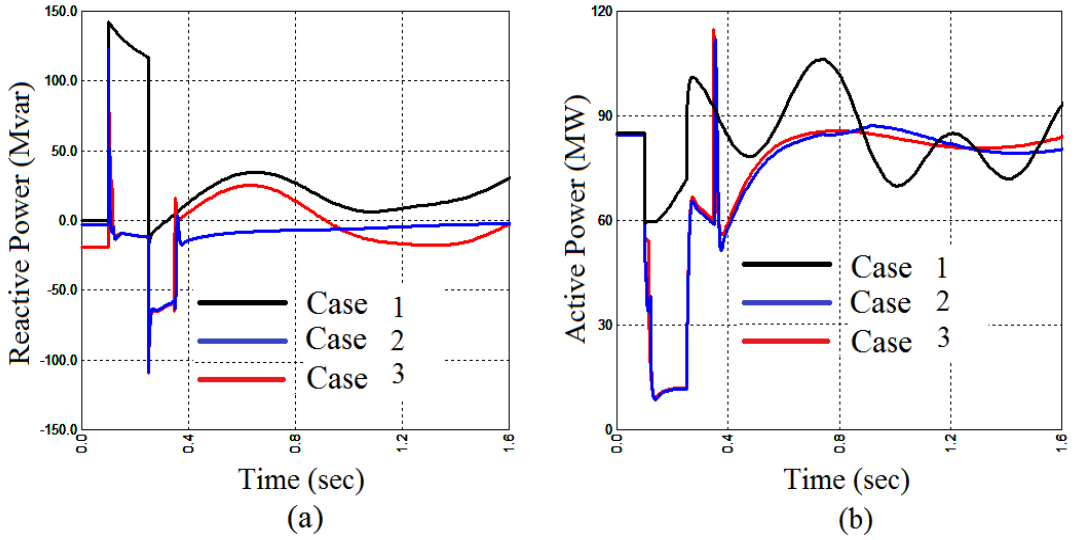

Figure 4.6 Simulation results of the (a) Generator's total reactive power, (b) Generator's total active power for the three cases.

Active power of G3 and DFIG based wind farm for each case can be seen in Figure 4.6 (b). The active power produced by DFIG in voltage control case is similar to the unity power factor case. However, the active power of wind farm cases and SG case are different during and after the fault is cleared. SG G3 is providing the grid with approximately 60 MW of active power during the fault period compared to just 12 MW injected from the wind farm. The active power of G3 after the fault oscillates because of its rotor inertial response. However, in the case of the wind farm, the active power output after the fault is relatively smooth.

The analysis and simulation results of previous cases clearly show that replacing a SG with a DFIG based wind farm has an adverse impact on the transient stability of the system, and the degree of the impact would depend on the control strategy used within the DFIG-RSC. The results of completed analysis demonstrate that although DFIG with voltage control can produce reactive power after crowbar deactivation time, both of unity power factor control and voltage control modes cannot provide any reactive power during active crowbar time. On the contrary, DFIG absorbs a large amount of reactive power leading to a severe voltage drop.

4.6.2 Transient Stability Analysis of the IEEE 39-bus System with Integration of DFIG Wind Turbines

IEEE 39-bus System is used to study the impact of DFIG wind turbine on power system transient stability as described in Section 4.5.2.

The analysis is carried out for three different cases, which are similar to the cases used to study small signal rotor angle stability:

- **Case 1:** SG case, this is a base case scenario in which all generators are considered to be conventional SGs without any PSS.
- **Case 2:** SG case with PSS, SGs G5, G7, G9 are equipped with (STAB1) PSS.
- **Case 3:** SGs G7 and G9, which are equipped with PSS, are replaced by DFIG wind farms controlled their terminal voltage at 1 p.u. (the reactive power is controlled to achieve a specified voltage value at the terminal bus).

To analyse the impact of wind power on IEEE 39-bus system transient stability, the three cases are simulated by a nonlinear simulation and therefore, the system has to be exposed to a significant disturbance such as a three-phase short circuit fault. The location of the disturbance is chosen to be near the most critical bus (bus 16). A 150 ms three-phase to ground permanent fault is applied at t = 0.1 s near critical bus 16 on transmission line 16–24. The fault was cleared by opening both sides of the faulted line simultaneously.

4.6.2.1 Results and Discussion

The rotor angles of each synchronous machine relative to the angle of largest SG G1, which is taken as a reference angle, are monitored. Figure 4.7 shows the rotor angles of G2 to G10 with respect to that of G1 in the first case where all PSSs are out of service. It is clear that the amplitude of the oscillation is increasing with time leading to system instability. As mentioned in the small signal stability analysis that

G9 is dominated the unstable oscillatory mode, G9 loses its synchronism after 11 s in the nonlinear transient stability simulation.

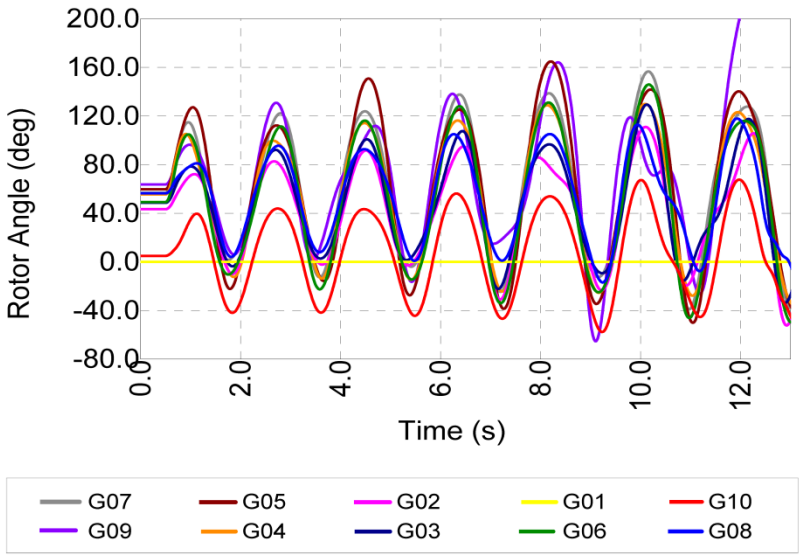

Figure 4.7 Rotor angles of SGs for case 1 (all generators without PSSs)

However, the system stability can be maintained by installing PSSs in G5, G7, and G9 as shown in Figure 4.8. This figure shows that rotor angle variation of the system in case 2 is better that in case 1. The unstable modes in the previous case, which are dominated by G1 and G9, are damped out by the installed PSSs leading to system stability. The steady state values of all rotor angles are reached in about 8 s as a result of PSSs damping torque.

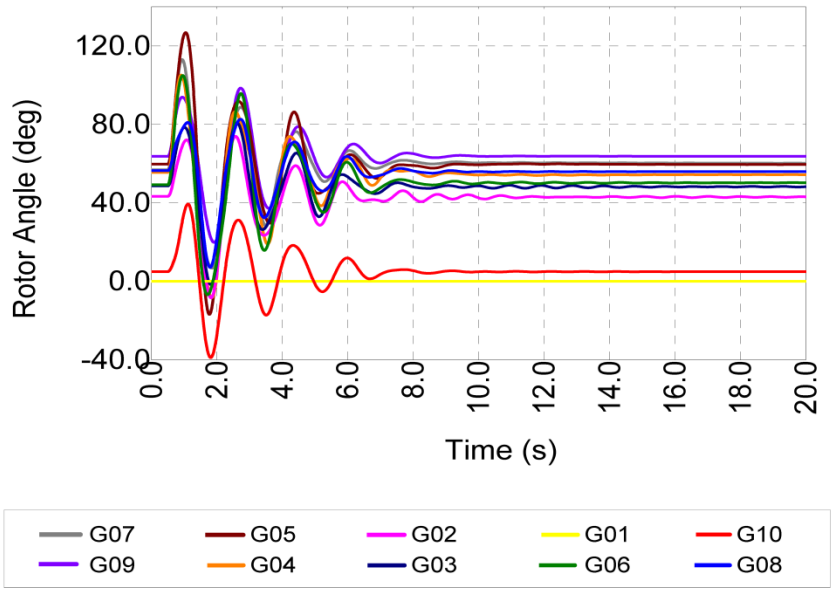

Figure 4.8 Rotor angles of SGs for case 2 (G5, G7, G9 are equipped with PSS).

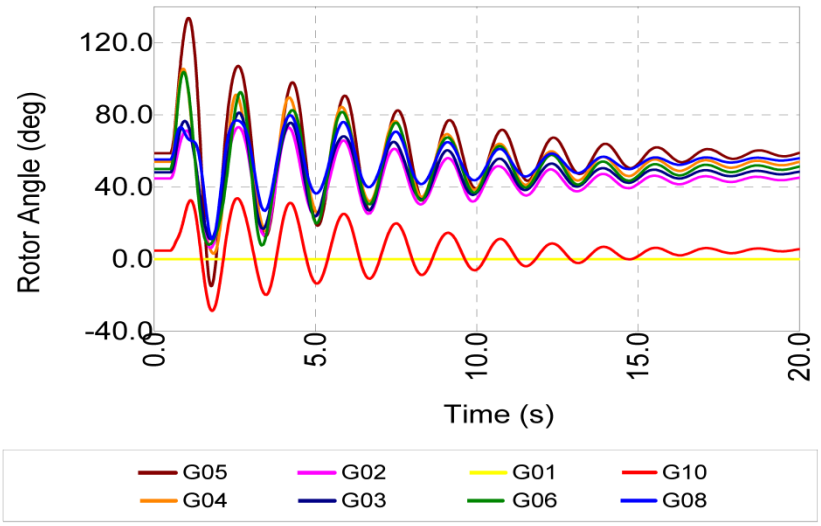

Figure 4.9 Rotor angles of each generator for case 3 (G7, G9 are replaced by an equivalent DFIG).

The rotor angles of each SG after G7 and G9 are replaced by two equivalent wind farms (case 3) are shown in Figure 4.9. The test system is affected adversely as a result of replacing the conventional SGs equipped with PSSs by an equivalent DFIG based wind farms. Due to the lack of damping torque provided by the replaced PSSs, the oscillations, in this case, last longer than those oscillations in case 2.

Moreover, a number of machines have larger rotor angle magnitudes than that in the second case. These results are similar to those obtained previously in the small signal stability analysis.

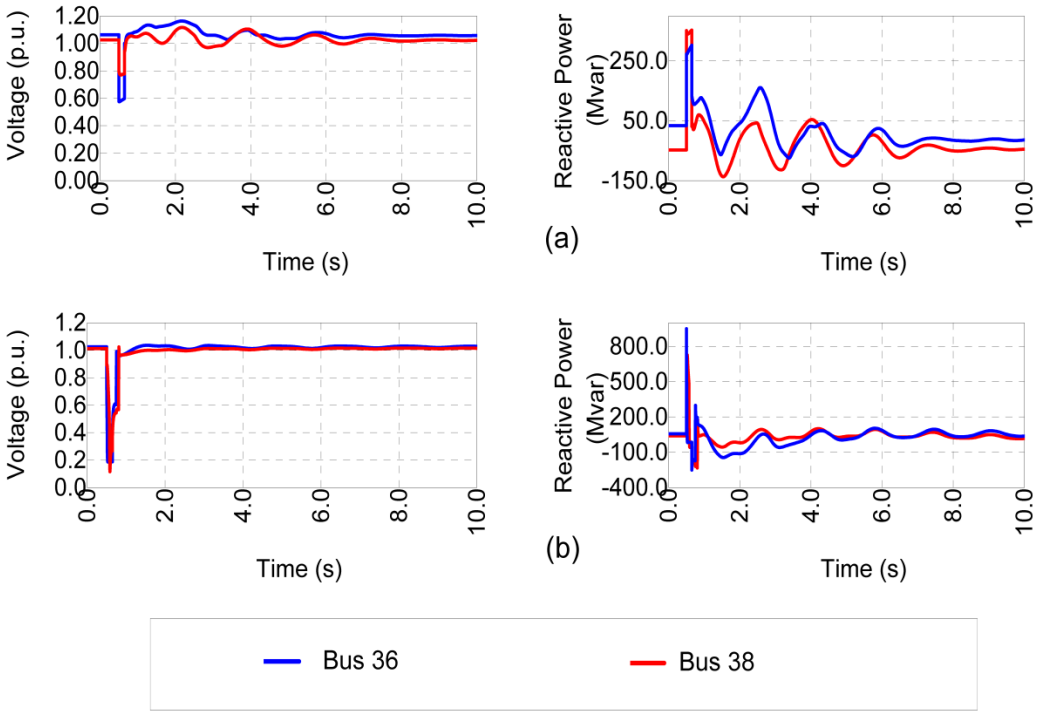

Figure 4.10 Transient responses of the studied system (a) (terminal voltages and reactive power of G7 and G9 in case 2), (b) (terminal voltages and reactive power of wind farm 1 &2 in case 3).

Figure 4.10 shows the terminal voltages of G7 (bus 36) and G9 (bus 38) for cases 2 and 3. In case 2, the terminal voltages of G7 and G9 fall to 0.6 p.u. and 0.77 p.u. respectively during the fault period and then recovered quickly to their normal values after the fault is cleared as indicated in Figure 4.10 (a). However, in cases 3, the terminal voltage falls to 0.2 p.u. during the fault period and then recovers to 0.6 p.u. after the fault clearance and when the crowbar is still active as shown in Figure 4.10 (b). The terminal voltage of both wind farms then recovered to their normal values after the crowbar is deactivated. It is clear that the terminal voltage of both G7 and G9 are variable after the fault period in comparison with the two wind farms, in which the terminal voltage is kept smooth after the crowbar deactivation. This is due to the fact that wind farms decoupled from the system and hence they did not contribute to the power system oscillations.

The SGs are producing approximately 300 MVAr each during the entire fault period, which in turn enables high voltage levels. Contrariwise, DFIG based wind farms absorb about 80 MVAr during the fault and 200 MVAr after the fault and during the operation time of the crowbar. This is for the reason that DFIGs crowbar will be activated following the short-circuit, and hence, the DFIG will operate as an induction generator.

Based on the results of small signal and transient stability analysis, damping of power system oscillations is reduced to some extent if a wind farm with DFIG replaced equivalent conventional SGs equipped with PSSs. Moreover, the terminal voltage of the SGs can be significantly reduced in the case of disturbance if the generator replaces by an equivalent wind farm due to the lack or reactive power during the disturbance.

4.7 Summary

In this chapter, wind power and power system stability were investigated. As the dynamic behaviour of power systems are highly influenced by the generators, the continuous increase of wind power integration into power systems can affect the stability of power systems, which currently becomes a very important issue. Therefore, investigate the effects of wind power integration on the three types of power system stability, which are rotor angle stability, frequency stability, and voltage stability, are discussed in this chapter.

The increased penetration of wind power indeed affects the stability of power system as the dynamic characteristics wind turbines are different from that of the SGs. Small signal stability is likely to be improved by wind power installation, particularly with fixed speed wind turbines due to the damping effect of the induction generator. However, power system transient stability is likely to be degraded with high penetration of wind power particularly fixed speed wind turbines. Similarly, large wind power penetration has a negative impact on power system voltage stability. Variable speed wind turbines have better voltage recovery than the fixed speed wind turbines since variable speed wind turbines are able to regulate reactive

power independently from the generated active power. Additionally, the increase of wind power penetration in electricity grid reduces the power system inertia, which is directly affecting frequency change rate.

To show the impacts of replacing SGs by equivalent DFIG based wind farms on rotor angle stability, two case studies were conducted on realistic power systems. The analysis and simulation results clearly show that replacing a SG by a DFIG based wind farm has a negative impact on transient stability of the power systems, and the degree of the impact would depend on the control strategy used within the DFIG-RSC. However, the impact on small signal stability depend on whether the replaced SG is fitted with PSS or not. Based on the results of small signal and transient stability analysis, damping of power system oscillations is reduced to some extent if a DFIG-based wind farm replaced an equivalent conventional SG.

Chapter 5

Proposed Control Approaches for DFIG

5.1 Introduction

The aim of this chapter is to develop control approaches for DFIG based wind farms to mitigate the impacts of high penetration of wind power on power systems small signal and transient stability. As the increase of wind power penetration continues, the impacts of wind power on power system stability will be significant. These effects have to be mitigated as wind power turbines should be able to contribute to network support and operation in order to keep the entire power system in stable condition. The most important contributions are fault ride through capability, power oscillations damping and voltage support capabilities during network disturbances. Poor damping of power oscillations and lack of reactive power support can deteriorate system stability and lead to blackouts.

Since DFIGs are not synchronously coupled to the power systems, the wind turbines do not produce any new electromechanical oscillations. However, damping of power system oscillations is reduced to some extent if a DFIG based wind farm replaced an equivalent conventional SG equipped with a PSS. This can be mitigated by equipping the DFIG wind turbines with PSSs. Moreover, as the ability of wind turbines to withstand network disturbances are very limited in comparison to conventional SGs, they are required to ride through grid disturbances and support the

grid voltage during and immediately after the grid disturbances. Therefore, a control approach to utilise the DFIG-GSC to provide reactive power support during grid faults is proposed.

5.2 Modal Analysis of Power Systems

In this section, the method used to assess power systems small signal stability is described, which is used to design power oscillations damping controller. As described in Chapter 4, small signal stability is the ability of the power system to remain synchronised after being subjected to a small disturbance. The equations of power system in small signal stability can be linearized for purposes of analysis as disturbances are considered small, for instance, small changes in load, which are frequently encountered in normal operation conditions.

Power systems can be described by sets of nonlinear ordinary differential-algebraic equations which can be represented in matrix format as follows [89]:

$$\dot{\mathbf{x}} = \mathbf{f}(\mathbf{x},\mathbf{u}) \tag{5.1}$$

$$\mathbf{y} = \mathbf{g}(\mathbf{x},\mathbf{u}) \tag{5.2}$$

where
$$\dot{\mathbf{x}} = \begin{bmatrix} \dot{x}_1 & \dot{x}_2 & \dots & \dot{x}_n \end{bmatrix}^T,\ \mathbf{x} = \begin{bmatrix} x_1 & x_2 & \dots & x_n \end{bmatrix}^T$$
$$\mathbf{u} = \begin{bmatrix} u_1 & u_2 & \dots & u_m \end{bmatrix}^T,\ \mathbf{f} = \begin{bmatrix} f_1 & f_2 & \dots & f_n \end{bmatrix}^T$$
$$\mathbf{y} = \begin{bmatrix} y_1 & y_2 & \dots & y_p \end{bmatrix}^T,\ \mathbf{g} = \begin{bmatrix} g_1 & g_2 & \dots & g_p \end{bmatrix}^T$$

In which **x** is a vector of *n* state variables, **u** is the vector of inputs to the system, *m* is the number of inputs, **f** is vector of non-linear equations, **y** is the vector of outputs, *p* is the number of outputs, and **g** is a vector of nonlinear functions relating state and input variables to output variables.

At equilibrium points, all the variables are constant and unvarying with time and therefore, (5.1) can be written as:

$$\dot{\mathbf{x}}_0 = \mathbf{f}(\mathbf{x}_0, \mathbf{u}_0) = \mathbf{0} \tag{5.3}$$

Where $\mathbf{X_0}$ is state vector and $\mathbf{U_0}$ is the input vector at the equilibrium point.

If small deviations from the equilibrium point (5.1) can be written as:

$$\dot{\mathbf{x}} = \dot{\mathbf{x}}_0 + \Delta\dot{\mathbf{x}} = \mathbf{f}\left[(\mathbf{x}_0 + \Delta\mathbf{x}), (\mathbf{u}_0 + \Delta\mathbf{u})\right] \tag{5.4}$$

As the deviation is a small, (5.4) can be expressed in terms of first order Taylor series expansion as follows:

$$\Delta\dot{\mathbf{x}} = \mathbf{A}\Delta\mathbf{x} + \mathbf{B}\Delta\mathbf{u} \tag{5.5}$$

where $\Delta\mathbf{x}$ is the incremental state vector of dimension n, $\Delta\mathbf{u}$ is the incremental input vector of dimension m, $\mathbf{A}$ is the state or plant matrix of size $n \times n$, and $\mathbf{B}$ is the control or input matrix of size $n \times m$.

$$\mathbf{A} = \begin{pmatrix} \frac{\partial f_1}{\partial x_1} & \cdots & \frac{\partial f_1}{\partial x_n} \\ \vdots & \ddots & \vdots \\ \frac{\partial f_n}{\partial x_1} & \cdots & \frac{\partial f_n}{\partial x_n} \end{pmatrix}, \quad \mathbf{B} = \begin{pmatrix} \frac{\partial f_1}{\partial u_1} & \cdots & \frac{\partial f_1}{\partial u_m} \\ \vdots & \ddots & \vdots \\ \frac{\partial f_n}{\partial u_1} & \cdots & \frac{\partial f_n}{\partial u_m} \end{pmatrix} \tag{5.6}$$

Similarly, (5.2) can be written as:

$$\Delta\mathbf{y} = \mathbf{C}\Delta\mathbf{x} + \mathbf{D}\Delta\mathbf{u} \tag{5.7}$$

where $\Delta\mathbf{y}$ is the incremental output vector of dimension p, $\Delta\mathbf{u}$ is the incremental input vector of dimension m, $\mathbf{C}$ is the observation (output) matrix of size $p \times n$, and $\mathbf{D}$ is the feed-forward matrix of size $p \times m$.

$$\mathbf{C}=\begin{pmatrix} \frac{\partial g_1}{\partial x_1} & \cdots & \frac{\partial g_1}{\partial x_n} \\ \vdots & \ddots & \vdots \\ \frac{\partial g_p}{\partial x_1} & \cdots & \frac{\partial g_p}{\partial x_n} \end{pmatrix}, \quad \mathbf{D}=\begin{pmatrix} \frac{\partial g_1}{\partial u_1} & \cdots & \frac{\partial g_1}{\partial u_m} \\ \vdots & \ddots & \vdots \\ \frac{\partial g_n}{\partial u_1} & \cdots & \frac{\partial g_n}{\partial u_m} \end{pmatrix} \tag{5.8}$$

5.2.1 Eigenvalues and Eigenvectors

In the linearized power system state space model, calculation of the eigenvalues of the system matrix **A** are required which are given by the values of the scalar parameter λ for which there exist non-trivial solutions to the following equation:

$$\mathbf{A\Phi} = \lambda\mathbf{\Phi} \tag{5.9}$$

where $\boldsymbol{\phi}$ is $n\times1$ vector

For any eigenvalue λ_i, the n-column vector $\boldsymbol{\phi}$ that satisfies (5.9) is called the right eigenvector of A associated with the eigenvalue λ_i. The right eigenvector is related to the mode shape, and it expresses the relative distribution of the mode through the system dynamic states. Information about the observability of the associated mode in the state variable can be extracted from the right eigenvector.

Similarly, there exists a left eigenvector, a $1\times n$ row vector $\boldsymbol{\psi_i}$ which satisfies λ_i is:

$$\boldsymbol{\psi}_\mathbf{i}\,\mathbf{A} = \boldsymbol{\psi}_\mathbf{i}\lambda_i \tag{5.10}$$

Information about the states distribution within any mode can be given by left eigenvector associated with that mode. Modes that excited by a particular input are directly affected by left eigenvector, which can measure the controllability of the associated mode.

The left and right eigenvectors related to various eigenvalues are orthogonal. This is mean that, if λ_i is not equal to λ_j then

$$\mathbf{\Phi_i \psi_j} = 0 \quad , i \neq j \tag{5.11}$$

If the eigenvectors corresponding to the same eigenvalue, then

$$\Phi_\mathbf{i} \mathbf{\psi_j} = \mathbf{C_i} \tag{5.12}$$

where $\mathbf{C_i}$ is a constant and non-zero. In practice, it is a common to normalise these vectors so that

$$\Phi_\mathbf{i} \mathbf{\psi_j} = 1 \tag{5.13}$$

The modal matrices $\boldsymbol{\phi}$, and right-left eigenvectors $\boldsymbol{\psi}$ are formed as follows

$$\Phi = \begin{bmatrix} \phi_1 & \phi_2 & \dots & \phi_n \end{bmatrix} \tag{5.14}$$

$$\boldsymbol{\psi} = \begin{bmatrix} \psi_1^T & \psi_2^T & \dots & \psi_n^T \end{bmatrix}^T \tag{5.15}$$

$$\boldsymbol{\psi\Phi} = \mathbf{I}, \quad \boldsymbol{\psi} = \Phi^{-1} \tag{5.16}$$

The behaviour of a mode λ_i as a function of time is expressed by (5.17) [160]

$$e^{\lambda_i t} \tag{5.17}$$

From equation (5.17), it is clear that real eigenvalues corresponding to a non-oscillatory mode where a negative value represents a decaying mode determined by its magnitude and positive real eigenvalues will lead to increasing amplitude. Complex eigenvalues occur only in conjugate pairs and correspond to oscillatory modes.

$$\lambda = \sigma \pm j\,\omega \tag{5.18}$$

where σ is the real component that provides damping and ω is the complex component that gives the frequency of oscillation in rad/s.

To determine the oscillation amplitude damping rate, the following formula is used

$$\zeta = \frac{-\sigma}{\sqrt{\sigma^2 + \omega^2}} \tag{5.19}$$

where ζ is the damping factor of a mode

Stability of a power system can be determined by the sign of the real part of eigenvalues. It is clear that if any eigenvalue has a positive real part, the power system is unstable. Similarly, eigenvalues with negative parts can lead to system instability if the damping factor is small. The oscillation frequency is calculated from the eigenvalues imaginary part while the real part can give information about the damping ratio. The damping ratio indicates the stability degree of a power system as the high positive value of a damping ratio indicates the system is more stable. Power systems with eigenvalues with high damping factors can restore steady state operation quickly following disturbances.

In this thesis, Neplan software [157] is used to linearize and calculate eigenvalues and eigenvectors of the test power systems.

5.2.2 Participation Factors

Participation factor is used to measure the degree of participation of a state in a mode. For state variable *j* in any selected mode *i*, the participation factor can be calculated as follows [161]:

$$\mathbf{P}_{ji} = \Phi_{ji}\ \boldsymbol{\psi}_{ij} \tag{5.20}$$

where $\mathbf{P_{ij}}$ is the participation factor, $\boldsymbol{\phi_{ji}}$ is the j^{th} entry of the i^{th} right eigenvector and $\boldsymbol{\psi_{ij}}$ is the j^{th} entry of the i^{th} left eigenvector.

The degree of i^{th} eigenvalue to changes in the j^{th} diagonal element of the **A** matrix can be measured by the participation factors which are associated completely with the mode. Inputs and outputs are not included in participation factors, which deal only with system state variables [162].

5.2.3 Modal System Representation

The power system linearized model expressed in (5.5) (5.7) is defined by state variables which are cross-coupled. A different description of the linearized power system model can be achieved by using modal transformation including the use of right eigenvector matrix. This linearized power system model is described by uncoupled modal state variables. The modal transformation between the state variables and the modal variables can be as follows:

$$\mathbf{\Delta x = \Phi z} \tag{5.21}$$

where $\mathbf{\Delta x}$ is state variables, $\boldsymbol{\phi}$ is the modal transformation matrix, and **z** is a vector of modal variables.

By substituting (5.21) in the equations (5.5) and (5.7)

$$\mathbf{z^{\cdot} = Fz + G\Delta u} \tag{5.22}$$

$$\mathbf{\Delta y = Hz + D\Delta u} \tag{5.23}$$

where $$\mathbf{F = \Phi^{-1}A\Phi} \tag{5.24}$$

$$\mathbf{G = \Phi^{-1}B = \psi B} \tag{5.25}$$

$$\mathbf{H = C\Phi} \tag{5.26}$$

Matrixes **F**, **G**, and **H** can be defined as follows [89]:

- Matrix **F** is a diagonal matrix, whose diagonal elements are the eigenvalues of **A**.
- Matrix **G** is referred to as the mode controllability matrix defines how controllable a mode is through a given input. If G_{ij} is equal to zero, then the j^{th} input will have no effect on the i^{th} mode.
- Matrix **H** is referred to as the mode observability matrix which defines how observable a mode is in a given output. If the element H_{ki} is equal to zero, then the i^{th} mode cannot be observed in the k^{th} output.

By applying the modal transformation to the transfer function representation of the linearised power system after applying Laplace transform to (5.5) and (5.7), and by assuming the feed-forward matrix **D** is zero since it has no effect on system modes and to simplify the analysis then will get [1], [163]:

$$G(s) = \sum_{i=1}^{n} \frac{R_i}{s - \lambda_i} \tag{5.27}$$

Where R_i is the open loop residual of the system transfer function.

Residual values have information of both modal observability for a given output and controllability through a given input.

5.3 Damping Controller Design

This section presents the design of a controller for DFIG based wind turbines to improve the damping of power system oscillations. The main function of the damping controller is to damp low-frequency power oscillations between 0.1 and 2 Hz, which are identified as local or inter-area modes, by adding an additional stabilising signal to compensate for undamped oscillations [164]. The widely used conventional PSS is used in this study as shown in Figure 5.1. It is a supplementary control device, which is connected to generator excitation systems.

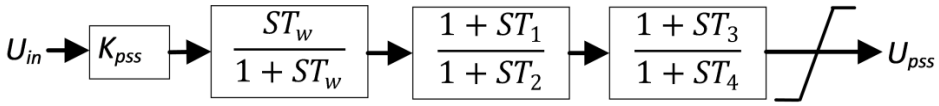

Figure 5.1 Power system stabiliser structure

The conventional PSS consists of a stabiliser gain K_{pss}, a washout filter with time constant T_w (s), a second-order lead-lag compensator with time constants T_1 *to* T_4 (s), and an output limiter. The gain determines the amount of damping introduced by the damping controller. The single washout filter with time constant $T_w = 5$ s is a high pass filter used to allow a certain range of frequency and is anticipated to be active only through transient periods. The two-stage compensator block provides an appropriate lead- lag phase of the output signal in order to enhance the damping of power system oscillations. The limiter is used to assure that the output signal is under the control limits. In this study, the values of the limiter are set to ±0.1 p.u. The transfer function of the PSS can be expressed by [165]:

$$u_{pss} = K_{pss}\left(\frac{ST_w}{1+ST_w}\right)\left(\frac{1+ST_1}{1+ST_2}\right)\left(\frac{1+ST_3}{1+ST_4}\right)u_{in} \tag{5.28}$$

where u_{in} and u_{pss} are input and output signals of the controller respectively, K_{pss} is the gain, T_w is a washout time constant (seconds) and T_1 to T_4 are time constants of the lead-lag compensator (seconds).

In this thesis, a PSS is used for DFIG wind turbines to damp power system oscillations as conventional SGs do [60, 166]. The output signal of PSS is attached to the reactive power controller within RSC to help to increase the damping torque by controlling the reactive power produced by DFIG as shown in Figure 5.2. The amplitude of oscillations can be reduced by changing the DFIG terminal voltage during the forward or the backward swing.

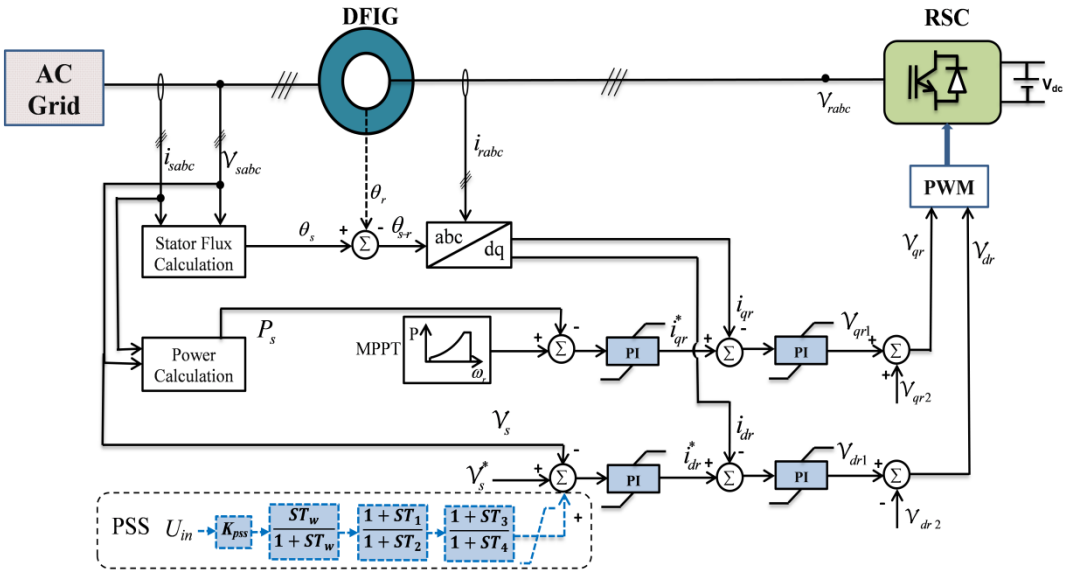

Figure 5.2 Proposed PSS (dashed blue lines) attached to DFIG-RSC.

In order to enhance the damping of the poorly damped low-frequency oscillations, critical oscillatory modes have to be modified. Therefore, the poorly damped oscillatory modes must be excited by the chosen input signal and have to be visible in the chosen output signal. Input signals with a higher magnitude of residual are more effective for damping the oscillatory modes [167].

Residual approach, which has been used for designing PSSs in SGs, can also be used for designing PSSs for DFIG based wind turbines. The feedback signal and phase angle that needs to be compensated can be determined by the residual approach. The residual is a comprehensive index that measures the degree to which the selected mode is influenced by the controller.

Considering the control system as shown in Figure 5.3 in which the control output Δy is sent back to the controller input signal Δu through a block filter $H(s)$, which has gain K from [168]:

$$\frac{d\lambda_i}{dk} = H(\lambda_i)R_i \tag{5.29}$$

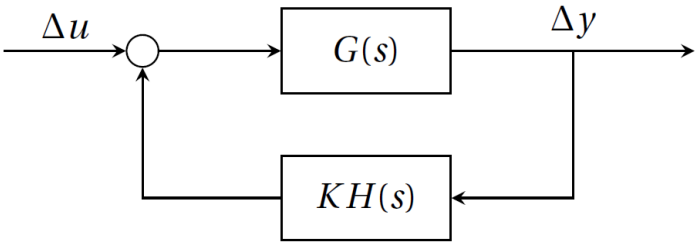

Figure 5.3 Generic control System

The residual R_i corresponding to a particular eigenvalue i_{th} for a transfer function between a selected input u and output y can provide a measure of the mode's sensitivity to the feedback control. Therefore, the residual method can give an indication of how the modes will be affected by the feedback control. Moreover, the residual is a complex value, and thus, the angle gives the direction in which the root locus leaves the associated pole. Hence, the required phase compensation between the input and output of PSS can be calculated by the residual angle to give a positive contribution to the damping of the selected mode [169]. Figure 5.4 shows a schematic illustration of the required phase compensation, where $\angle Ri$ represents the phase angle of residual R_i and $\angle Hi$ represents the PSS transfer function phase angle respectively.

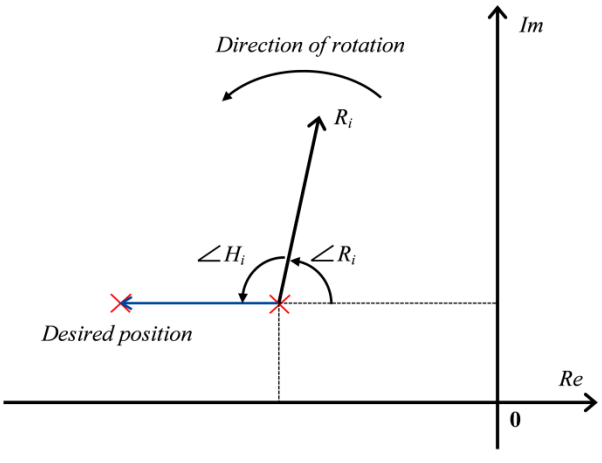

Figure 5.4 Schematic illustration of compensation concept.

As DFIG wind turbines are to some degree decoupled from the rest of the grid, the produced active power and the machine speed signals of DFIG wind turbines are not sensitive to the system oscillations. Moreover, these two signals are affected by tower shadow and torque variations. To avoid the use of wide area communications, the available local signals such as the deviations of the DFIG based wind farm terminal voltage and frequency are examined using residual analysis. The mode's sensitivity to the input signal of PSS can be provided by the residual of any specific mode. In [89], detailed information about how to calculate the residual from a transfer function is given. The required phase angle compensation and the time constants can be taken from [162]:

$$\varphi_{comp} = 180^{\mathrm{O}} - \angle Ri \tag{5.30}$$

$$\alpha_c = \frac{T_{lead}}{T_{lag}} = \frac{1-\sin\left(\frac{\varphi_{comp}}{m_c}\right)}{1+\sin\left(\frac{\varphi_{comp}}{m_c}\right)} \tag{5.31}$$

$$T_{lag} = \frac{1}{\omega_i \sqrt{\alpha_c}}, \quad T_{lead} = \alpha_c T_{lag} \tag{5.32}$$

$$m_c = \frac{\varphi_{comp}}{55^\circ} = \begin{cases} 1 & \varphi_{comp} \le 55^\circ \\ 2 & \varphi_{comp} \le 110^\circ \\ 3 & 110^\circ \angle \varphi_{comp} \le 180^\circ \end{cases} \tag{5.33}$$

where φ_{comp} is the required phase angle compensation given in degrees, $\angle Ri$ represents the phase angle of residual R_i and m_c represents the number of lead-lag blocks which are defined according to φ_{comp}.

As time constants of the lead-lag compensator have been defined, the following stage is to set the PSS gain K_{pss}. The gain of the controller is set to the minimum value that fulfils the requirement damping for the selected mode that to be damped. In this work, the PSS gain K_{pss} is chosen using data scanning tool of the software used in which the gain is increased incrementally and is recorded against the selected mode.

As the DFIG is partly decoupled from the grid by the partially rated converters, the power and rotational speed signals of DFIG wind turbines are less sensitive to grid oscillations. Moreover, these signals are influenced by torque variations due to tower shadow. Therefore, the available local signals are carefully chosen as PSS input signal to avoid the use of wide area communications.

Different approaches can be used to select the best feedback signal to damp power system oscillations [170-174]. A good method reported in [170, 173, 174] is the residual method mentioned earlier in this chapter. Based on residual analysis results, frequency deviation signal is carefully chosen for successful damping of oscillations. The output signal of the PSS is connected to the DFIG-RSC reference voltage signal as can be seen in Figure 5.2.

5.3.1 Designing DFIG-PSS for IEEE 9-bus Test System

The results of detailed small signal stability analysis conducted in Chapter 4 on IEEE 9-bus test system show that there is a critical mode with damping factor less than 5%. The critical mode (-0.306 ± 7.734) oscillating at 1.231 Hz with a damping factor of 3.9%. To move this critical mode away from the right-hand side of the complex plane the DFIG has to be fitted with a PSS. The proposed PSS is fitted to the reactive power control loop as mentioned previously.

To calculate the residual's phase angle $\angle Ri$ of the critical mode, the PSS is only implemented with a constant gain K_{pss} and washout filter with time constant $T_w = 5s$. No phase compensation blocks are involved at this stage. For different gain values, the critical mode must move in a straight line direction, as defined by the residual.

The analysis was performed under the cases were K_{pss} ranges from 0 to 50 with step of 5. The corresponding locations of the eigenvalues associated with the critical mode were recorded, and the results are displayed on Figure 5.5.

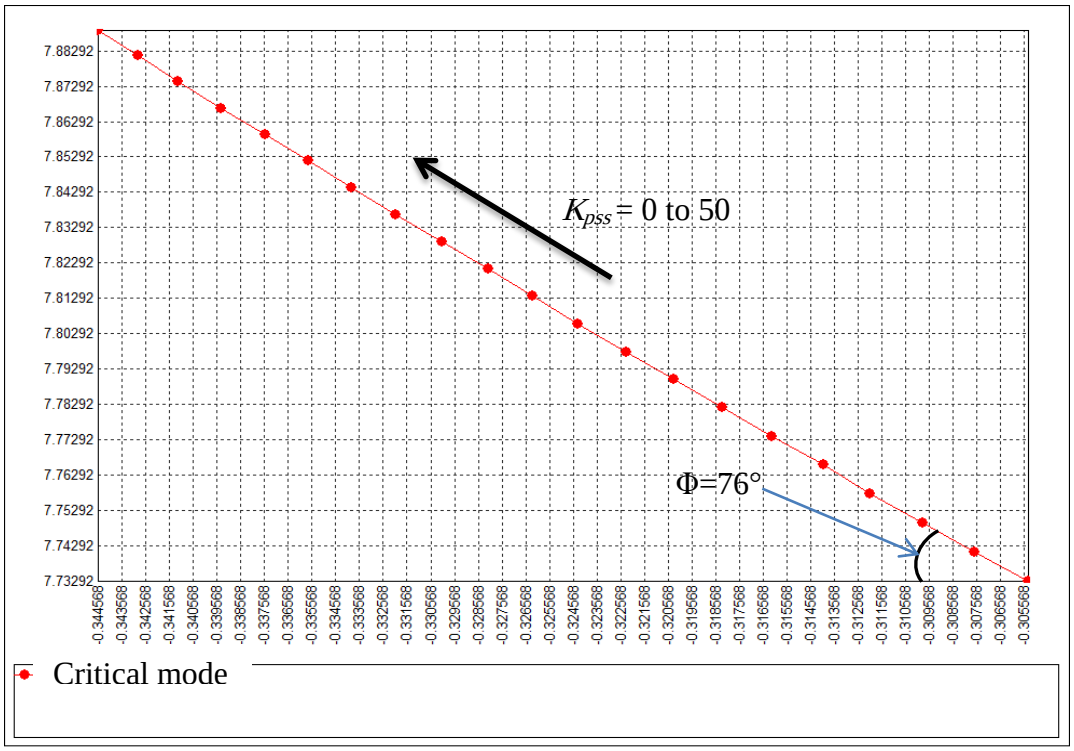

Figure 5.5 Residual's phase angle estimation for DFIG-PSS design

The required phase angle compensation was estimated to be 76° as shown in Figure 5.5. In this case, the phase compensation blocks have to introduce a phase shift of -76° as the applied feedback is positive instead of negative. The phase shift has to be introduced at 1.231Hz = -1.326 rad/s (the frequency of the critical mode).

As φ_{comp} is larger than 55° the number of lead-lag compensation blocks has to be two. Employing equations (5.31) and (5.32) the transfer function of the positive feedback are found to be:

$$u_{pss} = K_{pss}\left(\frac{5S}{1+5S}\right)\left(\frac{1+0.06308S}{1+0.26497S}\right)\left(\frac{1+0.06308S}{1+0.26497S}\right)u_{in} \qquad (5.34)$$

To define the value K_{pss} , the gain increased incrementally from 0 to 200 and recorded against the mode. The best gain of 170 was obtained against the mode (-0.967 ± 7.964). As a result, the completed transfer function of the positive feedback will be:

$$u_{pss} = 170\left(\frac{5S}{1+5S}\right)\left(\frac{1+0.06308S}{1+0.26497S}\right)\left(\frac{1+0.06308S}{1+0.26497S}\right)u_{in} \tag{5.35}$$

5.4 Reactive Power Support

When the terminal voltage at the DFIG decreases rapidly to a low level as a result of a close grid fault, a large current can occur in stator windings due to the stator's direct connection to the rest of the grid. The machine fluxes are forced to change suddenly leading to high rotor currents due to the magnetic coupling between the stator and the rotor. These currents can damage the DFIG-RSC. Therefore, in modern wind turbines, DFIG crowbar system is activated when overcurrent exists in the rotor windings. The crowbar system consists of a set of three-phase series resistances connected to the rotor windings [50].

Following the short circuit, the crowbar will be activated and hence the DFIG will work as an induction generator. In this case, a large amount of reactive power will be absorbed from the grid by the induction generator. The crowbar resistance should be high enough to limit the short-circuit rotor current, and it should be low enough to avoid excessive voltage in the rotor circuit. Therefore, the crowbar resistance must be chosen carefully. After the fault is cleared out, a delay time of 60 ms to 120 ms is needed to allow the machine flux transients to settle. Then the crowbar can be switched off, and the RSC goes back to normal operation to control the DFIG [175].

Since the RSC is deactivated during large transient disturbances, the GSC can be used as a STATCOM, as can be seen in Figure 5.6, to produce reactive power. The reactive power that can be produced by DFIG-GSC is limited by the rating of the converter. The GSC is similar to the traditional voltage source converter (VSC)

based STATCOM, which consists of a VSC and a DC capacitor. The control system of STATCOM is based on the standard *d-q* vector control scheme. The main objective of the STATCOM control circuit is to maintain the voltage of the DC capacitor constant and to regulate the interchanged reactive power between the converter and the grid. The detailed model of STATCOM can be found in [176], [177]. The control circuit of STATCOM is very similar to that already installed in the GSC. The same DC voltage control loop, which maintains the DC voltage constant in GSC, can be used without any modification to maintain the DC voltage of the STATCOM constant. The reactive power control loop, which controls reactive power flowing between the grid and the GSC, can be used without any change to produce the maximum reactive power of the GSC. It can also be used to regulate the DFIG terminal voltage when the switch (SW) is in position 2 in Figure 5.7.

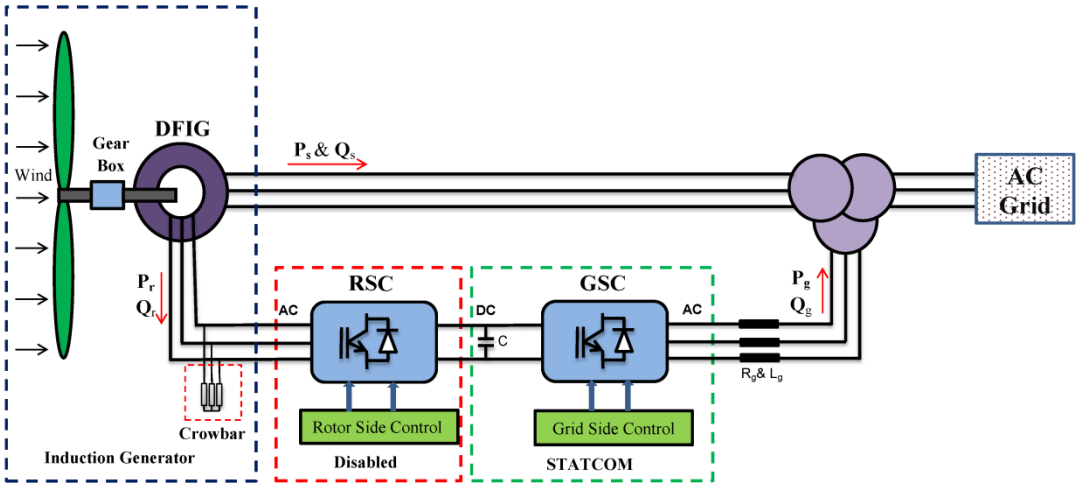

Figure 5.6 General structure of modelling DFIG-GSC as STATCOM.

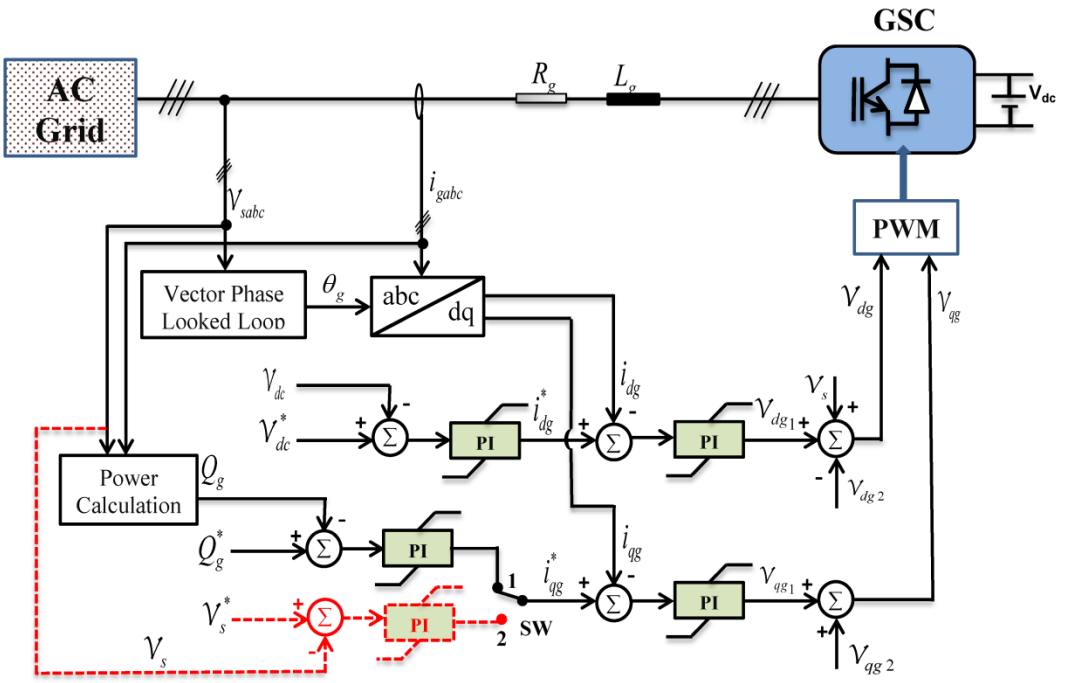

Figure 5.7 Overall vector control scheme of the GSC and STATCOM mode with red dashed lines.

During normal operation conditions, the RSC controls independently the stator active and reactive power, whilst the GSC independently controls the DC voltage and the exchange of reactive power between the GSC and the grid. The GSC is usually operated at a unity power factor to allow the rated rotor slip power to be exchanged through the converter. When the crowbar is activated, the rotor windings are short-circuited through the crowbar impedance and the RSC is deactivated. Since the GSC is decoupled from the rotor windings, there is no need for it to be disabled and hence can be used as STATCOM as long as the RSC is deactivated. The necessary time for the RSC to be blocked can be less than 1 ms [17]. Therefore, once the crowbar is triggered the set point of the GSC reactive power ($Q^*_{g)}$ can be changed to 1 p.u. to deliver its maximum reactive power or change the position of the switch (SW) to position 2 to regulate the terminal voltage. The reactive power that can be delivered from STATCOM mode is limited by the rating of GSC, which is about 30% of DFIG rating. The synchronisation of the RSC can be established after the fault and during the crowbar active time. When the crowbar is deactivated, the RSC is activated, and

the set point of the GSC reactive power is set back to zero or change the switch position back to 1 for normal operation condition.

5.5 Summary

This chapter has presented the proposed control approaches of DFIG wind turbines to mitigate the impacts of high penetration of wind power on power systems small signal and transient stability.

The chapter began by presenting power systems modal analysis and how models of nonlinear power systems can be linearised in order to perform small signal stability analysis from which power oscillations damping controller is designed. Residual approach, which has been used for designing PSSs in SGs, is used in this thesis to design DFIG stabiliser controller. The designed PSS will be assessed in next chapter when a DFIG based wind farm replaced an equivalent SG. Finally, a control approach to utilise the DFIG-GSC to provide reactive power support during grid faults is discussed in this chapter.

Chapter 6

Enhancement of Rotor Angle Stability by Utilising the DFIG Reactive Power using the Proposed Approaches

6.1 Introduction

With the continuous increasing integration of DFIG wind turbines into power systems, the overall power system performance can be influenced, and thus power system stability becomes a very important subject. Therefore, investigating the effects of DFIG wind turbines integration on the stability of existing conventional SGs is becoming an important issue in order to identify potential impacts and to develop measures to lessen those impacts.

This chapter provides illustrations of the impacts of replacing conventional SGs with equivalent DFIG wind farms on rotor angle stability of power systems and mitigate these impacts by the proposed control approaches described in Chapter 5. The effectiveness of the proposed control methods are examined in both standard Western System Coordinating Council (WSCC), which is known as IEEE 9-bus test system and the widely used New England 10-machine 39-bus system. Small and transient stability analysis are conducted on each test system without and with wind generation to show the impacts of replacing a SG by an equivalent DFIG wind turbine

on rotor angle stability of each system. Then the integrated DFIG wind turbines are equipped with the proposed control strategies to show how effective they are to improve rotor angle stability of the test system. Moreover, the capability of the proposed conventional fixed parameters PSS to damp power oscillations effectively under non-uniform variable wind speeds across the wind farm is assessed in multi-machines power system with two large wind farms.

6.2 Using IEEE 9-bus Test System to Evaluate Rotor Angle Stability using the Proposed Approaches

To investigate the effect of DFIG based wind farm on the power system rotor angle stability, a DFIG based wind farm is connected to the IEEE 9-bus test system. The test system has been described previously in Chapter 4, and its full static and dynamic data can be found in [178]. In this section, five different cases are analysed by small signal and transient stability to show the impact of DFIG on power systems rotor angle stability and how the disturbance can be mitigated by the proposed control strategies. The description of each case is as following:

- **Case 1**: SG case; this is a base case in which the three generators are conventional SGs where the three generators are equipped with an IEEE type 1 exciter and G1, G2 are equipped with turbine governor type TGOV1.
- **Case 2**: fixed unity power factor control mode (no reactive power injected into the system from DFIG). In this case, G3 is replaced by equivalent DFIG based wind farm. The single machine 85 MW wind farm was aggregated from 17 turbines of 5 MW each to achieve an equivalent generated power to replace SG G3, which is accounted as 27% of the consumed total power of the test system.
- **Case 3**: voltage control mode; to show the impact of reactive power on rotor angle stability, the wind farm operates to maintain its terminal voltage at 1 p.u. In this case, G3 is replaced by equivalent DFIG based wind farm with a voltage control mode.

- **Case 4**: STATCOM control mode; the use of DFIG-GSC as STATCOM control strategy, as explained in Chapter 5, will be investigated in this case.
- **Case 5**: DFIG-PSS; the DFIG will be equipped with the proposed PSS, as explained in Chapter 5.

6.2.1 Small signal stability analysis

A detailed small signal stability study on the test system was conducted for each case. The system eigenvalues for each case are shown in Figure 6.1. The system is stable for all cases as there are no modes in the right-hand side of the complex plane. However, there is a critical eigenvalue with damping factor less than 5% in the first three cases (case 1, 2 and 3). The critical mode is at its lowest damping factor in case 1, then improved slightly when the G3 is replaced by an equivalent wind farm but its damping factor is still less than 5% for cases 1 and 2.

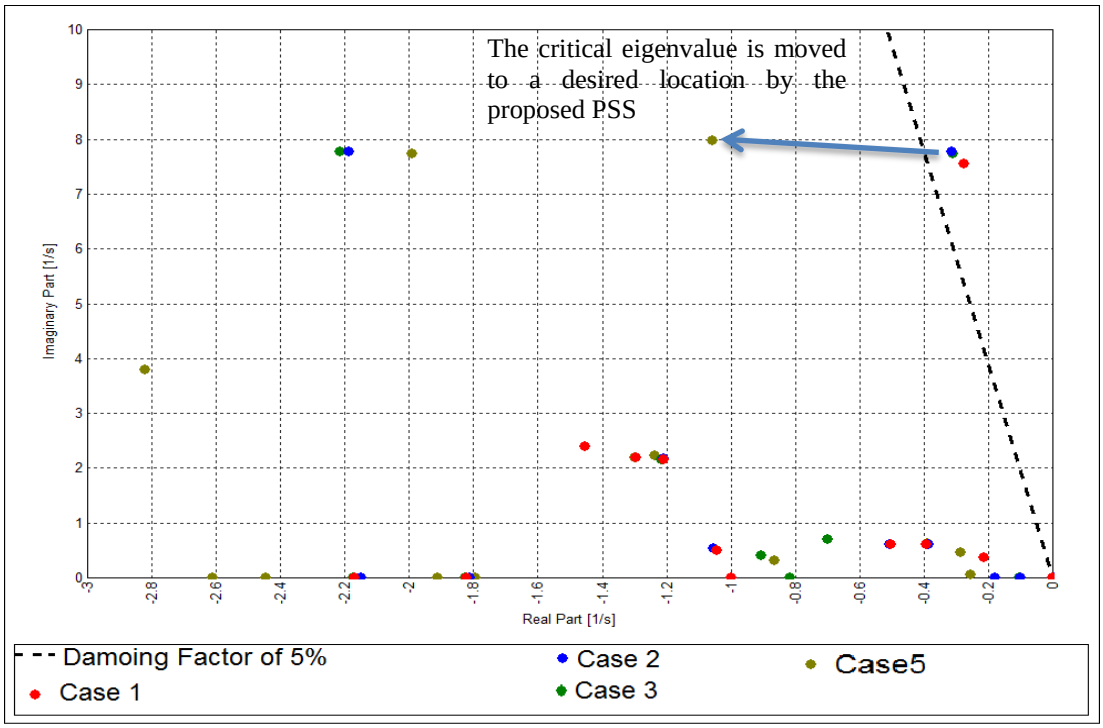

Figure 6.1 Overview of the complex plane with the test system eigenvalues for cases 1,2,3,5

However, the system is much more stable when the proposed PSS is attached to the DFIG based wind farm. The critical mode moved away from the right-hand side to the left of the complex plane leading to a more stable system. The damping factor of the critical mode improved beyond 5% as a result of fitting the wind farm with the proposed PSS.

The dominant eigenvalue and their frequency, damping factor, main machine and the participation factor for each main state variable for each case are shown in Table 6.1. The critical mode for each case is dominated by rotor angle ρ and speed ω of generator G2. The frequency of each mode is relatively unchanged for each case. However, rotor angle oscillation of case 5 is much more stable than other cases. The damping factor of the main mode is improved slightly from 3.5% to 3.8% when the SG is replaced by an equivalent wind farm. This improvement is further enhanced slightly to 3.9% when the voltage at the connection point is regulated by the wind farm. However, with the proposed PSS, the damping factor of the main mode increased significantly from 3.9% (without PSS) to 12% (with PSS). These results indicate that rotor angle stability of the system is enhanced due to the effectiveness of the proposed PSS.

Table 6.1 Main electromechanical modes of case 1 (SG case), case 2 (G3 is replaced by DFIG based wind farm operating at fixed unity power factor), case 3 (G3 is replaced by DFIG based wind farm controlled its terminal voltage at 1 p.u.), and case 5 (the DFIG is equipped with the proposed PSS).

Cases	**Case 1**	**Case 2**	**Case 3**	**Case 5**
Eigenvalue $\lambda = \sigma + j\omega$ (p.u.)	-0.265 ±j7.615	-0.297±j7.778	-0.306 ± 7.734	-0.967 ± 7.964
Frequency f (Hz)	1.212	1.238	1.231	1.268
Damping Factor ζ (%)	3.5	3.8	3.9	12
Dominant variable	ρ, ω	ρ, ω	ρ, ω	ρ, ω

Cases	Case 1	Case 2	Case 3	Case 5
Dominant Machine	G2	G2	G2	G2
Participation factor (%)	35.8, 37.5	40.3, 42.1	40.2, 42.3	48.3, 50.8

The used PSS is designed in Chapter 5, and its parameters are given in the following equation:

$$u_{pss} = 170\left(\frac{5S}{1+5S}\right)\left(\frac{1+0.06308S}{1+0.26497S}\right)\left(\frac{1+0.06308S}{1+0.26497S}\right)u_{in} \tag{6.1}$$

6.2.2 Transient stability analysis

The result of small signal stability study shows G2 has the highest participation factor. Therefore, the location of the disturbance has to be near G2. A disturbance lasting 150 ms of a 3-phase to ground fault was imposed near Bus 7 on line 5-7 as shown in Figure 6.2. The fault was cleared by opening both sides of the faulted line simultaneously.

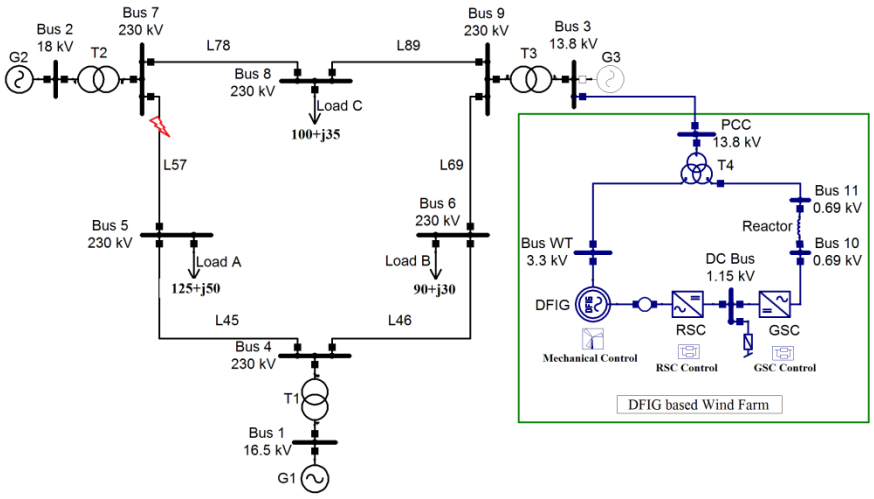

Figure 6.2 Test system with DFIG based wind farm

In order to assess the effect of DFIG based wind farm on transit stability of the test system, rotor angle of each generator is observed, from which the transient stability index is calculated. The terminal voltage of the replaced SG (Bus 3), active, and reactive power are also monitored. The angle of the largest SG G1, which is the slack generator, was taken as a reference angle.

Rotor angle oscillation of the G2 relevant to G1 for the first three cases is shown in Figure 6.3. The figure shows that rotor angle variation of the G2 when G3 is replaced by a wind farm with an equivalent size has a larger rotor angular swing than that in the base case. Therefore, replacing SG by equivalent DFIG based wind farm has a negative impact on transient stability of power systems. However, there is an improvement when the DFIG based wind farm controls its terminal (case 3). This indicates that DFIG reactive power can be used to reduce the deviations between synchronous machines rotor angles and consequentially enhancing the power system rotor angle stability.

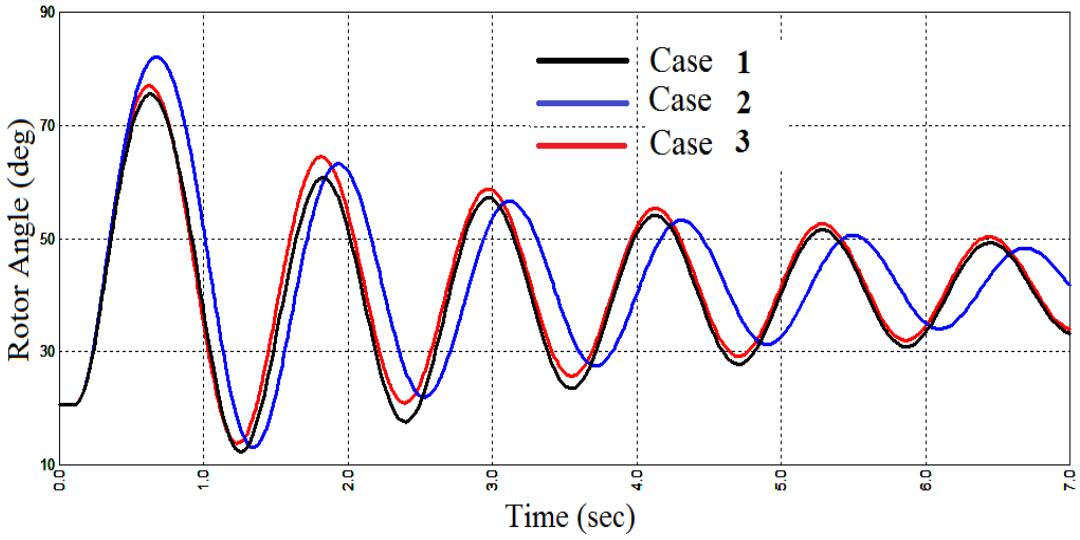

Figure 6.3 Rotor angle of G2 relevant to G1 for cases 1, 2 and 3

As the RSC is deactivated during large transient disturbances, the GSC can be used as a STATCOM, to produce reactive power as shown in Figure 6.4. The utilising of GSC to produce reactive power is well explained in Chapter 5.

Figure 6.4 shows the amount of reactive power that can be delivered from DFIG-GSC during normal operation and STATCOM mode. In the case of normal operation, GSC cannot provide any reactive power support during fault. In this case, the GSC has no contribution towards transient stability improvement. However, in the case of STATCOM mode, GSC provides reactive power support during and after the fault when the DFIG crowbar is still active. The 3-phase short-circuit fault is applied at (t_1 = 0.1 s). The DFIG crowbar is triggered at (t_2 = 0.12 s) to initiate the STATCOM mode after few milliseconds. During the fault period, the DFIG-GSC provides 20 MVAr, which helps to improve the terminal voltage of DFIG wind farm. Although, the fault is cleared at (t_3 = 0.25 s), the STATCOM mode is deactivated at (t_4 = 0.35 s) when the DFIG crowbar system is also deactivated. After fault clearance, DFIG-GSC provides its full rated reactive power to support the terminal voltage of wind farm.

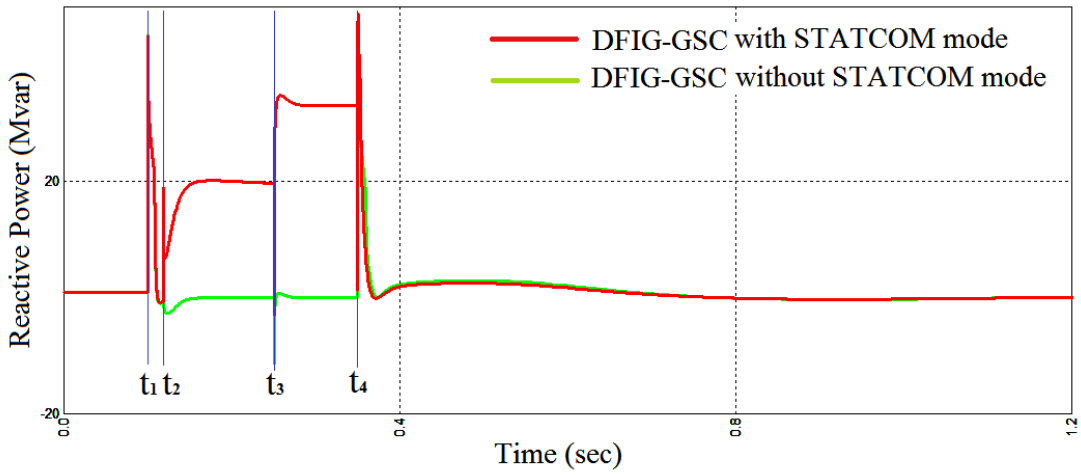

Figure 6.4 Reactive power of DFIG-GSC during normal operation (green line) and STATCOM modes (red line).

The produced reactive power helps to improve the terminal voltage of the wind farm. The wind farm terminal voltage is improved from 0.37 p.u. to 0.42 p.u. with STATCOM mode during the fault and from 0.81 p.u. to 0.88 p.u. after the fault when the crowbar is still on as shown in Figure 6.5.

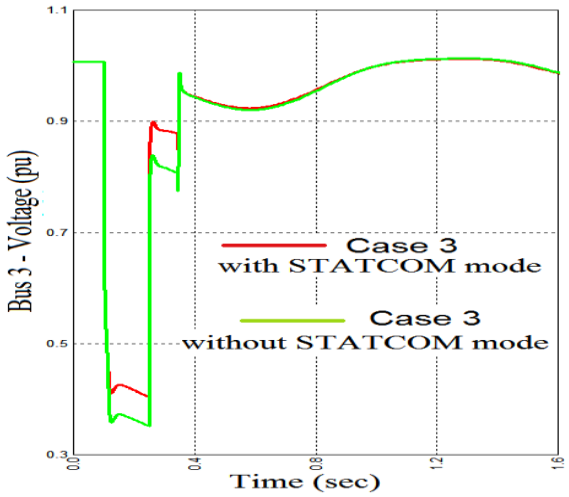

Figure 6.5 DFIG terminal voltage with and without STATCOM mode.

As the DFIG act as an induction generator when the crowbar is on, a large amount of reactive power is absorbed from the grid by the induction generator as shown in Figure 6.6. The amount of reactive power absorbed from the grid by the wind farm is reduced from 63 MVAr (without STATCOM mode) to 34 MVAr (with STATCOM mode). The amount of reactive power produced in STATCOM mode helps to decrease the amount of reactive power absorbed from the grid leading to better voltage recovery.

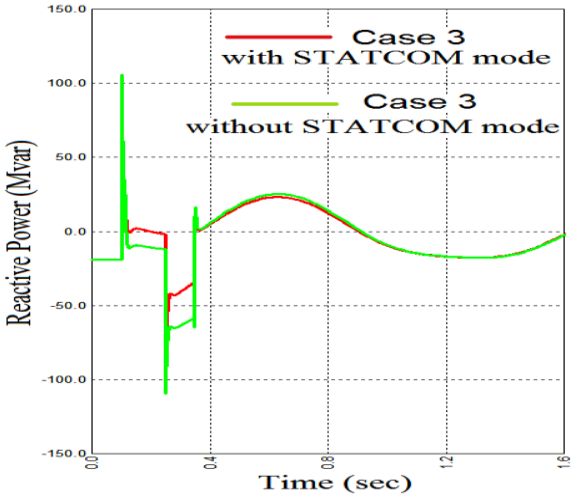

Figure 6.6 DFIG reactive power absorbed from the grid with and without STATCOM mode.

Figure 6.7 presents the rotor angle of G2 when STATCOM mode is used. The magnitude of the rotor angles in cases 2 and 3 is slightly lower when it is compared to those in Figure 6.3. A smaller rotor angle deviation of G2 has been gained in the case of STATCOM mode as a result of the injected reactive power. The rotor angle magnitude and oscillation in the case 3 with STATCOM mode has similar performance to SG case. Therefore, replacing a SG by DFIG based wind farm controlling its terminal voltage and equipped with STATCOM mode has no negative impacts on the transient stability of the power system.

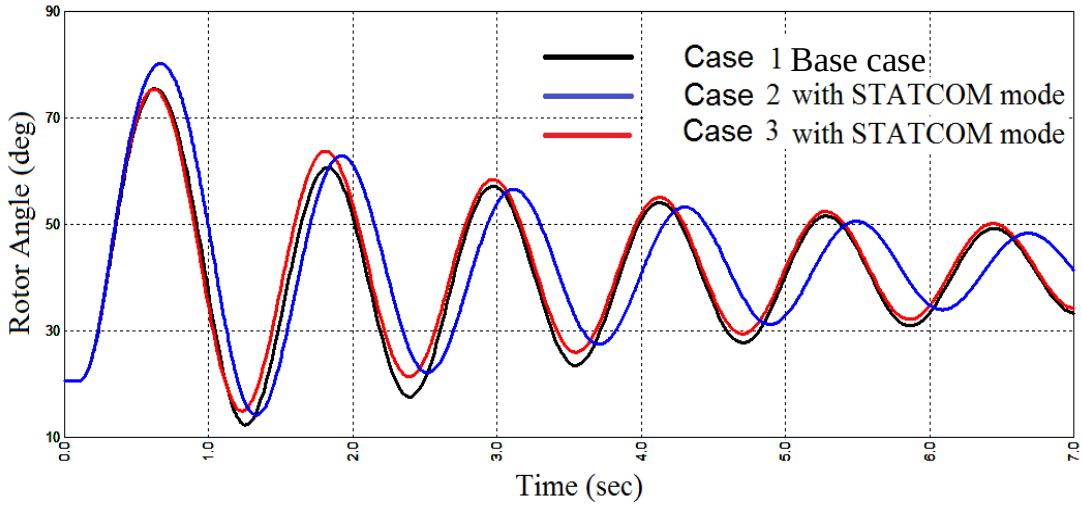

Figure 6.7 Rotor angle of G2 relevant to G1 for case 1, 4 (case 2, 3 with and without STATCOM mode)

The transient stability index of case 1, 2, 3 and 4 are shown in

Table 6.2. The transient stability index is reduced when the DFIG wind farm replaced the SG G3. However, using the proposed method of using the GSC as STATCOM increases the transient stability of the power system to reach a similar performance to case1. The stability index of case 3 is improved from 64.77 to 65.38 in case 4, which is similar to the case 1 (65.3).

Table 6.2 Transient stability index of cases 1-4

TSI	Case 1	Case 2	Case 3	Case 4
η	65.3	62.87	64.77	65.38

The results of case4 indicate that transient stability of the system is improved by using DFIG-GSC as STATCOM. The reactive power provided by STATCOM mode improves the terminal voltage of wind farm during the disturbance and hence resulting in better system stability. Since the terminal voltage of DFIG based wind farm can be controlled by the voltage control strategy of RSC during normal operation conditions, the STATCOM mode can provide a voltage support during transient periods when the crowbar is active.

The results of small signal stability indicate that rotor angle stability of the system is enhanced due to the effectiveness of the proposed PSS. The effectiveness of the proposed model of PSS that is designed in Chapter 5 has to be examined further by time domain simulation. Figure 6.8 show the dynamic response of G2 rotor angle when there is no PSS (case 3) and when the PSS is attached to a DFIG based wind farm with both voltage control strategy and STATCOM mode (case 5).

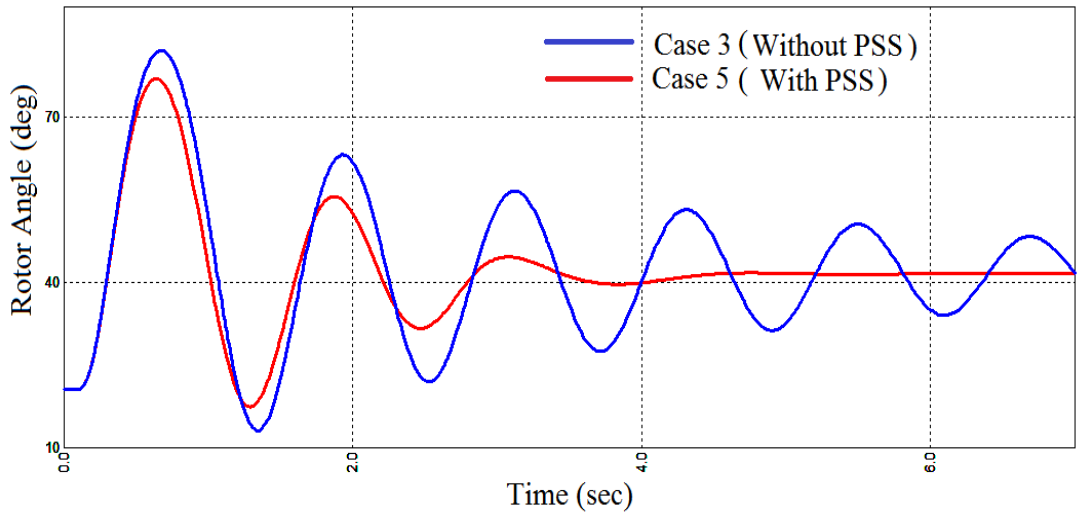

Figure 6.8 Rotor angle of G2 relevant to G1 for cases 3 and 5

The time domain simulation clearly shows the oscillation damps down quickly, and the rotor angle steady state value is reached in a time of less than 4 s. Therefore, it is clear that DFIG based wind farm has the capability to improve rotor angle oscillations.

The PSS output signal that is attached to the reactive power control loop of the DFIG is shown in Figure 6.9. During rotor angle oscillations, the frequency deviation at the wind farm terminal bus is passed through the PSS blocks to form the output signal. The output of PSS is limited by ±0.1 p.u. to assure that the DFIG terminal voltage is within limits. The PSS output signal goes to zero when the rotor angle oscillation reaches new steady state point.

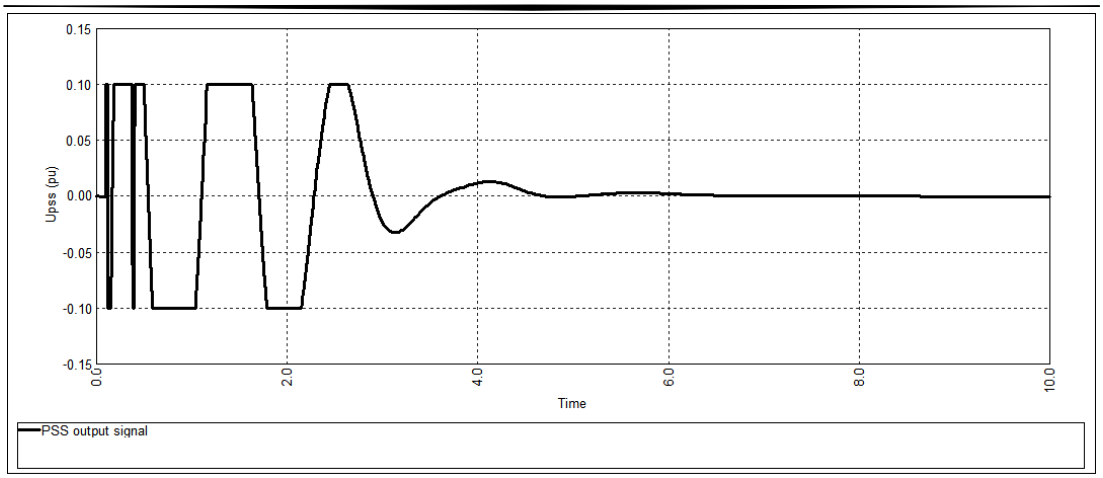

Figure 6.9 Power system stabiliser output signal

Since PSS output signal is connected to the reactive power loop, the difference between the two cases (with and without PSS) is only in the reactive power output as can be seen in Figure 6.10. The DFIG stator for with and without PSS cases produces a similar amount of reactive power before, and during the fault when the crowbar protection is on. This is because the PSS signal before the fault is zero and the control of reactive power is disabled during the fault by the crowbar. After the fault is cleared and the crowbar is deactivated, the PSS is activated to damp the rotor angle oscillations leading to reactive power variation different from the case when there is no PSS. The variation of reactive power in the case of PSS is damped in about 4s when the PSS output goes to zero.

DFIG based wind farms equipped with PSS can use STATCOM mode to improve system transient stability. The DFIG-GSC can be used as a reactive power support during the time when DFIG crowbar is active. Figure 6.10 shows the reactive power output of the STATCOM mode when the wind farm is equipped with PSS. The GSC provides a reactive power support during the time when DFIG crowbar is active only. Conversely, the PSS starts to control the DFIG stator reactive power after the crowbar is deactivated.

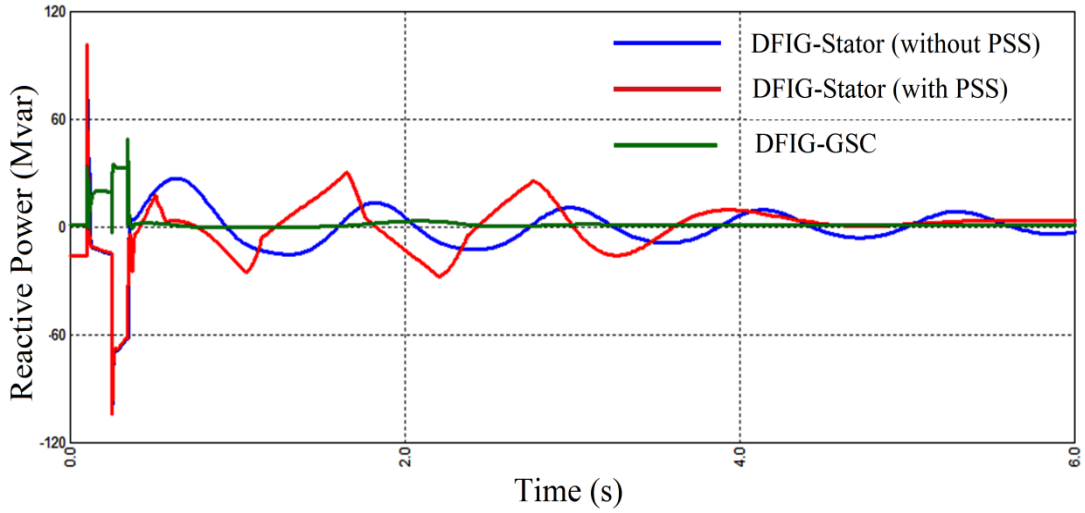

Figure 6.10 DFIG-GSC reactive power during STATCOM mode, and DFIG stator reactive power with and without PSS

In a similar way to the reactive power, the terminal voltage of the wind farm with PSS is more variable, as shown in Figure 6.11. This variation also occurs after the crowbar is deactivated. However, this variation is limited and is effectively damped in a short time.

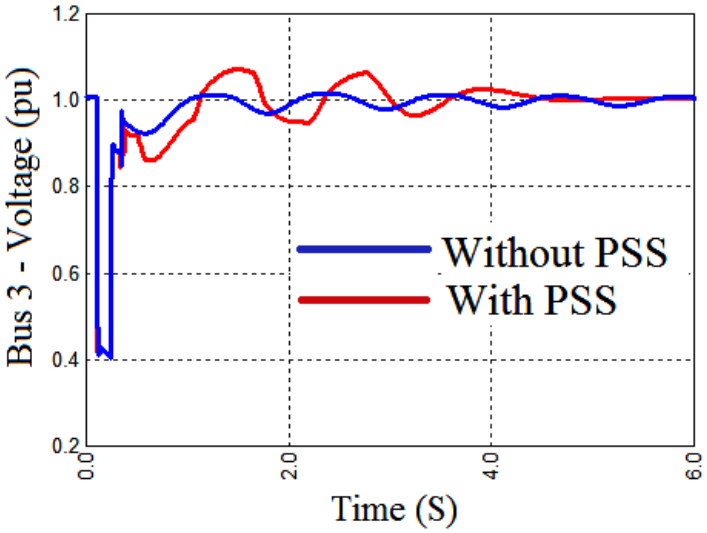

Figure 6.11 DFIG terminal voltage for cases 3 and 5.

As the PSS is attached to the reactive power control loop, the difference between case 3 and 5 is the only reactive power that is produced by the generator. The active power is similar for both cases (with and without PSS) as shown in Figure 6.12.

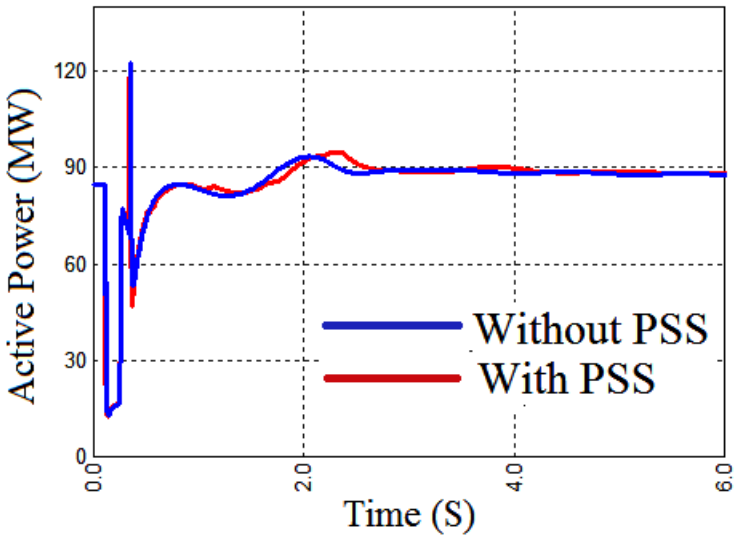

Figure 6.12 DFIG active power for cases 3 and 5.

The transient stability results indicate that DFIG based wind farms can damp rotor angle oscillation effectively by using a PSS attached to the DFIG-RSC reactive power control loop. Moreover, the transient stability results indicate that the DFIG-GSC control strategy can be used on the same DFIG based wind farm that is fitted with PSS to improve transient stability of the power system.

6.3 Using IEEE 39-bus Test System to Evaluate Rotor Angle Stability using the Proposed Approaches

To investigate the effect of DFIG based wind farm on multi machines power system rotor angle stability, two DFIG based wind farms are connected to the IEEE 39-bus test system, which is also known as New England 10-machine test system. The test system has been described previously in Chapter 4 and its full static, and dynamic data can be found in [158]. In this section, four different cases are analysed by small signal and transient stability to show the impact of DFIG on power systems

rotor angle stability and how the disturbance can be mitigated by the proposed control strategies. The description of each case is as following:

- **Case 1:** SG case; this is a base case in which all generators are conventional SGs where every generator is equipped with TGOV1 turbine governor, IEEE type 1 exciter. However, only SGs G5, G7, G9 are equipped with (STAB1) PSS.
- **Case 2:** SGs G7 and G9 in case 1, which are equipped with PSS, are replaced by equivalent DFIG1 and DFIG2 wind farms respectively. These two wind farms are controlling their terminal voltage (the reactive power is controlled to achieve a specified voltage value at the terminal bus). Each wind farm was aggregated from several 5 MW wind turbines to achieve an equivalent generated power of the replaced generator. The generated power from the two wind farms is accounted for 22.6% of the total consumed power of the test system.
- **Case 3**: STATCOM control mode; the use of DFIG-GSC as STATCOM control strategy, as explained in Chapter 5, will be investigated in this case.
- **Case 4**: DFIG-PSS case; each DFIG will be equipped with the proposed PSS, as explained in Chapter 5.

6.3.1 Small signal Stability Analysis

A detailed small signal stability study on the test system was conducted for each case. The whole system eigenvalues for each case are shown in Figure 6.13. It can be seen that the system is stable for all cases as there are no modes in the right-hand side of the complex plane. However, there are four critical eigenvalues with damping factor less than 5%.

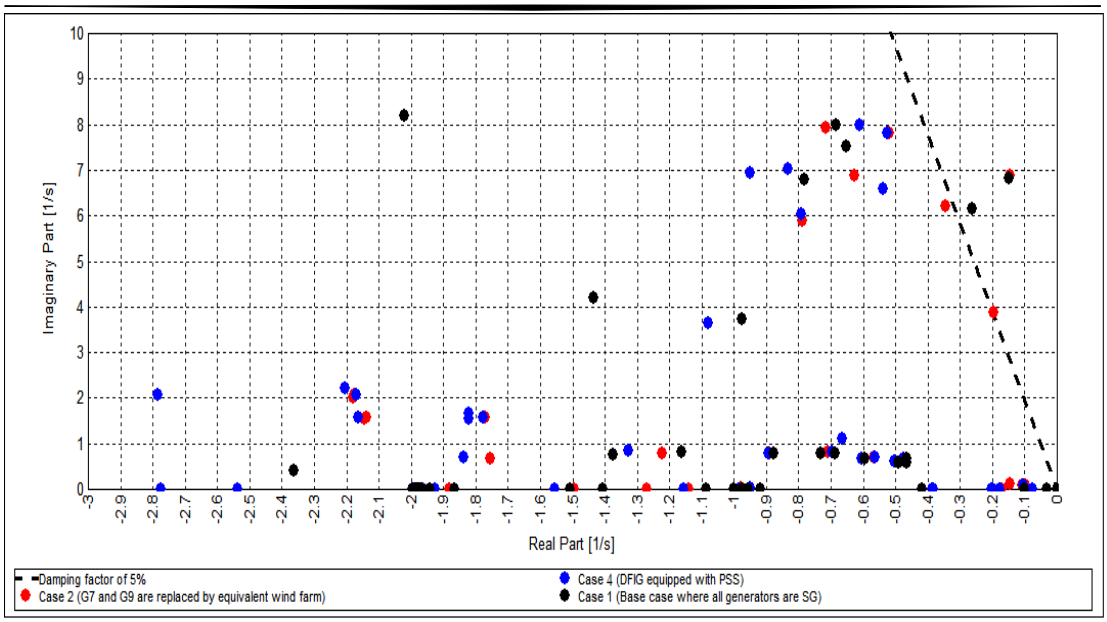

Figure 6.13 Overview of the complex plane with the test system eigenvalues for cases 1, 2 and4

In the first case, there are two critical modes with damping factor of less than 5%. These two critical modes (-0.151± j 6.83) and (-0.264± j 6.16) are dominated by synchronous machines G03 and G02 respectively as shown in Table 6.3. The numbers of oscillatory modes with damping factors of less than 10% are increased in case 2 as compared to case 1. This indicates that replacing synchronous machines equipped with PSS by equivalent DFIG based wind farm degrade the small signal stability of the power system. However, this can be mitigated by the proposed DFIG PSS as presented in case 4. There are just three oscillatory modes in case 4 with damping factors of less than 10%, and none of them has a damping factor of less than 5%. The critical oscillatory mode (-0.149± j6.85) with damping factor of 2.2% in case 2 moved toward the stable region by the proposed PSS. The new position of the oscillatory mode is (-0.445 ± j6.63) with damping factor of 6.7%, and it is still dominated by the SG G3. The other critical oscillatory mode (-0.19± j3.89) with damping factor of 4.9% in case 2 is damped out in case 4. Moreover, the mode that dominated by SG G6 is damped out by DFIG1 PSS. The other two modes dominated by SGs G4 and G8, which have a damping factor of 6.6% and 9% respectively, are unaffected by the damping torque of the two wind farms.

Small signal stability results indicate that replacing large-scale SGs equipped with PSSs by an equivalent DFIG based wind farms can have a negative impact on the damping of power system oscillations. However, these impacts can be mitigated by the equipping the DFIG based wind farm with the proposed PSS to damp power system oscillations. Although the installed wind farms are not synchronously coupled to the test system, they can provide a damping effect if they are equipped with PSSs as shown in case 4. In this case, the system is much more stable than all previous cases and in which no damping factor less than 6.7% is observed.

Table 6.3 Main electromechanical modes of case 1 (SG case), case 2 (G7 and G9 are replaced by DFIG based wind farms), case 4 (the DFIG is equipped with the proposed PSS).

Case	Eigenvalue $\lambda = \sigma + j\omega$ (p.u.)	Damping Factor ζ (%)	Frequency f (Hz)	Dominant Machine
1	-0.151± j 6.83	2.2	1.086	G03
	-0.264± j 6.16	4.3	0.98	G02
	-0.654 ±j 7.53	8.7	1.199	G04
	-0.683 ± j7.99	8.5	1.272	G08
2	-0.149± j6.85	2.2	1.091	G03
	-0.19± j3.89	4.9	0.619	G01
	-0.354± j6.22	5.7	0.99	G02
	-0.52± j7.821	6.6	1.245	G04
	-0.625± j6.87	9.1	1.094	G06
	-0.717± j7.93	9	1.262	G08
4	-0.445 ± j6.63	6.7	1.056	G03
	-0.519 ± j7.82	6.6	1.244	G04
	-0.722 ± j7.98	9.0	1.271	G08

The selected location of the PSS used for SGs is based on participation factor [91, 179-181] for each generator except G1, which is the equivalent external generator. Moreover, the parameters of the PSS used in the SGs and the two DFIG

based wind farms are designed according to the method described in Chapter 5, and its parameters are given in the following table:

Table 6.4 PSS parameters used for SGs and DFIG based wind farms

Synchronous generators PSS				**DFIG based wind farms PSS**			
	K	$T_1=T_3$	$T_2=T_4$		*K*	*T1=T3*	*T2=T4*
G5	18	0.4757	0.1535	DFIG1	120	0.1599	0.1325
G7	38	0.3814	0.1851	DFIG2	140	0.3179	0.2106
G9	22	0.3533	0.0901				

6.3.2 Transient Stability Analysis

To evaluate the effectiveness of the damping controller and the proposed STATCOM mode in a large multi-machines power system, the four cases are simulated by a nonlinear simulation. To conduct transient stability analysis, the system has to be exposed to a large disturbance such as a three-phase short circuit fault. The location of the disturbance is chosen to be near the most critical busbar in the test system, which is the bus 16. A 150 ms three-phase to ground permanent fault is applied at t = 0.1 s near critical bus 16 on transmission line 16–24. The fault was cleared by opening switches on both sides of the faulted line simultaneously.

The rotor angles of each synchronous machine relative to the angle of largest synchronous machine G1, which is taken as a reference angle, are monitored. Figure 6.14 shows the rotor angles of G2 to G10 with respect to that of G1 for the first case where all generators are synchronous machines and G5, G7, and G9 are equipped with PSS. It is clear that the system is stable, and the system oscillations are damped out in less than 8 s.

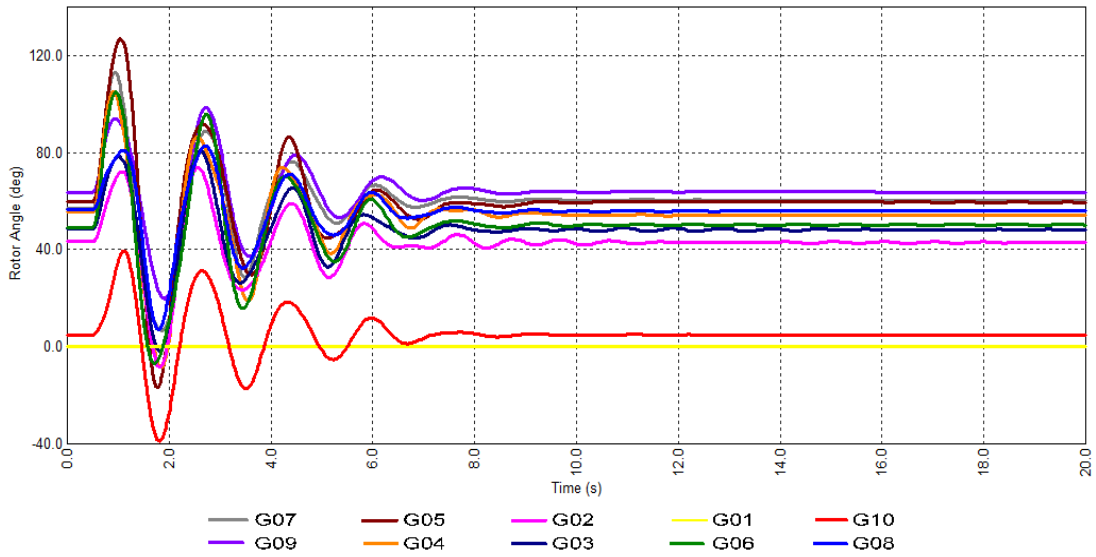

Figure 6.14 Rotor angles of all SGs for case 1 (G5, G7, G9 are equipped with PSS).

However, the rotor angle stability of the test system is affected adversely as a result of replacing conventional SGs G7 and G9, which are both equipped with PSSs, by an equivalent DFIG based wind farms as shown in Figure 6.15. Although the system is still stable in case 2, the oscillations of synchronous machines rotor angles last much longer than those oscillations in case 1. This is due to a lack of damping torque provided by the replaced PSSs. Moreover, some machines have larger rotor angle magnitude than that in the first case. These results are similar to those obtained previously in the small signal stability analysis.

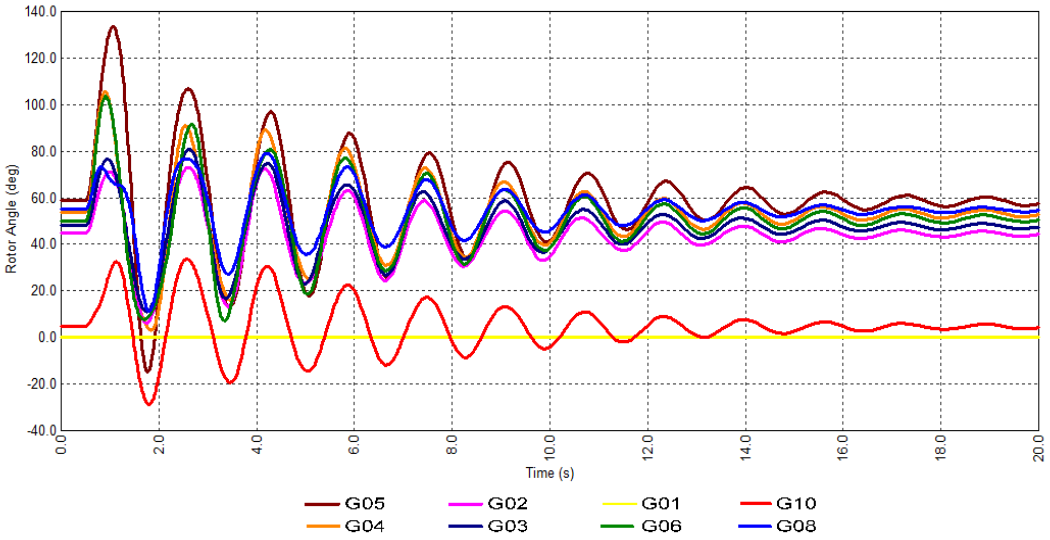

Figure 6.15 Rotor angles of each generator for case 2 (G7, G9 are replaced by equivalent DFIGs).

The evaluate the use of DFIG-GSC as STATCOM control strategy, GSC of the two DFIG is modelled to provide a reactive power support when the crowbar is enabled as explained in Chapter 5. Figure 6.16 presents the rotor angle of all generators when STATCOM mode is used. The magnitudes of the rotor angles, in this case, are slightly lower when they are compared to those in Figure 6.15 (case 2). Smaller rotor angle deviations of all SGs have been gained in the case of STATCOM mode as a result of the injected reactive power from DFIGs-GSC. From Figure 6.15 and Figure 6.16, the generator that has the largest rotor angle magnitude in the case 3 (with STATCOM mode) has a similar magnitude in case 1 (SGs case).

Table 6.5 shows the transient stability index for each case. It is clear that the transient stability of the test system degraded when two of the SGs are replaced by equivalent wind farms. The transient stability index is decreased from 47.84 in case 1 to 45.89 in case 2. However, replacing a SG by DFIG based wind farm equipped with STATCOM mode has no negative impacts on the transient stability of the test system. The transient stability index improved in case 3 to reach 47.24, which is comparable to the base case.

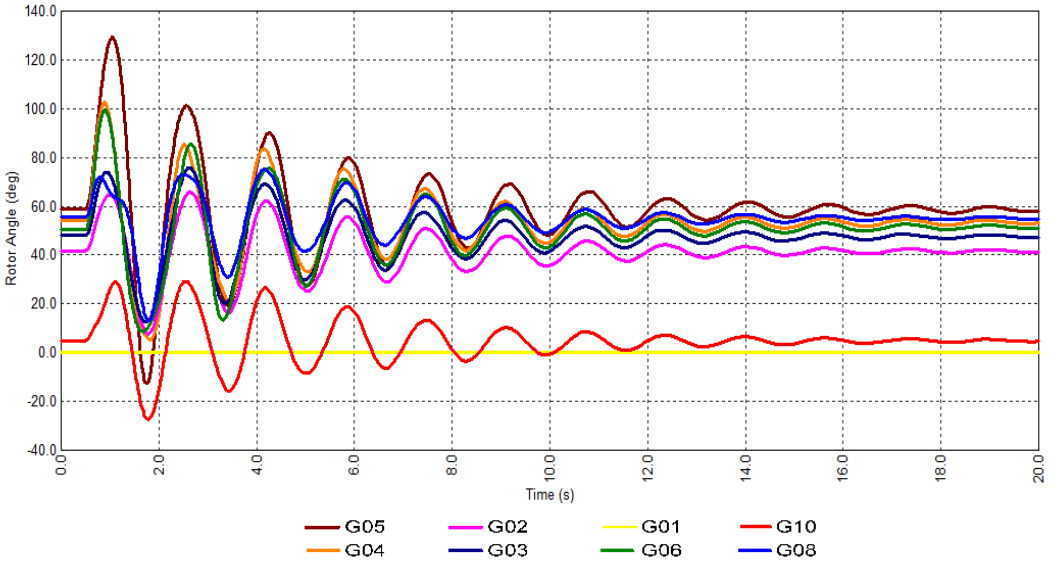

Figure 6.16 Rotor angles of all generators for case 3 (STATCOM mode).

Table 6.5 Transient stability index of cases 1-3

TSI	Case 1	Case 2	Case 3
η	47.84	45.89	47.24

Figure 6.17 shows the amount of reactive power that can be delivered from the wind farms during STATCOM mode. In the case of normal operation, (the crowbar is deactivated), the amount of reactive power produced by GSC is almost zero. However, in this case of a disturbance, GSC of both wind farms provides reactive power support during and after the fault when the DFIG crowbar is still active. Approximately 140 MVAr is produced from the first wind farm (DFIG1) while the second wind farm (DFIG2) produced about 230 MVAr.

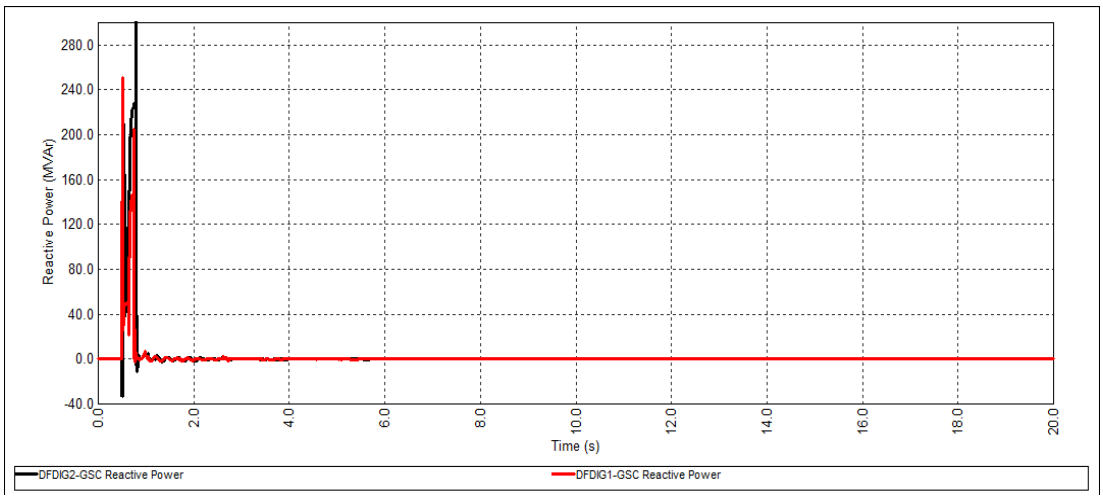

Figure 6.17 Reactive power of DFIG1 and 2 GSC during STATCOM mode.

The use of STATCOM mode can be combined with the use of the proposed PSS to damp power system oscillations as shown in Figure 6.18. It is noticeable that the test system can reach steady state in a short time by equipping the two wind farms with the proposed PSS. The time domain simulation clearly shows that the oscillation is damped quickly and the rotor angle steady state value is reached in about 5s. This indicates that the tested DFIG-PSS is robust even in large power systems.

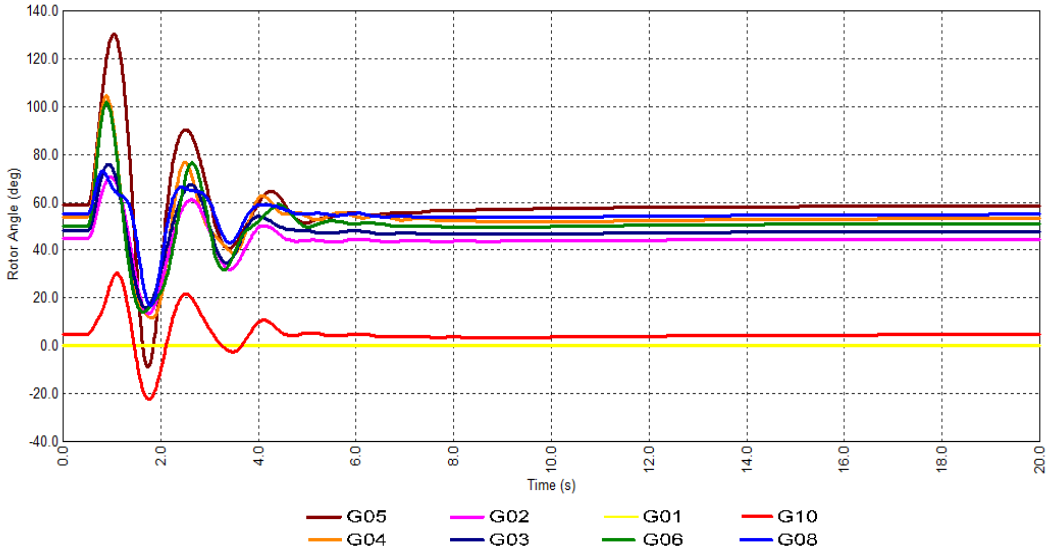

Figure 6.18 Rotor angles of all generators for case 4 (Proposed PSS).

The transient stability results indicate that DFIG based wind farms equipped with PSS have the capability to improve rotor angle oscillations better than SGs. As can be seen from Figure 6.14 and Figure 6.18, the rotor angle of all SGs damped in case 4 reached the steady state operation point faster than those in case 1. Moreover, the magnitudes of the SGs rotor angles in case 4 are slightly lower than that in case 1.

Once again, the stability index is improved from 45.89 in case 2 to reach 48.15 in case 4 as illustrated in Table 6.6. The degree of stability reached when the DFIG wind farm equipped with both STATCOM mode and PSS is better than the base case when all generators are conventional SGs.

Table 6.6 Transient stability index of cases 1-4

TSI	**Case 1**	**Case 2**	**Case 3**	**Case 4**
η	47.84	45.89	47.24	48.15

The PSS output signal that is attached to the reactive power control loop of the DFIG is shown in Figure 6.19. During rotor angle oscillations, the frequency deviation at the terminal bus of each wind farm is passed through the PSS blocks to form the output signal. As the location of the fault is electrically closer to DFIG1 than DFIG2, the output signals are slightly different. The PSS output signal of both wind farms goes to zero when the rotor angle oscillations reach new steady-state point.

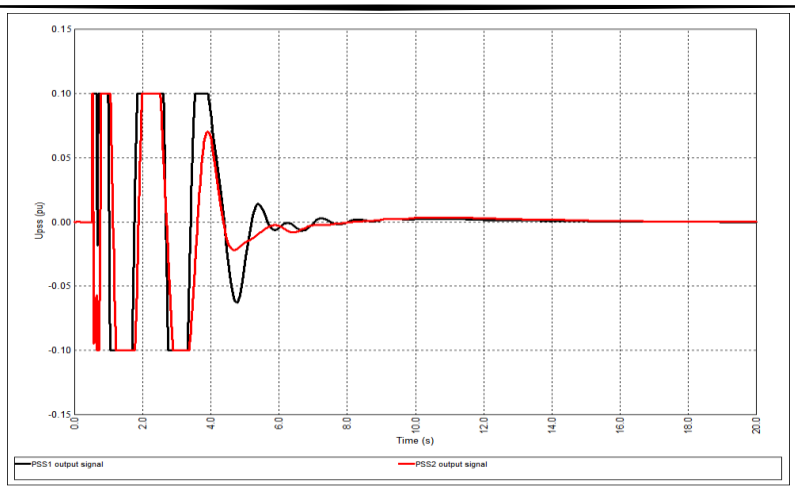

Figure 6.19 The output signals of PSS1 at DFIG1 wind farm and PSS2 at DFIG2 wind farm

Since PSS output signal is connected to the reactive power loop, the PSS output signal will alter only the DFIG reactive power to damp rotor angle oscillations. The two wind farms reactive power variations, when the proposed PSS is used with and without STATCOM mode, is shown in Figure 6.20. Both wind farms were producing about 50 MVAr prior the disturbance to maintain their terminal voltage at predefined values. During the disturbance, approximately 150 MVAr and 200 MVAr are absorbed by DFIG1 and DFIG2 respectively. However, this amount of absorbed reactive power can be reduced by using the DFIG-GSC as STATCOM. When the STATCOM mode is used 50 MVAr and 90 MVAr are absorbed by DFIG1 and DFIG2 respectively. After the crowbar protection is deactivated, the PSS is activated to damp the rotor angle oscillations leading to reactive power variation. The reactive power fluctuations reached a steady state point in a similar time to the PSS signals, which are damped out in about 6s.

The available DFIG reactive power can be utilised by proposed control strategy to improve rotor angle stability. DFIG based wind farms equipped with PSS can use STATCOM mode to improve system transient stability. The DFIG-GSC provides a reactive power support during the time when DFIG crowbar is active only. Conversely, the PSS starts to control the DFIG stator reactive power after the crowbar is deactivated.

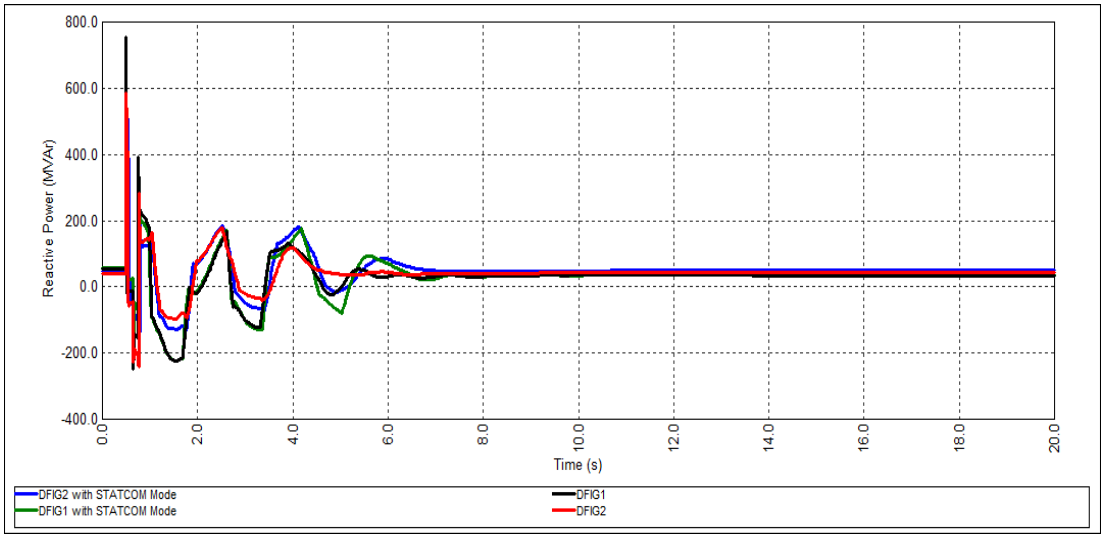

Figure 6.20 Reactive power of DFIG 1 and 2 when the proposed PSS is used with and without STATCOM mode.

The produced reactive power by the DFIG-GSC helps to improve the terminal voltage of the wind farm when the STATCOM mode is used as shown in Figure 6.21. The DFIG1 wind farm terminal voltage is improved from 0.20 p.u. to 0.28 p.u. with STATCOM mode during the fault and from 0.65 p.u. to 0.80 p.u. after the fault when the crowbar is still on as shown in Figure 6.21. Moreover, the terminal voltage of DFIG2 wind farm is increased from 0.29 p.u. to 0.42 p.u. with STATCOM mode during the fault and from 0.63 p.u. to 0.84 p.u. after the fault when the crowbar is still on. After the crowbar is deactivated, the terminal voltages of both wind farms fluctuate between 0.9 p.u. and 1.1 p.u. as a result of reactive power variations. The voltages at DFIG1 and DFIG2 become stable after 6 s when all rotor angle oscillations are damped out.

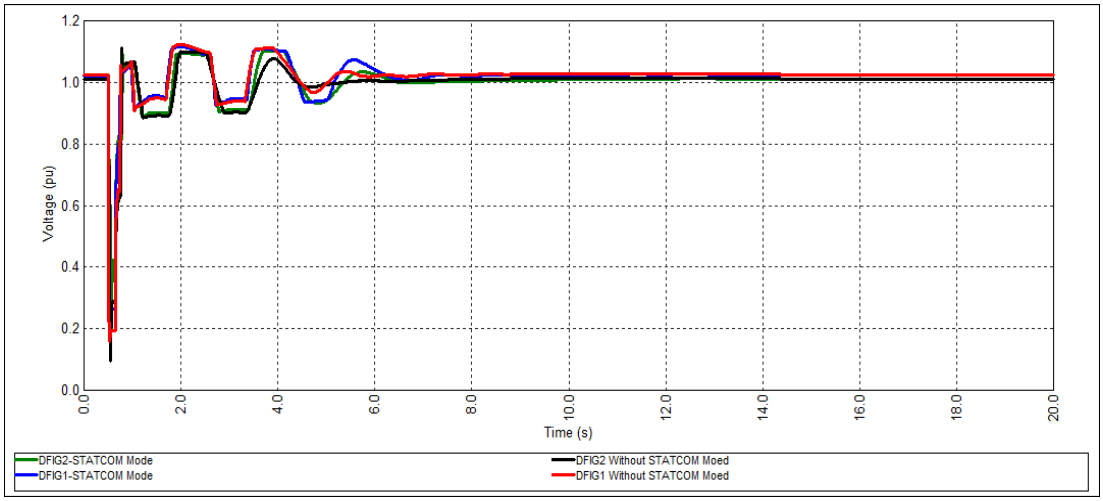

Figure 6.21 Terminal voltage of wind farms DFIG 1 and DFIG2 when the proposed PSS is used with and without STATCOM mode.

6.4 Evaluating the Proposed Approach under a Wide Range of Operating Conditions

As wind power is stochastic and fluctuates with the variation of wind speed, the capability of a wind farm to damp power system oscillations may be reduced. Therefore, the proposed conventional fixed parameters PSS should have the capability to damp power oscillations effectively under non-uniform variable wind speeds across the wind farm. In this Section, the feasibility of the proposed fixed parameters PSS is evaluated using IEEE 39-bus test system taking into account the non-uniform and variable wind speed profiles.

To investigate the capability of the proposed approach to damp power system oscillations, two large-scale DFIG wind farms equipped with the proposed PSS and STATCOM mode are installed in the test system to replace the two large synchronous machines G7 and G9 respectively.

The most used aggregation method assumes that all wind turbines within the wind farm are receiving the same wind speed and thus operating at the same operating point to produce the same power. However, in practice, powers produced by wind turbines are different depending on wind speed variation and their location

inside the wind farm due to the wake effect. Hence, a multi-machine equivalent method is used in this Section, and it is more accurate when the turbines within the wind farm are facing different wind speeds [127].

Each wind farm is represented by three DFIG based wind turbines as shown in Figure 6.22. The three DFIG base wind turbines in each wind farm are operating at different operating points, which are defined in

Table 6.7. Moreover, each wind farm is exposed to a short-term wind speed variation which is a measured wind speed obtained by [17] from wind turbine manufacturers. Figure 6.23 shows the wind speed patterns for each wind turbine in both wind farms.

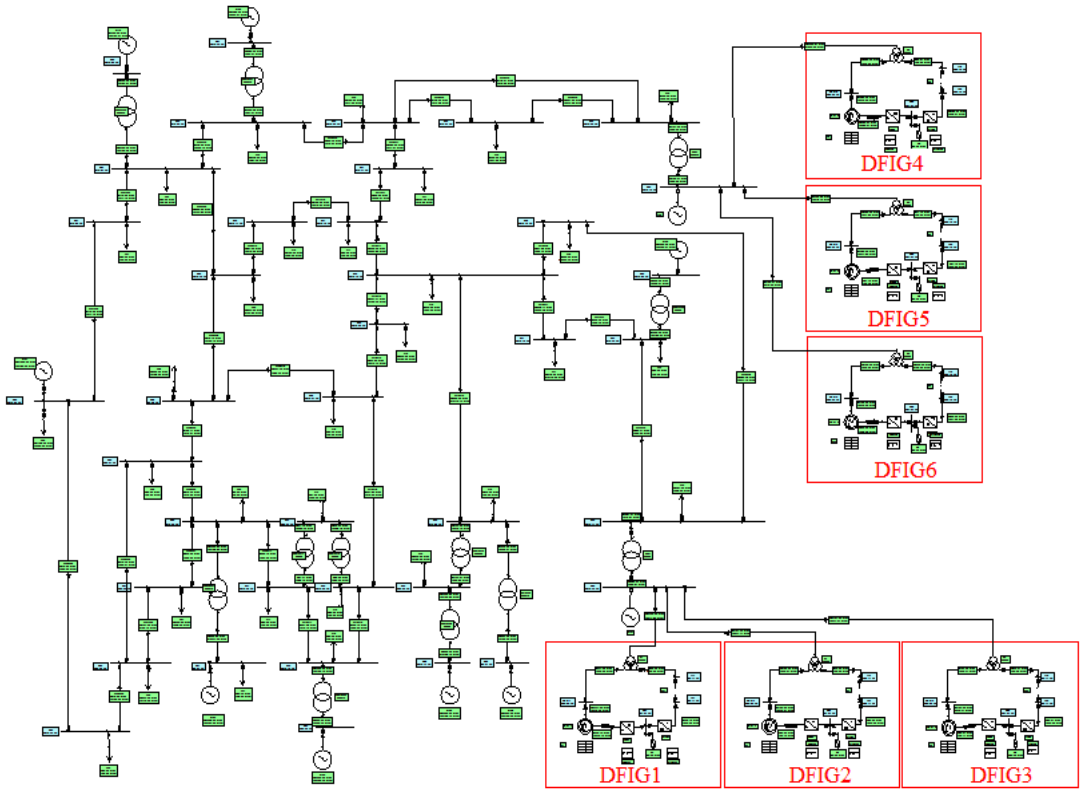

Figure 6.22 Single line diagram of the IEEE 39-bus test system with two wind farms each represented by three DFIG wind turbines.

Table 6.7 Different modes of operation for each wind turbine in the two wind farms

Wind Farm	Turbine	Operation Mode	Wind Pattern	Stator Power (MW)	Rotor Power (MW)	Total Power (MW)
1	DFIG1	Super-synchronous	Figure 6.23-a	240	36	276
	DFIG2	Normal	Figure 6.23-a	167	-2	165
	DFIG3	Sub- synchronous	Figure 6.23-a	139	-21	118
2	DFIG4	Super-synchronous	Figure 6.23-b	350	53	403
	DFIG5	Normal	Figure 6.23-b	245	3	248
	DFIG6	Sub- synchronous	Figure 6.23-b	206	-31	175

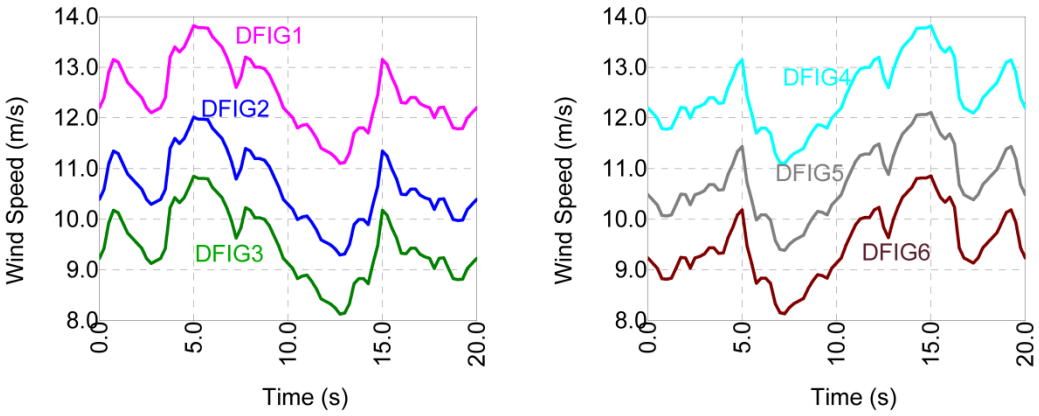

Figure 6.23 (a) wind speed patterns for each wind turbine in wind farms 1, (b) wind speed patterns for each wind turbine in wind farms 2

In a similar way to Section 6.3, four different cases are analysed by small signal and transient stability to evaluate the effect of the proposed strategy on power systems rotor angle stability when the three DFIG base wind turbines in each wind farm are operating at different operating points. The description of each case is as following:

- **Case 1:** SG case; this is a base case in which all generators are conventional SGs where every generator is equipped with TGOV1 turbine governor, IEEE type 1 exciter. However, only SGs G5, G7, G9 are equipped with (STAB1) PSS.
- **Case 2**: SGs G7 and G9, which are equipped with PSS, are replaced by two equivalent wind farms. Wind farm 1 consists of three (DFIG1, DFIG2, and DFIG3) wind turbines operating according to
- Table 6.7 and Figure 6.23. The second wind farm consists of three (DFIG4, DFIG5, and DFIG7) wind turbines operating according to
- Table 6.7 and Figure 6.23. The two wind farms are controlling their terminal voltage.
- **Case 3**: STATCOM control mode; the use of DFIG-GSC as STATCOM control strategy in each wind turbine in case 2.
- **Case 4**: DFIG-PSS case; each DFIG will be equipped with the proposed PSS with the same parameters used in Section 6.3.

6.4.1 Small signal stability analysis

The small signal stability results for each case are shown in

Table 6.8. It is interesting to note that in this case representing the whole wind farm as a single aggregated DFIG has a similar impact on power system small signal stability as that of representing the wind farm as three aggregated DFIGs operating at different modes.

In the second case, there are 6 modes with a damping factor of less than 10%. The dominant machine and frequency of each oscillatory mode are similar to the results obtained when each wind farm is represented by a single equivalent DFIG wind turbine. There are three modes in case 4 which have a similar frequency and are dominated by the same machine to that when the wind farm is represented by a single turbine. However, the damping factors of the two modes are slightly different.

Table 6.8 Main electromechanical modes of case 1and 3.

Case	Eigenvalue $\lambda = \sigma + j\omega$ (p.u.)	Damping Factor ζ (%)	Frequency f (Hz)	Dominant Machine
1	-0.151± j 6.83	2.2	1.086	G03
	-0.264± j 6.16	4.3	0.98	G02
	-0.654 ±j 7.53	8.7	1.199	G04
	-0.683 ± j7.99	8.5	1.272	G08
2	-0.145 ± j687	2.1	1.093	G03
	-0.198 ± j3.89	5.1	0.619	G01
	-0.345 ± j6.22	5.5	0.99	G02
	-0.521 ± j7.82	6.6	1.245	G04
	-0.628 ± j6.87	9.1	1.094	G06
	-0.716 ± j7.93	9	1.262	G08
4	-0.527 ± j7.81	6.7	1.244	G04
	-0.538 ± j6.60	8.1	1.051	G03
	-0.611 ± j7.98	7.6	1.27	G08

6.4.2 Transient Stability Analysis

To evaluate the effectiveness of the proposed control strategy under non-uniform and variable wind speeds across the wind farm and compare the obtained results to those previously obtained, the system is exposed to the same disturbance in the previous Section. A 150 ms three-phase to ground permanent fault is applied at t = 0.1 s near critical bus 16 on transmission line 16–24. The fault was cleared by opening switches on both sides of the faulted line simultaneously.

The rotor angles of SGs after G7 and G9 are replaced by two equivalent wind farms each represented by three DFIG wind turbines (case 2) are shown in Figure 6.24. The oscillations, in this case, are very similar to the results obtained previously when the whole wind farm is represented by a single DFIG wind turbine. Therefore,

representing the wind farm as a single machine has a similar impact on the rotor angle of synchronous machines to representing the wind farm as three separate machines operating at different modes. These results are similar to those obtained in the small signal stability analysis.

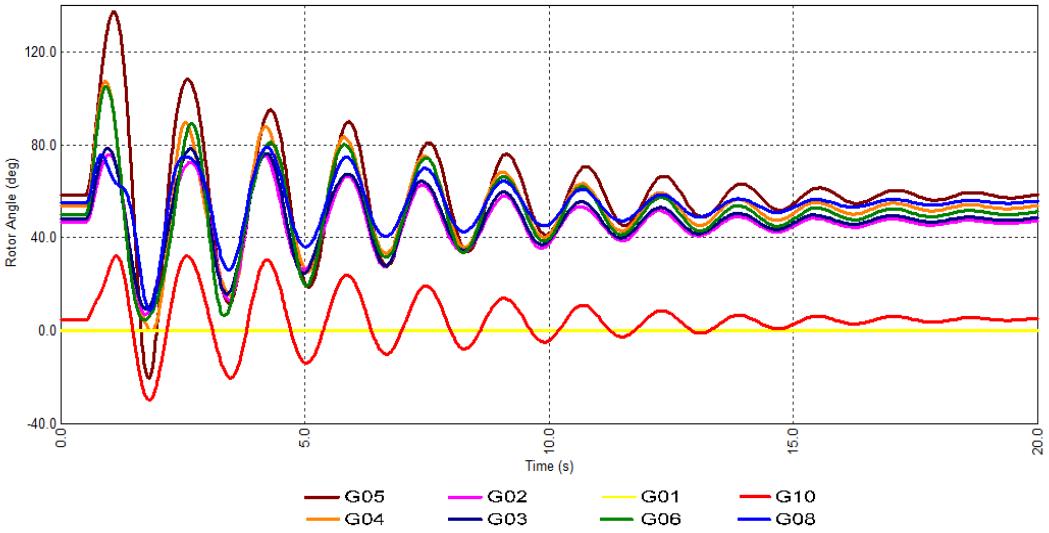

Figure 6.24 SGs rotor angles for case 2

However, when the STATCOM mode is used (case 3) as shown in Figure 6.25, the magnitudes of synchronous machines rotor angles are lower when they are compared to those obtained when the wind farm represented by a single equivalent turbine. Smaller rotor angle deviations of all synchronous machines have been gained in the case of representing the wind farm as three separate wind turbines. This is a result of more reactive power being injected from DFIGs-GSC than that injected in the case of representing the wind farm as a single equivalent wind turbine.

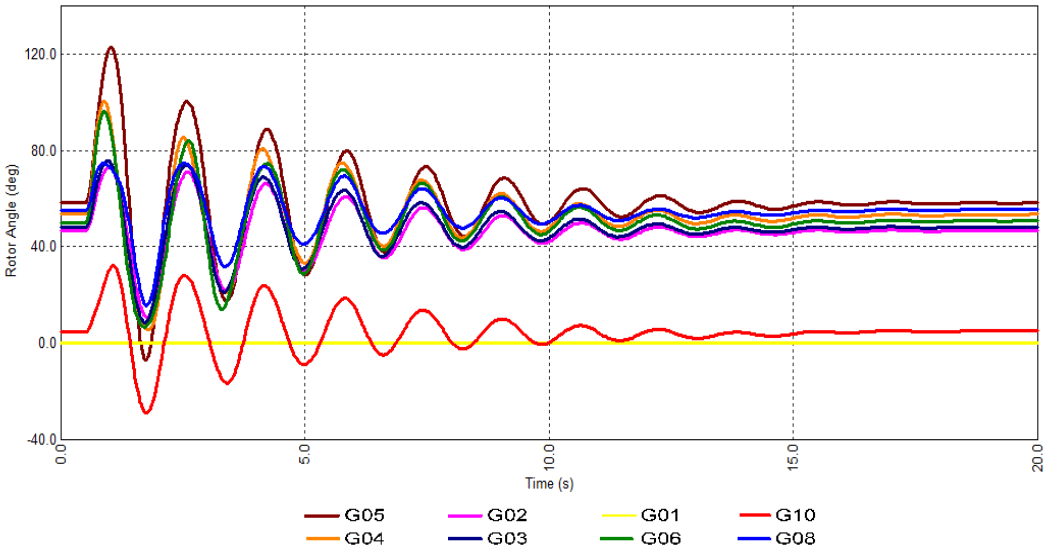

Figure 6.25 SGs rotor angles for case 3

Figure 6.26 show synchronous machines rotor angle oscillations for case 4 (each wind turbine equipped with the proposed PSS and STATCOM mode). It is noticeable that the proposed control strategy is very effective under non-uniform variable wind speeds across the wind farm. The time domain simulation clearly shows that the test system can reach steady state in short time, less than 5s, by equipping each wind turbine with the proposed PSS.

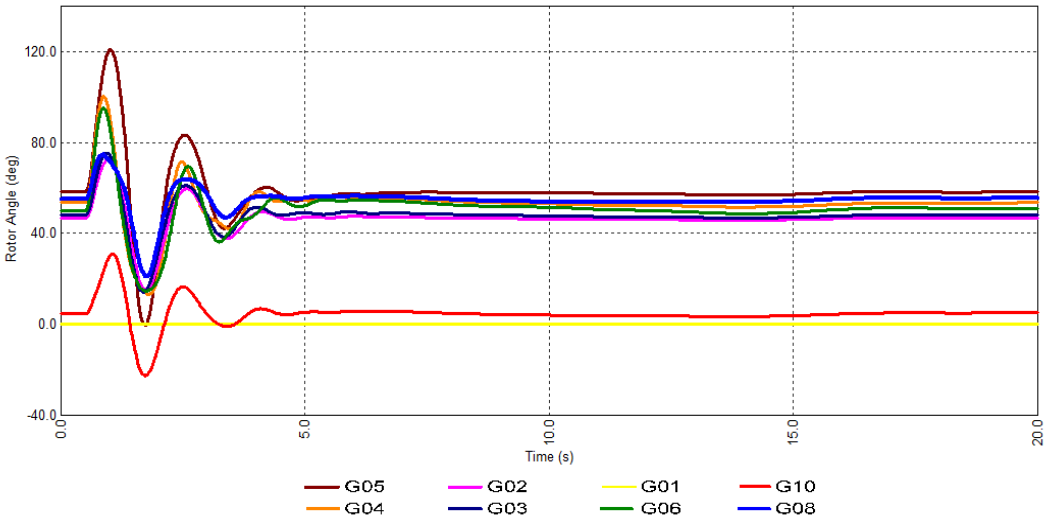

Figure 6.26 SGs rotor angles for case 4

The transient stability index for all cases is shown in Table 6.9. The transient stability index improved from 45.73 in case 2 to reach 49.06 in case 3. The maximum degree of stability is reached when the DFIG wind farm equipped with STATCOM mode and PSS. The degree of stability, in this case, is better than the base case when all generators are conventional SGs. Although the transient stability index is not affected by the wind farm representation in case 2, the transient stability index in case 3 is different. A higher index is obtained when the wind farm represented by three separate wind turbine operating at different operation modes. This is as a result of a higher amount of reactive power being injected, in the case of three wind turbine representation, by the STATCOM mode during the time when the crowbar is active.

Table 6.9 Transient stability index of cases 1-4 compared to resulted obtained when each wind farm represented as a single equivalent wind turbine

TSI	Wind farm representation	Case 1	Case 2	Case 3	Case 4
η	Single wind turbine with uniform fixed wind speed across the wind farm	47.84	45.89	47.24	48.15
	Three wind turbines with non-uniform variable wind speeds across the wind farm	47.84	45.73	49.06	49.69

The two wind farms reactive power variations, when the proposed PSS is used with and without STATCOM mode, is shown in Figure 6.27. Both wind farms were producing 50MVAr prior the disturbance to maintain their terminal voltage at predefined values. During the disturbance, 60 MVAr is produced by the GSC of each wind turbine (STATCOM mode) in wind farm 1. This amount of produced reactive power helps to reduce the absorbed reactive power and hence improves the terminal voltage of wind farm 1. The voltage of first wind farm improved from 0.2 p.u. (without STATCOM mode) to 0.29 p.u. (with STATCOM mode) as shown in Figure 6.28.

Since the produce reactive power helps to improve the voltage across the system, the crowbar system in the second wind farm has not been activated. There is no high rotor current detected by the crowbar system as the terminal voltage did not drop under 0.9 p.u. In this case, wind farm 2 did not lose the control over active and reactive power. Therefore, the three wind turbines (DFIG 4, 5 and 6) produce 750 MVAr during the disturbance, as shown in Figure 6.27, to support the terminal voltage of the wind farm.

After the crowbar protection is deactivated, the PSS is activated to damp the rotor angle oscillations leading to reactive power variation. The variation of the reactive power in the case of with and without STATCOM mode is similar as the GSC is providing reactive power only during a disturbance when the crowbar system is active.

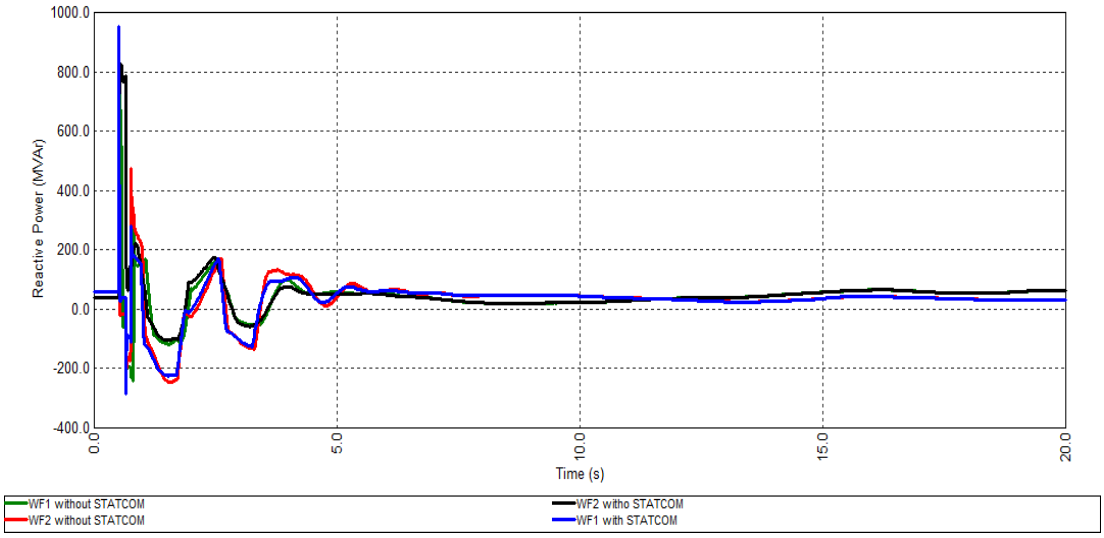

Figure 6.27 Reactive power of the two wind farms for case 4 with and without STATCOM mode.

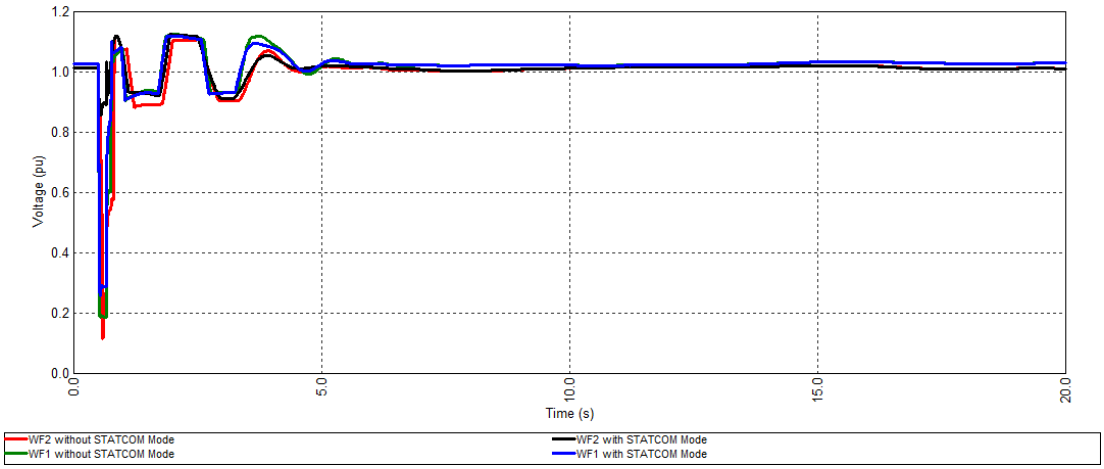

Figure 6.28 Terminal voltages of the two wind farms for case 4 with and without STATCOM mode.

6.5 Summary

The studies of this chapter have investigated the impacts of DFIG base wind farms on rotor angle stability of power systems. An existing SG in IEEE 9-bus test system is replaced by an equivalent DFIG based wind farm to show the impacts of replacing SGs by equivalent DFIG based wind farms on rotor angle stability. The obtained results show that SGs rotor angles can be affected if a conventional SG is replaced by an equivalent wind farm. The transient stability of the test system is reduced when the DFIG replaces the existing SG as a result of lack of reactive power support from the DFIG during the disturbance. However, this can be mitigated by using the proposed control approach of STATCOM mode for reactive power support. The results also show that DFIG wind turbines have no contribution to the power system oscillation; however, the implementation of the proposed PSS within the reactive power control loop of the wind farm helps to damp the oscillation effectively.

Studies on the impact of high penetration of DFIG wind power on the rotor angle stability of large system are also carried out in this chapter. Two large-scale SGs in IEEE 39-bus test system is replaced by an equivalent DFIG based wind farms to show the impacts of replacing large-scale SGs by equivalent DFIG based wind farms on rotor angle stability. The results of the large system enhanced the results obtained

in the previous test system. The proposed control approaches for DFIG wind turbines can mitigate the impacts of high penetration of wind power on power systems rotor angle stability. Moreover, it is interesting to observe that replacing a SG fitted out with PSS by an equivalent DFIG based wind farm equipped with the proposed control strategies has no negative impacts on the power system rotor angle stability. The power system oscillations are damped out more quickly by the DFIG proposed PSSs when compared to those in conventional SGs.

Additionally, the simulation results show that the proposed fixed parameters DFIG PSS can damp power system oscillations under a wide range of operating conditions of the wind farm and under various wind speeds. Therefore, a farm level PSS is possible by applying the same PSS signal to the reactive power control loop of all DFIG wind turbines.

Chapter 7

Conclusions and Future Work

7.1 Conclusions

This thesis has thoroughly evaluated the impacts of increased penetration levels of DFIG based wind turbines on rotor angle stability of power systems and how these impacts could be mitigated. In completing this research, a novel cost-effective control approach is developed to lessen the impacts of DFIG on the rotor angle stability through a more creative use of the existing DFIG equipment's (utilised DFIG-GSC as STATCOM and the designed PSS). The results show that the developed PSS has the capability to damp power oscillations effectively under variable operating conditions.

The proposed control approach is both important and relevant for power system operators. As wind power penetration into power systems increases, additional integration considerations are needed, and the most important considerations are fault ride through capability, damping of power oscillations and voltage support capabilities during network disturbances. Therefore, it is important to exploit the fast controllability of DFIG wind turbines in order to improve the stability of power systems, as well as carefully assessing any designed controllers to ensure that they perform satisfactorily across all system conditions. As the level of wind penetration

is increased, the benefit of such control scheme is that the DFIG-based wind turbines are able to take over the SGs responsibility to support power system stability.

The thesis began by presenting the development of wind power generation and wind turbine generator types concentrating on the relevant technologies in use today. The aim was to put forward an understanding of the dramatic increase of wind power integration and developments of wind power around the world. The main reasons behind the rapid growth of wind power integration are environmental and economic issues that are normally associated with fossil fuels [67]. A detailed discussion was presented on present wind generation and potential status globally. The integration of wind power has grown significantly from 17.4 GW in 2000 to more than 432 GW in 2015 and may reach 712 GW by 2020 [10, 14]. The integration of wind power is expected to continue as more countries have implemented encouraging policies to speed up the wind power development. Moreover, this thesis has presented a detailed analysis of different wind turbine technologies in use, their main components, and their advantages and disadvantages. The requirements for wind power integration such as frequency and voltage tolerance, reactive power and voltage control capability, frequency regulation and fault ride-through capabilities are also presented along with future technical requirements that may include inertial response and power system stabiliser. These special requirements are set for wind power integration to avoid any potential negative impacts that wind power may has on the operation and stability of power systems.

This thesis has also presented the modelling of the various components of a power system with emphasis on DFIG based wind turbines with the help of mathematical equations and diagrams. A dynamic model of commercial DFIG wind turbines is developed in this thesis to investigate the effect of DFIG wind turbines on power system rotor angle stability and to design an appropriate controller to mitigate these impacts [39, 182]. The model describes operational and mathematical equations of DFIG various subsystems, mainly wind turbine rotor aerodynamic model, a mechanical model, induction generator model, power converters model and associated control systems model, crowbar system and aggregated DFIG wind farm

model. In addition, operating range of DFIG wind turbines, characteristics, and the maximum power tracking curve for various wind speeds have also been discussed. Throughout the thesis, a detailed model of power system components, including DFIG wind turbines has provided a clear understanding of the impacts of high penetration of wind power on power system rotor angle stability especially when DFIG based wind farms are used to replace conventional SGs [39].

In this thesis, the impacts of increased penetration of wind generation on power system rotor angle stability have been examined carefully. The increased penetration of wind power indeed affects the stability of power system, as the dynamic characteristics of wind turbines are different from those of the SGs [42]. Moreover, the effects of wind generation on rotor angle stability depend on the type of the installed wind turbine [134]. Small signal stability is likely to be improved by wind power installation, particularly with fixed speed wind turbines due to the damping effect of induction generators. However, power system transient stability is likely to be degraded with high penetration of wind power particularly fixed speed wind turbines. To show the impacts of replacing SG by equivalent DFIG based wind farms on rotor angle stability, two case studies were conducted on realistic power systems using time domain simulation [39, 183]. IEEE 9-bus and IEEE 39 bus test systems have been utilised to show the impact of high penetration of wind power on power system rotor angle stability. The wind farm rating is equivalent to the replaced SG and produces the same amount of power that is generated by the replaced SG. The test system is evaluated by small and transient stability analysis without and with wind power under the same operation conditions. The results obtained clearly show that replacing a SG by a DFIG based wind farm has a negative impact on the transient stability of the power system, and the degree of the impact would depend on the control strategy used within the DFIG-RSC. Replacing an existing SG by an equivalent wind farm controlling its terminal voltage has less impact on rotor angle stability of the power system than replacing it with an equivalent wind farm operating at a unity power factor. However, the impact on small signal stability depends on whether the replaced SG is fitted with PSS or not. The damping of power

system oscillations is reduced if a DFIG based wind farm replaced an equivalent conventional SG equipped with PSS [39, 183].

A novel control strategy has been reported in this thesis to mitigate the impacts of DFIG wind turbines on rotor angle stability due to increased penetration levels of DFIGs into existing power systems. A control strategy for both DFIG rotor side and the grid side converters are proposed to mitigate DFIGs impacts on the system rotor angle stability. DFIG-GSC is utilised as static synchronous compensator (STATCOM) to provide reactive power support during grid faults. Since the terminal voltage of DFIG based wind farm can be controlled by the DFIG-RSC during normal operation conditions, the STATCOM mode can provide a voltage support during transient periods when the crowbar is active. The results obtained show that the produced reactive power helps to improve the terminal voltage of the wind farm during the disturbance and hence resulting in better system stability [39].

A PSS has been designed for reactive power control loop of DFIG-RSC. Although DFIGs are not synchronously coupled to the power systems, the damping of power system oscillations is reduced to some extent if a DFIG based wind farm replaced an equivalent conventional SG equipped with a PSS. This can be mitigated by equipping the DFIG wind turbines with the proposed PSS. This is a novel research into the use of DFIG reactive power to damp power system oscillations taking into account the influence of the crowbar system when the control of active and reactive power is lost, and a large amount of reactive power is absorbed. The PSS used in this thesis is based on conventional PSS, which has been used with SGs. This type of PSS is still preferred for its high robustness and a good performance which can be achieved with an easy tuning. Residual approach [169], which has been used for designing PSSs in SGs, is used in this thesis to design the DFIG-PSS. The obtained results show that the implementation of the proposed PSS within the reactive power control loop of the wind farm can influence the rotor angle of SGs and thus damp the power system oscillations effectively. The proposed PSS was validated further under a wide range of operation conditions to ensure it has the capability damp power oscillations effectively under non-uniform variable wind

speeds across the wind farm. The results confirm the robustness and stabilising effect against various operating modes and under various wind speeds [183]. Moreover, the results demonstrate clearly that DFIG based wind farms equipped with PSS can damp power system oscillations more effectively than SGs PSS. Furthermore, based on the obtained results, a farm level PSS is possible by applying the same PSS signal to reactive power control loop of all DFIG wind turbines within the wind farm. Such control scheme will be very beneficial as the levels of wind penetration are increased and to allow DFIG based wind farms take over SGs responsibility to damping power system oscillations. In addition, the obtained results show that DFIG based wind farms equipped with PSS can use STATCOM mode to improve system transient stability. The DFIG-GSC provides a reactive power support during the time when DFIG crowbar is active only. Conversely, the PSS starts to control the DFIG stator reactive power after the crowbar is deactivated.

7.2 Future Work

This thesis contributes to the impacts of high penetration of DFIG base wind turbines have on rotor angle stability of power systems and proposes a novel control strategy to lessen these impacts. The work presented within this thesis has fulfilled all of the research aims, which were initially defined. Nevertheless, there are a number of areas where this work could be extended in order to further develop the ideas and methods, which have been established.

- The proposed control strategy that used within this thesis for mitigating the impacts of DFIG based wind turbines on system rotor angle stability was applied to IEEE 9-bus and IEEE 39-bus test systems. It would be worthwhile for utilities to apply the proposed method to actual networks and compare the results obtained with those presented in this thesis.
- It would be useful to implement and validate the proposed control strategy with full-scale power converter wind turbines. As the GSC of Type IV wind turbines is designed for full rated power, more capacity is available to support the grid voltage and therefore better ride through capability during a typical grid faults

[17]. The grid-side converter of full-scale power converter wind turbines can be used as a STATCOM during fault [52]. Moreover, the proposed conventional power oscillation damping controller can be attached to the reactive power control loop of the Type IV wind turbines [184].

- The developed methods can be extended to include HVDC systems and also photovoltaic systems [17]. Both HVDC and photovoltaic systems are using power converters, which can be used in a similar way to the Type IV wind turbines [182].
- In the present work, the PSS input signal and its parameters are obtained according to residual approach results. Other methods [185] could be used to design the PSS and compare the obtained results with those presented in this thesis. Moreover, other types of PSS such as proportional-integral and proportional- integral-derivative can be examined instead of the proposed PSS and compare the obtained results with those presented in this thesis.
- It would be useful to investigate the use of STATCOM mode for both DFIG grid-side converter and rotor-side converter. When DFIG crowbar system is activated, the rotor-side converter will be deactivated. The mechanism of using both DFIG-RSC and GSC in parallel to provide more reactive power during grid disturbances could be examined.

The author hopes that this list of suggestions for future work will inspire other researchers working in this area.

References

[1] John Twidell and Tony Weir, *Renewable energy resources*: Routledge, 2015.

[2] Joseph Cullen, "Measuring the environmental benefits of wind-generated electricity," *American Economic Journal: Economic Policy,* vol. 5, pp. 107-133, 2013.

[3] S Bilgen, "Structure and environmental impact of global energy consumption," *Renewable and Sustainable Energy Reviews,* vol. 38, pp. 890-902, 2014.

[4] Kyoto Protocol, "United Nations framework convention on climate change," *Kyoto Protocol, Kyoto,* vol. 19, 1997.

[5] R Saidur, Mr Islam, Na Rahim, and Kh Solangi, "A review on global wind energy policy," *Renewable and Sustainable Energy Reviews,* vol. 14, pp. 1744-1762, 2010.

[6] Ryan Wiser and Mark Bolinger. (2013, Accessed: April 2016). *Wind Technologies Market Report*. Available at: https://www1.eere.energy.gov/wind/pdfs/2012_wind_technologies_market_report.pdf

[7] Global Wind Energy Council, "Global wind report: Annual market update 2011," *Global Wind Energy Council: Brussels, Belgium,* 2012.

[8] Brendan Fox, *Wind power integration: connection and system operational aspects* vol. 50: Iet, 2007.

[9] Ryan Wiser and Mark Bolinger. (2016, Accessed: November 2016). *Wind Technologies Market Report* Available at: https://energy.gov/sites/prod/files/2016/08/f33/2015-Wind-Technologies-Market-Report-08162016.pdf

[10] Global Wind Energy Council. (2014, Accessed: May 2016). *Global Wind Report 2014* Available at: http://www.gwec.net/wp-content/uploads/2015/03/GWEC_Global_Wind_2014_Report_LR.pdf

[11] Iea. (2013, Accessed: October 2016). *Technology Roadmap, Wind Energy*. Available at: http://www.iea.org/publications/freepublications/publication/Wind_2013_Roadmap.pdf

[12] Steven Chu and Arun Majumdar, "Opportunities and challenges for a sustainable energy future," *nature,* vol. 488, pp. 294-303, 2012.

[13] Renewable Energy Policy Network for the 21st Century, "Renewables 2016 global status report-Annual Reporting on Renewables: Ten years of excellence," 2016.

[14] Global Wind Energy Council. (2014, Accessed). *Global Wind Energy Outlook 2014*. Available at: http://www.gwec.net/wp-content/uploads/2014/10/GWEO2014_WEB.pdf

[15] Serhiy Bozhko, Greg Asher, Risheng Li, Jon Clare, and Liangzhong Yao, "Large offshore DFIG-based wind farm with line-commutated HVDC connection to the main grid: engineering studies," *IEEE Transactions on Energy Conversion*, vol. 23, pp. 119-127, 2008.

[16] F. Blaabjerg and Ma Ke, "Future on Power Electronics for Wind Turbine Systems," *Emerging and Selected Topics in Power Electronics, IEEE Journal of*, vol. 1, pp. 139-152, 2013.

[17] Thomas Ackermann, *Wind Power in Power Systems*: John Wiley & Sons, 2012.

[18] Roberto Cardenas, Ruben Pena, Salvador Alepuz, and Greg Asher, "Overview of control systems for the operation of DFIGs in wind energy applications," *IEEE Transactions on Industrial Electronics*, vol. 60, pp. 2776-2798, 2013.

[19] Jg Slootweg and Wl Kling, "The impact of large scale wind power generation on power system oscillations," *Electric Power Systems Research*, vol. 67, pp. 9-20, 2003.

[20] Vladislav Akhmatov, Hans Knudsen, Arne Hejde Nielsen, Jørgen Kaas Pedersen, and Niels Kjølstad Poulsen, "Modelling and transient stability of large wind farms," *International Journal of Electrical Power & Energy Systems*, vol. 25, pp. 123-144, 2003.

[21] Zhe Chen, "Issues of connecting wind farms into power systems," in *Transmission and Distribution Conference and Exhibition: Asia and Pacific, 2005 IEEE/PES*, 2005, pp. 1-6.

[22] Marina Tsili and S Papathanassiou, "A review of grid code technical requirements for wind farms," *IET Renewable Power Generation*, vol. 3, pp. 308-332, 2009.

[23] Oriol Gomis-Bellmunt, Adria Junyent-Ferre, Andreas Sumper, and Joan Bergas-Jane, "Ride-through control of a doubly fed induction generator under unbalanced voltage sags," *IEEE Transactions on Energy Conversion*, vol. 23, pp. 1036-1045, 2008.

[24] National Grid Electricity Transmission Plc. (2016 Accessed: January 2017). *The grid code, Issue 5, Revision 19*. Available at:

http://www2.nationalgrid.com/uk/industry-information/electricity-codes/grid-code/the-grid-code/

[25] Zhe Chen and Frede Blaabjerg, "Wind farm—A power source in future power systems," *Renewable and Sustainable Energy Reviews,* vol. 13, pp. 1288-1300, 2009.

[26] Olimpo Anaya-Lara, Nick Jenkins, Janaka Ekanayake, Phill Cartwright, and Michael Hughes, *Wind energy generation: modelling and control*: John Wiley & Sons, 2011.

[27] José Luis Domínguez-García, Oriol Gomis-Bellmunt, Lluís Trilla-Romero, and Adrià Junyent-Ferré, "Indirect vector control of a squirrel cage induction generator wind turbine," *Computers & Mathematics with Applications,* vol. 64, pp. 102-114, 2012.

[28] Manfred Stiebler, *Wind energy systems for electric power generation*: Springer Science & Business Media, 2008.

[29] José Luis Domínguez-García, Oriol Gomis-Bellmunt, Fernando D Bianchi, and Andreas Sumper, "Power oscillation damping supported by wind power: a review," *Renewable and Sustainable Energy Reviews,* vol. 16, pp. 4994-5006, 2012.

[30] Y. Mishra, S. Mishra, M. Tripathy, N. Senroy, and Z. Y. Dong, "Improving Stability of a DFIG-Based Wind Power System With Tuned Damping Controller," *Energy Conversion, IEEE Transactions on,* vol. 24, pp. 650-660, 2009.

[31] F Michael Hughes, Olimpo Anaya-Lara, Nicholas Jenkins, and Goran Strbac, "A power system stabilizer for DFIG-based wind generation," *Power Systems, IEEE Transactions on,* vol. 21, pp. 763-772, 2006.

[32] Prabha Kundur, John Paserba, Venkat Ajjarapu, Göran Andersson, Anjan Bose, Claudio Canizares, Nikos Hatziargyriou, David Hill, Alex Stankovic, and Carson Taylor, "Definition and classification of power system stability IEEE/CIGRE joint task force on stability terms and definitions," *Power Systems, IEEE Transactions on,* vol. 19, pp. 1387-1401, 2004.

[33] F. R. Schleif and J. H. White, "Damping for the northwest-southwest tieline oscillations-An analog study," *IEEE Transactions on Power Apparatus and Systems,* pp. 1239-1247, 1966.

[34] Dmitry N Kosterev, Carson W Taylor, and William A Mittelstadt, "Model validation for the August 10, 1996 WSCC system outage," *IEEE transactions on power systems,* vol. 14, pp. 967-979, 1999.

[35] Vaithianathan Venkatasubramanian and Yuan Li, "Analysis of 1996 Western American electric blackouts," *Bulk Power System Dynamics and Control-VI, Cortina d'Ampezzo, Italy,* pp. 22-27, 2004.

[36] Graham Rogers, *Power system oscillations*: Springer Science & Business Media, 2012.

[37] Bikash Pal and Balarko Chaudhuri, *Robust control in power systems*: Springer Science & Business Media, 2006.

[38] Yi Wang, Jianhui Meng, Xiangyu Zhang, and Lie Xu, "Control of PMSG-based wind turbines for system inertial response and power oscillation damping," *IEEE Transactions on Sustainable Energy,* vol. 6, pp. 565-574, 2015.

[39] Mohamed Edrah, Kwok L Lo, and Olimpo Anaya-Lara, "Impacts of high penetration of DFIG wind turbines on rotor angle stability of power systems," *IEEE Transactions on Sustainable Energy,* vol. 6, pp. 759-766, 2015.

[40] Aiguo Tan, Xiangning Lin, Jinwen Sun, Ran Lyu, Zhengtian Li, Long Peng, and Muhammad Shoaib Khalid, "A Novel DFIG Damping Control for Power System with High Wind Power Penetration," *Energies,* vol. 9, p. 521, 2016.

[41] Wu Feng, Zhang Xiao-Ping, K. Godfrey, and Ju Ping, "Modeling and Control of Wind Turbine with Doubly Fed Induction Generator," in *Power Systems Conference and Exposition, 2006. PSCE '06. 2006 IEEE PES*, 2006, pp. 1404-1409.

[42] M. J. Hossain, H. R. Pota, M. A. Mahmud, and R. A. Ramos, "Investigation of the Impacts of Large-Scale Wind Power Penetration on the Angle and Voltage Stability of Power Systems," *Systems Journal, IEEE,* vol. 6, pp. 76-84, 2012.

[43] Mk Döşoğlu, A Basa Arsoy, and U Güvenç, "Application of STATCOM-supercapacitor for low-voltage ride-through capability in DFIG-based wind farm," *Neural Computing and Applications,* pp. 1-10, 2016.

[44] Wei Qiao, Ronald G Harley, and Ganesh Kumar Venayagamoorthy, "Coordinated reactive power control of a large wind farm and a STATCOM using heuristic dynamic programming," *IEEE Transactions on Energy Conversion,* vol. 24, pp. 493-503, 2009.

[45] Marta Molinas, Jon Are Suul, and Tore Undeland, "Low voltage ride through of wind farms with cage generators: STATCOM versus SVC," *IEEE Transactions on power electronics,* vol. 23, pp. 1104-1117, 2008.

[46] E. Vittal, M. O'malley, and A. Keane, "Rotor Angle Stability With High Penetrations of Wind Generation," *Power Systems, IEEE Transactions on,* vol. 27, pp. 353-362, 2012.

[47] Graham Pannell, David J Atkinson, and Bashar Zahawi, "Minimum-threshold crowbar for a fault-ride-through grid-code-compliant DFIG wind turbine," *Energy Conversion, IEEE Transactions on,* vol. 25, pp. 750-759, 2010.

[48] A. H. Kasem, E. F. El-Saadany, H. H. El-Tamaly, and M. A. A. Wahab, "An improved fault ride-through strategy for doubly fed induction generator-based wind turbines," *Renewable Power Generation, IET,* vol. 2, pp. 201-214, 2008.

[49] Anca D. Hansen and Gabriele Michalke, "Fault ride-through capability of DFIG wind turbines," *Renewable Energy,* vol. 32, pp. 1594-1610, 2007.

[50] Lasantha Gunaruwan Meegahapola, Tim Littler, and Damian Flynn, "Decoupled-DFIG fault ride-through strategy for enhanced stability performance during grid faults," *Sustainable Energy, IEEE Transactions on,* vol. 1, pp. 152-162, 2010.

[51] R Pena, Jc Clare, and Gm Asher, "Doubly fed induction generator using back-to-back PWM converters and its application to variable-speed wind-energy generation," *IEE Proceedings-Electric Power Applications,* vol. 143, pp. 231-241, 1996.

[52] Thanh Hai Nguyen and Dong-Choon Lee, "Advanced fault ride-through technique for PMSG wind turbine systems using line-side converter as STATCOM," *Industrial Electronics, IEEE Transactions on,* vol. 60, pp. 2842-2850, 2013.

[53] Arjen A Van Der Meer, Ralph L Hendriks, and Wil L Kling, "A survey of fast power reduction methods for VSC connected wind power plants consisting of different turbine types," *EPE wind energy,* pp. 23-24, 2009.

[54] G Ramtharan, Atputharajah Arulampalam, Janaka Bandara Ekanayake, Fm Hughes, and Nick Jenkins, "Fault ride through of fully rated converter wind turbines with AC and DC transmission systems," *IET Renewable Power Generation,* vol. 3, pp. 426-438, 2009.

[55] Durga Gautam, Vijay Vittal, and Terry Harbour, "Impact of increased penetration of DFIG-based wind turbine generators on transient and small signal stability of power systems," *IEEE transactions on power systems,* vol. 24, pp. 1426-1434, 2009.

[56] Georgios Tsourakis, Basil M Nomikos, and Costas D Vournas, "Contribution of doubly fed wind generators to oscillation damping," *Energy Conversion, IEEE Transactions on,* vol. 24, pp. 783-791, 2009.

[57] Georgios Tsourakis, Basil M Nomikos, and Costas D Vournas, "Contribution of doubly fed wind generators to oscillation damping," *IEEE Transactions on Energy Conversion,* vol. 24, pp. 783-791, 2009.

[58] D. Gautam, V. Vittal, R. Ayyanar, and T. Harbour, "Supplementary control for damping power oscillations due to increased penetration of doubly fed induction generators in large power systems," in *Power Systems Conference and Exposition (PSCE), 2011 IEEE/PES*, 2011, pp. 1-6.

[59] Zhixin Miao, Lingling Fan, Dale Osborn, and Subbaraya Yuvarajan, "Control of DFIG-based wind generation to improve interarea oscillation damping," *Energy Conversion, IEEE Transactions on,* vol. 24, pp. 415-422, 2009.

[60] Mohamed Edrah, Kwok L Lo, Abdussalam Elansari, and Olimpo Anaya-Lara, "Power oscillation damping capabilities of doubly fed wind generators," in *Power Engineering Conference (UPEC), 2014 49th International Universities*, 2014, pp. 1-6.

[61] S Muller, M Deicke, and Rik W De Doncker, "Doubly fed induction generator systems for wind turbines," *Industry Applications Magazine, IEEE,* vol. 8, pp. 26-33, 2002.

[62] Fan Lingling, Yin Haiping, and Miao Zhixin, "On Active/Reactive Power Modulation of DFIG-Based Wind Generation for Interarea Oscillation Damping," *Energy Conversion, IEEE Transactions on,* vol. 26, pp. 513-521, 2011.

[63] F. M. Hughes, O. Anaya-Lara, G. Ramtharan, N. Jenkins, and G. Strbac, "Influence of Tower Shadow and Wind Turbulence on the Performance of Power System Stabilizers for DFIG-Based Wind Farms," *Energy Conversion, IEEE Transactions on,* vol. 23, pp. 519-528, 2008.

[64] Yin Haiping, Fan Lingling, and Miao Zhixin, "Reactive power modulation for inter-area oscillation damping of DFIG-based wind generation," in *Power and Energy Society General Meeting, 2010 IEEE*, 2010, pp. 1-9.

[65] R. D. Fernandez, R. J. Mantz, and P. E. Battaiotto, "Contribution of wind farms to the network stability," in *Power Engineering Society General Meeting, 2006. IEEE,* 2006, p. 6 pp.

[66] International Energy Agency. (2015, Accessed: May 2016). *CO2 emissions from fuel combustion 2015*. Available at: https://www.iea.org/publications/freepublications/publication/CO2EmissionsFromFuelCombustionHighlights2015.pdf

[67] European Commission. (2009, Accessed: November 2016). *National Renewable Energy Action Plan for the United Kingdom*. Available at: https://ec.europa.eu/energy/en/topics/renewable-energy/national-action-plans

[68] Thomas Ackermann, *Wind Power in Power Systems*: John Wiley & Sons, Ltd, 2005.

[69] Global Wind Energy Council. (2015, Accessed: May 2016). *Global Wind Report*. Available at: http://www.gwec.net/wp-content/uploads/vip/GWEC-Global-Wind-2015-Report_April-2016_22_04.pdf

[70] Dennis Yc Leung and Yuan Yang, "Wind energy development and its environmental impact: A review," *Renewable and Sustainable Energy Reviews,* vol. 16, pp. 1031-1039, 2012.

[71] Jianzhong Xu, Dexin He, and Xiaolu Zhao, "Status and prospects of Chinese wind energy," *Energy,* vol. 35, pp. 4439-4444, 2010.

[72] Global Wind Energy Council. (2015, Accessed: June 2016). *Overview of China's wind development*. Available at: http://www.gwec.net/news/china-focus/graphs-chinese-marke/

[73] Fr Pazheri, Mf Othman, and Nh Malik, "A review on global renewable electricity scenario," *Renewable and Sustainable Energy Reviews,* vol. 31, pp. 835-845, 2014.

[74] Inga Margrete Ydersbond and Marius Korsnes, "Wind Power in China and in the EU: Comparative Analysis of Key Political Drivers," *Energy Procedia,* vol. 58, pp. 95-102, 2014.

[75] European Wind Energy Association. (2015, Accessed: June 2016). *Wind in power 2014 European statistics*. Available at: http://www.ewea.org/fileadmin/files/library/publications/statistics/EWEA-Annual-Statistics-2014.pdf

[76] Liyan Qu and Wei Qiao, "Constant power control of DFIG wind turbines with supercapacitor energy storage," *Industry Applications, IEEE Transactions on,* vol. 47, pp. 359-367, 2011.

[77] Renewableuk. (2015, Accessed: May 2016). *Wind Energy in the UK, State of the Industry Report Summary* Available at: http://c.ymcdn.com/sites/www.renewableuk.com/resource/resmgr/publications/reports/soi_report_summary_2015.pdf

[78] O. Anaya-Lara, N. Jenkins, J. Ekanayake, P. Cartwright, and M. Hughes, *Wind Energy Generation: Modelling and Control*: Wiley, 2009.

[79] Ahmed M. Ewais, Carlos Ugalde-Loo, Janaka B. Ekanayake, Jun Liang, and Nick Jenkins, "Influence of Fixed-Speed Induction Generator-Based Wind Turbines on Subsynchronous Resonance," in *Universities' Power Engineering Conference (UPEC), Proceedings of 2011 46th International*, 2011, pp. 1-6.

[80] H. Polinder, D. Bang, R. P. J. O. M. Van Rooij, A. S. Mcdonald, and M. A. Mueller, "10 MW Wind Turbine Direct-Drive Generator Design with Pitch or Active Speed Stall Control," in *Electric Machines & Drives Conference, 2007. IEMDC '07. IEEE International*, 2007, pp. 1390-1395.

[81] Tony Burton, David Sharpe, Nick Jenkins, and Ervin Bossanyi, *Wind energy handbook*: John Wiley & Sons, 2001.

[82] Panos Pardalos, Steffen Rebennack, Mario Vf Pereira, Niko A Iliadis, and Vijay Pappu, *Handbook of Wind Power Systems*: Springer, 2014.

[83] Tony Burton, David Sharpe, Nick Jenkins, and Ervin Bossanyi, *Wind energy handbook*: John Wiley & Sons, 2011.

[84] L Holdsworth, Janaka Bandara Ekanayake, and Nicholas Jenkins, "Power system frequency response from fixed speed and doubly fed induction generator-based wind turbines," *Wind Energy*, vol. 7, pp. 21-35, 2004.

[85] Dd Banham-Hall, Ga Taylor, Ca Smith, and Mr Irving, "Towards large-scale direct drive wind turbines with permanent magnet generators and full converters," in *Power and Energy Society General Meeting, 2010 IEEE*, 2010, pp. 1-8.

[86] Alan Mullane and Mark O'malley, "The inertial response of induction-machine-based wind turbines," *Power Systems, IEEE Transactions on*, vol. 20, pp. 1496-1503, 2005.

[87] Ye Wang, Gauthier Delille, Herman Bayem, Xavier Guillaud, and Bruno Francois, "High wind power penetration in isolated power systems—assessment of wind inertial and primary frequency responses," *Power Systems, IEEE Transactions on*, vol. 28, pp. 2412-2420, 2013.

[88] Johan Morren, Sjoerd Wh De Haan, Wil L Kling, and Ja Ferreira, "Wind turbines emulating inertia and supporting primary frequency control," *IEEE Transactions on Power Systems, 21 (1)*, 2006.

[89] Prabha Kundur, *Power system stability and control*: McGraw-hill New York, 1994.

[90] "IEEE Guide for Synchronous Generator Modeling Practices and Applications in Power System Stability Analyses," *IEEE Std 1110-2002 (Revision of IEEE Std 1110-1991)*, pp. 0_1-72, 2003.

[91] Peter W Sauer and M. A. Pal, *Power system dynamics and stability*: Prentice Hall, 1998.

[92] "IEEE Recommended Practice for Excitation System Models for Power System Stability Studies," *IEEE Std 421.5-2005 (Revision of IEEE Std 421.5-1992)*, pp. 0_1-85, 2006.

[93] S Kalyani, M Prakash, and G Angeline Ezhilarasi, "Transient stability studies in SMIB system with detailed machine models," in *Recent Advancements in Electrical, Electronics and Control Engineering (ICONRAEeCE), 2011 International Conference on*, 2011, pp. 459-464.

[94] W. W. Price, H. D. Chiang, H. K. Clark, C. Concordia, D. C. Lee, J. C. Hsu, S. Ihara, C. A. King, C. J. Lin, and Y. Mansour, "Load representation for dynamic performance analysis " *IEEE transactions on power systems,* vol. 8, pp. 472-482, 1993.

[95] C. Concordia and S. Ihara, "Load Representation in Power System Stability Studies," *Power Apparatus and Systems, IEEE Transactions on,* vol. PAS-101, pp. 969-977, 1982.

[96] Richard G Farmer, "Power system dynamics and stability," *The Electric Power Engineering Handbook,* 2001.

[97] Ww Price, Cw Taylor, and Gj Rogers, "Standard load models for power flow and dynamic performance simulation," *IEEE transactions on power systems,* vol. 10, 1995.

[98] James F Manwell, Jon G Mcgowan, and Anthony L Rogers, *Wind energy explained: theory, design and application*: John Wiley & Sons, 2010.

[99] Magdi Ragheb and Adam M Ragheb, *Wind turbines theory-the betz equation and optimal rotor tip speed ratio*: INTECH Open Access Publisher, 2011.

[100] Sm Muyeen, Junji Tamura, and Toshiaki Murata, *Stability augmentation of a grid-connected wind farm*: Springer Science & Business Media, 2008.

[101] S. M. Muyeen, M. H. Ali, R. Takahashi, T. Murata, J. Tamura, Y. Tomaki, A. Sakahara, and E. Sasano, "Comparative study on transient stability analysis of wind turbine generator system using different drive train models," *Renewable Power Generation, IET,* vol. 1, pp. 131-141, 2007.

[102] Nicholas W Miller, William W Price, and Juan J Sanchez-Gasca, "Dynamic modeling of GE 1.5 and 3.6 wind turbine-generators," *GE-Power systems energy consulting,* 2003.

[103] Salman K Salman and Anita Lj Teo, "Windmill modeling consideration and factors influencing the stability of a grid-connected wind power-based embedded generator," *Power Systems, IEEE Transactions on,* vol. 18, pp. 793-802, 2003.

[104] Ren-Jie Ye, Hui Li, Zhe Chen, and Qiang Gao, "Comparison of transient behaviors of wind turbines with DFIG considering the shaft flexible models," in *Electrical Machines and Systems, 2008. ICEMS 2008. International Conference on*, 2008, pp. 2585-2590.

[105] Miguel García-Gracia, M Paz Comech, Jesus Sallan, and Andrés Llombart, "Modelling wind farms for grid disturbance studies," *Renewable Energy,* vol. 33, pp. 2109-2121, 2008.

[106] Wei Qiao, "Dynamic modeling and control of doubly fed induction generators driven by wind turbines," in *Power Systems Conference and Exposition, 2009. PSCE'09. IEEE/PES*, 2009, pp. 1-8.

[107] Jiang Zhenhua and Yu Xunwei, "Modeling and control of an integrated wind power generation and energy storage system," in *Power & Energy Society General Meeting, 2009. PES '09. IEEE*, 2009, pp. 1-8.

[108] M. V. A. Nunes, J. A. Peas Lopes, H. H. Zurn, U. H. Bezerra, and R. G. Almeida, "Influence of the variable-speed wind generators in transient stability margin of the conventional generators integrated in electrical grids," *Energy Conversion, IEEE Transactions on*, vol. 19, pp. 692-701, 2004.

[109] Anca D Hansen, Clemens Jauch, Poul Ejnar Sørensen, Florin Iov, and Frede Blaabjerg, *Dynamic wind turbine models in power system simulation tool DIgSILENT*, 2004.

[110] Johannes Gerlof Slootweg, *Wind power: Modelling and impact on power system dynamics*: TU Delft, Delft University of Technology, 2003.

[111] E Tremblay, A Chandra, and Pj Lagace, "Grid-side converter control of DFIG wind turbines to enhance power quality of distribution network," in *Power Engineering Society General Meeting, 2006. IEEE*, 2006, p. 6 pp.

[112] Arantxa Tapia, Gerardo Tapia, J Xabier Ostolaza, and Jose Ramon Saenz, "Modeling and control of a wind turbine driven doubly fed induction generator," *Energy Conversion, IEEE Transactions on*, vol. 18, pp. 194-204, 2003.

[113] Qiao Wei, G. K. Venayagamoorthy, and R. G. Harley, "Real-Time Implementation of a STATCOM on a Wind Farm Equipped With Doubly Fed Induction Generators," *Industry Applications, IEEE Transactions on*, vol. 45, pp. 98-107, 2009.

[114] Jouko Niiranen, "Voltage dip ride through of a doubly-fed generator equipped with an active crowbar," in *Nordic wind power conference*, 2004.

[115] Ralf Lohde, Simon Jensen, André Knop, and Friedrich W Fuchs, "Analysis of three phase grid failure and doubly fed induction generator ride-through using crowbars," in *Power Electronics and Applications, 2007 European Conference on*, 2007, pp. 1-8.

[116] Dawei Xiang, Li Ran, Peter J Tavner, and Shunchang Yang, "Control of a doubly fed induction generator in a wind turbine during grid fault ride-through," *IEEE Transactions on Energy Conversion*, vol. 21, pp. 652-662, 2006.

[117] Qiao Wei, Zhou Wei, J. M. Aller, and R. G. Harley, "Wind Speed Estimation Based Sensorless Output Maximization Control for a Wind Turbine Driving a

DFIG," *Power Electronics, IEEE Transactions on*, vol. 23, pp. 1156-1169, 2008.

[118] Morten H Hansen, Anca Daniela Hansen, Torben J Larsen, Stig Øye, Poul Sørensen, and Peter Fuglsang, *Control design for a pitch-regulated, variable speed wind turbine*, 2005.

[119] M Carolin Mabel and E Fernandez, "Estimation of energy yield from wind farms using artificial neural networks," *Energy Conversion, IEEE Transactions on*, vol. 24, pp. 459-464, 2009.

[120] Anca Hansen, Poul Sørensen, Florin Iov, and Frede Blaabjerg, "Control of variable speed wind turbines with doubly-fed induction generators," *Wind Engineering*, vol. 28, pp. 411-432, 2004.

[121] Bin Wu, Yongqiang Lang, Navid Zargari, and Samir Kouro, *Power conversion and control of wind energy systems*: John Wiley & Sons, 2011.

[122] Luis M Fernández, Francisco Jurado, and José Ramón Saenz, "Aggregated dynamic model for wind farms with doubly fed induction generator wind turbines," *Renewable Energy*, vol. 33, pp. 129-140, 2008.

[123] Janaka B Ekanayake, Lee Holdsworth, Xueguang Wu, and Nicholas Jenkins, "Dynamic modeling of doubly fed induction generator wind turbines," *Power Systems, IEEE Transactions on*, vol. 18, pp. 803-809, 2003.

[124] Markus Pÿller and Sebastian Achilles, "Aggregated wind park models for analyzing power system dynamics," 2003.

[125] Lm Fernandez, Ca Garcia, Jr Saenz, and F Jurado, "Equivalent models of wind farms by using aggregated wind turbines and equivalent winds," *Energy conversion and management*, vol. 50, pp. 691-704, 2009.

[126] Shenghu Li, Zhengkai Liu, and Yudong Jia, "Dynamic aggregation of doubly-fed induction generators (DFIGs) for stability analysis of wind power systems," in *Power and Energy Society General Meeting, 2011 IEEE*, 2011, pp. 1-6.

[127] Vladislav Akhmatov and Hans Knudsen, "An aggregate model of a grid-connected, large-scale, offshore wind farm for power stability investigations—importance of windmill mechanical system," *International Journal of Electrical Power & Energy Systems*, vol. 24, pp. 709-717, 2002.

[128] Jan Machowski, Janusz Bialek, and Jim Bumby, *Power system dynamics: stability and control*: John Wiley & Sons, 2011.

[129] Mania Pavella, Damien Ernst, and Daniel Ruiz-Vega, *Transient stability of power systems: a unified approach to assessment and control*: Springer Science & Business Media, 2012.

[130] Carson W Taylor, *Power system voltage stability*: McGraw-Hill, 1994.

[131] Gk Morison, B Gao, and P Kundur, "Voltage stability analysis using static and dynamic approaches," *Power Systems, IEEE Transactions on,* vol. 8, pp. 1159-1171, 1993.

[132] J. G. Slootweg and W. L. Kling, "The impact of large scale wind power generation on power system oscillations," *Electric Power Systems Research,* vol. 67, pp. 9-20, 2003.

[133] Ahmadreza Tabesh and Reza Iravani, "Small-signal model and dynamic analysis of variable speed induction machine wind farms," *Renewable Power Generation, IET,* vol. 2, pp. 215-227, 2008.

[134] Yuanzhang Sun, Lixin Wang, Guojie Li, and Jin Lin, "A review on analysis and control of small signal stability of power systems with large scale integration of wind power," in *Power System Technology (POWERCON), 2010 International Conference on*, 2010, pp. 1-6.

[135] Olimpo Anaya-Lara, F. Michael Hughes, Nicholas Jenkins, and Goran Strbac, "Influence of Windfarms on Power System Dynamic and Transient Stability," *Wind Engineering,* vol. 30, pp. 107-127, 2006.

[136] N. R. Chaudhuri and B. Chaudhuri, "Impact of wind penetration and HVDC upgrades on dynamic performance of future grids," in *Power and Energy Society General Meeting, 2011 IEEE*, 2011, pp. 1-8.

[137] Nilesh Modi, Tapan K Saha, and N Mithulananthan, "Effect of wind farms with doubly fed induction generators on small-signal stability—a case study on Australian equivalent system," in *Innovative Smart Grid Technologies Asia (ISGT), 2011 IEEE PES*, 2011, pp. 1-7.

[138] Zhixin Miao, Lingling Fan, Dale Osborn, and Subbaraya Yuvarajan, "Control of DFIG-based wind generation to improve interarea oscillation damping," *IEEE Transactions on Energy Conversion,* vol. 24, pp. 415-422, 2009.

[139] Huang Huazhang and C. Y. Chung, "Design of a Power Oscillation Damper for DFIG-based Wind Energy Conversion System Using Modified Particle Swarm Optimizer," in *Modelling Symposium (AMS), 2012 Sixth Asia*, 2012, pp. 161-166.

[140] Costas D Vournas, Emmanuel G Potamianakis, Cédric Moors, and Thierry Van Cutsem, "An educational simulation tool for power system control and stability," *Power Systems, IEEE Transactions on,* vol. 19, pp. 48-55, 2004.

[141] F Michael Hughes, Olimpo Anaya-Lara, Nicholas Jenkins, and Goran Strbac, "Control of DFIG-based wind generation for power network support," *Power Systems, IEEE Transactions on,* vol. 20, pp. 1958-1966, 2005.

[142] Jg Slootweg and Wl Kling, "Modelling and analysing impacts of wind power on transient stability of power systems," *Wind Engineering*, vol. 26, pp. 3-20, 2002.

[143] Liu Chengxi, Chen Zhe, C. L. Bak, Liu Zhou, P. Lund, and P. Ronne-Hansen, "Transient stability assessment of power system with large amount of wind power penetration: The Danish case study," in *IPEC, 2012 Conference on Power & Energy*, 2012, pp. 461-467.

[144] Qiao Wei and R. G. Harley, "Effect of grid-connected DFIG wind turbines on power system transient stability," in *Power and Energy Society General Meeting - Conversion and Delivery of Electrical Energy in the 21st Century, 2008 IEEE*, 2008, pp. 1-7.

[145] Chi Yongning, Liu Yanhua, Wang Weisheng, and Dai Huizhu, "Voltage Stability Analysis of Wind Farm Integration into Transmission Network," in *Power System Technology, 2006. PowerCon 2006. International Conference on*, 2006, pp. 1-7.

[146] C Samarasinghe and G Ancell, "Effects of large scale wind generation on transient stability of the New Zealand power system," in *Power and Energy Society General Meeting-Conversion and Delivery of Electrical Energy in the 21st Century, 2008 IEEE*, 2008, pp. 1-8.

[147] N. R. Ullah and T. Thiringer, "Variable Speed Wind Turbines for Power System Stability Enhancement," *Energy Conversion, IEEE Transactions on*, vol. 22, pp. 52-60, 2007.

[148] A. Dittrich and A. Stoev, "Comparison of fault ride-through strategies for wind turbines with DFIM generators," in *Power Electronics and Applications, 2005 European Conference on*, 2005, pp. 8 pp.-P.8.

[149] A. A. Tamimi, A. Pahwa, and S. Starrett, "Effective Wind Farm Sizing Method for Weak Power Systems Using Critical Modes of Voltage Instability," *Power Systems, IEEE Transactions on*, vol. 27, pp. 1610-1617, 2012.

[150] R. S. Al Abri, E. F. El-Saadany, and Y. M. Atwa, "Optimal Placement and Sizing Method to Improve the Voltage Stability Margin in a Distribution System Using Distributed Generation," *Power Systems, IEEE Transactions on*, vol. 28, pp. 326-334, 2013.

[151] M. El-Shimy, M. A. L. Badr, and O. M. Rassem, "Impact of large scale wind power on power system stability," in *Power System Conference, 2008. MEPCON 2008. 12th International Middle-East*, 2008, pp. 630-636.

[152] G. Lalor, A. Mullane, and M. O'malley, "Frequency control and wind turbine technologies," *Power Systems, IEEE Transactions on*, vol. 20, pp. 1905-1913, 2005.

[153] Yuan-Zhang Sun, Zhao-Sui Zhang, Guo-Jie Li, and Jin Lin, "Review on frequency control of power systems with wind power penetration," in *Power System Technology (POWERCON), 2010 International Conference on*, 2010, pp. 1-8.

[154] M. Kayikci, Milanovic, X, and J. V., "Dynamic Contribution of DFIG-Based Wind Plants to System Frequency Disturbances," *Power Systems, IEEE Transactions on*, vol. 24, pp. 859-867, 2009.

[155] Dominic D Banham-Hall, Gareth A Taylor, Chris A Smith, and Malcolm R Irving, "Flow batteries for enhancing wind power integration," *IEEE transactions on power systems*, vol. 27, pp. 1690-1697, 2012.

[156] P.M. Anderson and A.A. Fouad, *POWER SYSTEM CONTROL AND STABILITY*: Wiley-IEEE Press 2003.

[157] Bcp Busarello. (2010, Accessed: May 2016). *Cott+ Partner AG,"NEPLAN, power system analysis,"* Available at: www. neplan. ch

[158] Ma Pai, *Energy Function Analysis for Power System Stability*: Springer Science & Business Media, 1989.

[159] Libao Shi, Shiqiang Dai, Yixin Ni, Liangzhong Yao, and Masoud Bazargan, "Transient stability of power systems with high penetration of DFIG based wind farms," in *Power & Energy Society General Meeting, 2009. PES'09. IEEE*, 2009, pp. 1-6.

[160] Jan Machowski, Janusz Bialek, and James Richard Bumby, *Power system dynamics and stability*: John Wiley & Sons, 1997.

[161] A Elices, L Rouco, H Bourles, and T Margotin, "Design of robust controllers for damping interarea oscillations: Application to the European power system," *Power Systems, IEEE Transactions on*, vol. 19, pp. 1058-1067, 2004.

[162] International Conference on Large High Voltage Electric Systems, *Analysis and Control of Power System Oscillations: Final Report*: CIGRE, 1996.

[163] Nelson Martins and Leonardo Tg Lima, "Determination of suitable locations for power system stabilizers and static var compensators for damping electromechanical oscillations in large scale power systems," *Power Systems, IEEE Transactions on*, vol. 5, pp. 1455-1469, 1990.

[164] Ev Larsen and Da Swann, "Applying power system stabilizers part ii: Performance objectives and tuning concepts," *Power Apparatus and Systems, IEEE Transactions on*, pp. 3025-3033, 1981.

[165] M. A. Abido, "A novel approach to conventional power system stabilizer design using tabu search," *International Journal of Electrical Power & Energy Systems*, vol. 21, pp. 443-454, 1999.

[166] Mohamed Edrah, Kwok L Lo, and Olimpo Anaya-Lara, "Impacts of High Penetration of DFIG Wind Turbines on Rotor Angle Stability of Power Systems," *Sustainable Energy, IEEE Transactions on,* vol. 6, pp. 759-766, 2015.

[167] Ram B Gupta, *Hydrogen fuel: production, transport, and storage*: CRC Press, 2008.

[168] F Luis Pagola, Ignacio J Pérez-Arriaga, and George C Verghese, "On sensitivities, residues and participations: applications to oscillatory stability analysis and control," *Power Systems, IEEE Transactions on,* vol. 4, pp. 278-285, 1989.

[169] J Eichman, Kevin William Harrison, and Michael Peters, *Novel Electrolyzer Applications: Providing More Than Just Hydrogen*: National Renewable Energy Laboratory, 2014.

[170] L Rouco and Fl Pagola, "An eigenvalue sensitivity approach to location and controller design of controllable series capacitors for damping power system oscillations," *Power Systems, IEEE Transactions on,* vol. 12, pp. 1660-1666, 1997.

[171] Mm Farsangi, Yh Song, and Kwang Y Lee, "Choice of FACTS device control inputs for damping interarea oscillations," *Power Systems, IEEE Transactions on,* vol. 19, pp. 1135-1143, 2004.

[172] Annissa Heniche and Innocent Kamwa, "Assessment of two methods to select wide-area signals for power system damping control," *Power Systems, IEEE Transactions on,* vol. 23, pp. 572-581, 2008.

[173] Yong Li, Christian Rehtanz, Sven Rüberg, Longfu Luo, and Yijia Cao, "Assessment and choice of input signals for multiple HVDC and FACTS wide-area damping controllers," *Power Systems, IEEE Transactions on,* vol. 27, pp. 1969-1977, 2012.

[174] Malihe M Farsangi, Hossein Nezamabadi-Pour, Yong-Hua Song, and Kwang Y Lee, "Placement of SVCs and selection of stabilizing signals in power systems," *Power Systems, IEEE Transactions on,* vol. 22, pp. 1061-1071, 2007.

[175] I. Erlich, H. Wrede, and C. Feltes, "Dynamic Behavior of DFIG-Based Wind Turbines during Grid Faults," in *Power Conversion Conference - Nagoya, 2007. PCC '07*, 2007, pp. 1195-1200.

[176] P. Rao, M. L. Crow, and Yang Zhiping, "STATCOM control for power system voltage control applications," *Power Delivery, IEEE Transactions on,* vol. 15, pp. 1311-1317, 2000.

[177] Shuhui Li, Ling Xu, and Timothy A. Haskew, "Control of VSC-based STATCOM using conventional and direct-current vector control strategies,"

International Journal of Electrical Power & Energy Systems, vol. 45, pp. 175-186, 2013.

[178] Paul M Anderson and Aziz A Fouad, *Power system control and stability*: John Wiley & Sons, 2008.

[179] Yuan-Yih Hsu and Chern-Lin Chen, "Identification of optimum location for stabiliser applications using participation factors," in *Generation, Transmission and Distribution, IEE Proceedings C,* 1987, pp. 238-244.

[180] Lokman H Hassan, M Moghavvemi, Haider Af Almurib, Km Muttaqi, and Velappa G Ganapathy, "Optimization of power system stabilizers using participation factor and genetic algorithm," *International Journal of Electrical Power & Energy Systems,* vol. 55, pp. 668-679, 2014.

[181] Vahid Keumarsi, Mohsen Simab, and Ghazanfar Shahgholian, "An integrated approach for optimal placement and tuning of power system stabilizer in multi-machine systems," *International Journal of Electrical Power & Energy Systems,* vol. 63, pp. 132-139, 2014.

[182] Mohamed Edrah, Kwok L Lo, Olimpo Anaya-Lara, and Abdussalam Elansari, "Impact of DFIG based offshore wind farms connected through VSC-HVDC link on power system stability," in *AC and DC Power Transmission, 11th IET International Conference on*, 2015, pp. 1-7.

[183] Mohamed Edrah, Kwok L Lo, and Olimpo Anaya-Lara, "Reactive power control of DFIG wind turbines for power oscillation damping under a wide range of operating conditions," *IET Generation, Transmission & Distribution,* vol. 10, pp. 3777-3785, 2016.

[184] Thyge Knüppel, Jørgen N Nielsen, Kim H Jensen, Andrew Dixon, and Jacob Østergaard, "Power oscillation damping capabilities of wind power plant with full converter wind turbines considering its distributed and modular characteristics," *IET Renewable Power Generation,* vol. 7, pp. 431-442, 2013.

[185] Vk Tayal and Js Lather, "Reduced order H∞ TCSC controller & PSO optimized fuzzy PSS design in mitigating small signal oscillations in a wide range," *International Journal of Electrical Power & Energy Systems,* vol. 68, pp. 123-131, 2015.

Appendix A: Network Data

This appendix will provide the data required in order to perform dynamic studies on the test systems used throughout this thesis.

A.1 IEEE 9-Bus Test System Data

Original data are taken from [178]. The system base is 100 MVA.

A.1.1 Lines/Transformers

The lines and transformers data for the network is presented in Table A.1.

Table A.1 Line and transformers data for the IEEE 9-bus test system [178].

From Bus	*To Bus*	*R (p.u.)*	*X (p.u.)*	*B (p.u.)*
1	4	0.0000	0.0576	0.0000
4	6	0.0170	0.0920	0.1580
6	9	0.0390	0.1700	0.3580
9	3	0.0000	0.0586	0.0000
9	8	0.0119	0.1008	0.2090
8	7	0.0085	0.0720	0.1490
7	2	0.0000	0.0625	0.0000
7	5	0.0320	0.1610	0.3060
5	4	0.0100	0.0850	0.1760

A.1.2 Power and Voltage Set points

Data required to complete load flow is included in Table A.2; G01 connected to bus 1 is the slack.

Table A.2 Load flow data for the IEEE 9-Bus test system [178].

Bus	*Type*	*Voltage (p.u.)*	*Load*		*Generator*		
			MW	*MVAr*	*MW*	*MVAr*	*Unit No*
1	PV	1.04	0.0	0.0	-	-	G01
2	PV	1.025	0.0	0.0	163	-	G02
3	PV	1.025	0.0	0.0	85	-	G03
4	PQ	-	0.0	0.0	0.0	0.0	
5	PQ	-	125	50	0.0	0.0	
6	PQ	-	90	30	0.0	0.0	
7	PQ	-	0.0	0.0	0.0	0.0	
8	PQ	-	100	35	0.0	0.0	
9	PQ	-	0.0	0.0	0.0	0.0	

A.1.3 Generators

The generator dynamic presented is given in Table A.3.

Table A.3 Generator dynamic in p.u. data for the IEEE 9-bus test system [178].

Unit No	*G01*	*G02*	*G03*
H (s)	23.64	6.4	3.01
x_d	0.1460	0.8958	1.3125
x'_d	0.0608	0.1198	0.1813
x_q	0.0969	0.8645	1.2578
x'_q	0.0608	0.1198	0.1813
T'_{do}	8.96	6.0	5.89
T'_{qo}	0.3100	0.5350	0.6000

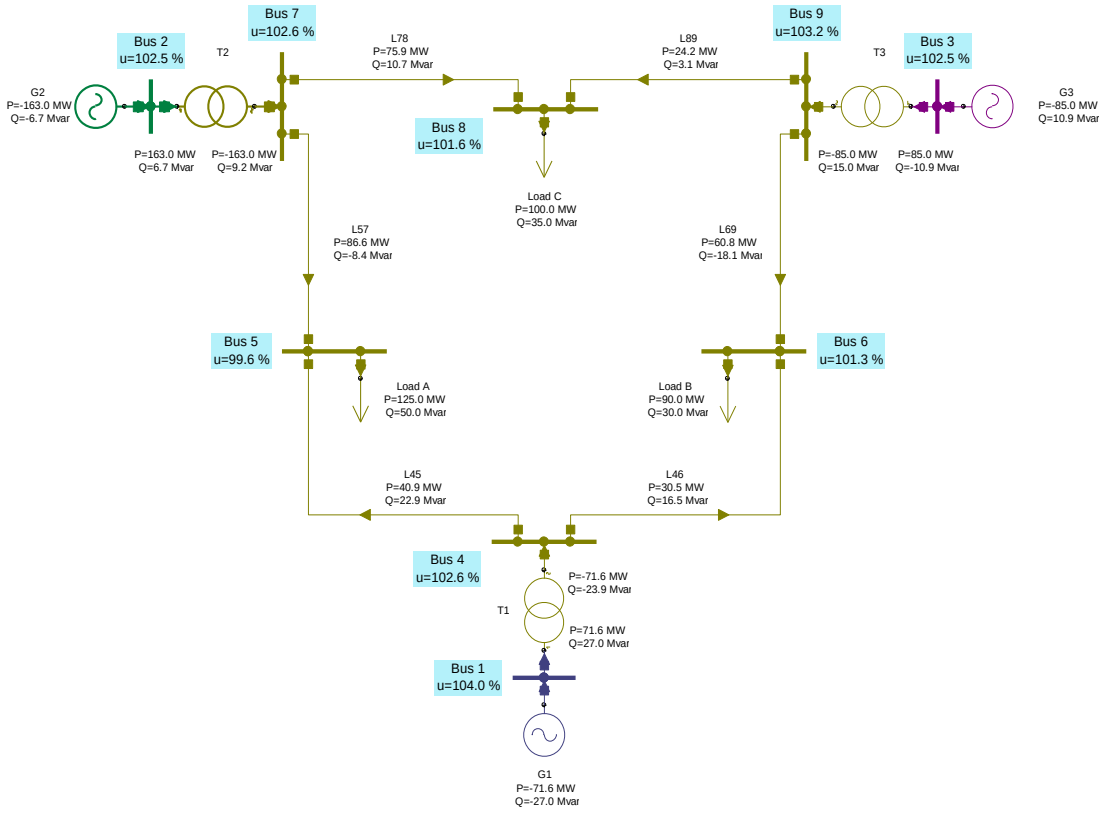

Figure A.1 Load flow results of IEEE 9-bus test system

A.2 IEEE 39-Bus Test System Data

All original data is adopted from [158]. The system base is 100 MVA.

A.2.1 Lines and Transformers

The lines and transformers data for the network is presented in Table A.4.

Table A.4 Line and transformers data for the IEEE 39-bus test system [158].

		Line Data			*Transformer Tap*	
From Bus	***To Bus***	***R (p.u.)***	***X (p.u.)***	***B (p.u.)***	***Magnitude***	***Angle***
1	2	0.0035	0.0411	0.6987	0.000	0.00
1	39	0.0010	0.0250	0.7500	0.000	0.00

		Line Data			*Transformer Tap*	
From Bus	***To Bus***	***R (p.u.)***	***X (p.u.)***	***B (p.u.)***	***Magnitude***	***Angle***
2	3	0.0013	0.0151	0.2572	0.000	0.00
2	25	0.0070	0.0086	0.1460	0.000	0.00
3	4	0.0013	0.0213	0.2214	0.000	0.00
3	18	0.0011	0.0133	0.2138	0.000	0.00
4	5	0.0008	0.0128	0.1342	0.000	0.00
4	14	0.0008	0.0129	0.1382	0.000	0.00
5	6	0.0002	0.0026	0.0434	0.000	0.00
5	8	0.0008	0.0112	0.1476	0.000	0.00
6	7	0.0006	0.0092	0.1130	0.000	0.00
6	11	0.0007	0.0082	0.1389	0.000	0.00
7	8	0.0004	0.0046	0.0780	0.000	0.00
8	9	0.0023	0.0363	0.3804	0.000	0.00
9	39	0.0010	0.0250	1.2000	0.000	0.00
10	11	0.0004	0.0043	0.0729	0.000	0.00
10	13	0.0004	0.0043	0.0729	0.000	0.00
13	14	0.0009	0.0101	0.1723	0.000	0.00
14	15	0.0018	0.0217	0.3660	0.000	0.00
15	16	0.0009	0.0094	0.1710	0.000	0.00
16	17	0.0007	0.0089	0.1342	0.000	0.00
16	19	0.0016	0.0195	0.3040	0.000	0.00
16	21	0.0008	0.0135	0.2548	0.000	0.00
16	24	0.0003	0.0059	0.0680	0.000	0.00
17	18	0.0007	0.0082	0.1319	0.000	0.00
17	27	0.0013	0.0173	0.3216	0.000	0.00
21	22	0.0008	0.0140	0.2565	0.000	0.00
22	23	0.0006	0.0096	0.1846	0.000	0.00
23	24	0.0022	0.0350	0.3610	0.000	0.00
25	26	0.0032	0.0323	0.5130	0.000	0.00
26	27	0.0014	0.0147	0.2396	0.000	0.00

		Line Data			Transformer Tap	
From Bus	***To Bus***	***R (p.u.)***	***X (p.u.)***	***B (p.u.)***	***Magnitude***	***Angle***
26	28	0.0043	0.0474	0.7802	0.000	0.00
26	29	0.0057	0.0625	1.0290	0.000	0.00
28	29	0.0014	0.0151	0.2490	0.000	0.00
12	11	0.0016	0.0435	0.0000	1.006	0.00
12	13	0.0016	0.0435	0.0000	1.006	0.00
6	31	0.0000	0.0250	0.0000	1.070	0.00
10	32	0.0000	0.0200	0.0000	1.070	0.00
19	33	0.0007	0.0142	0.0000	1.070	0.00
20	34	0.0009	0.0180	0.0000	1.009	0.00

A.2.2 Load Flow Data

Data required to complete load flow is included in Table A.5; G02 connected to bus 31 is the slack.

Table A.5 Load flow data for the IEEE 39-Bus test network [158].

Bus	***Type***	***Voltage (p.u.)***	***Load***		***Generator***		
			MW	***MVAr***	***MW***	***MVAr***	***Unit No***
1	PQ	-	0.0	0.0	0.0	0.0	
2	PQ	-	0.0	0.0	0.0	0.0	
3	PQ	-	322.0	2.4	0.0	0.0	
4	PQ	-	500.0	184.0	0.0	0.0	
5	PQ	-	0.0	0.0	0.0	0.0	
6	PQ	-	0.0	0.0	0.0	0.0	
7	PQ	-	233.8	84.0	0.0	0.0	
8	PQ	-	522.0	176.0	0.0	0.0	
9	PQ	-	0.0	0.0	0.0	0.0	
10	PQ	-	0.0	0.0	0.0	0.0	

Bus	*Type*	*Voltage (p.u.)*	*Load*		*Generator*		
			MW	*MVAr*	*MW*	*MVAr*	*Unit No*
11	PQ	-	0.0	0.0	0.0	0.0	
12	PQ	-	7.5	88.0	0.0	0.0	
13	PQ	-	0.0	0.0	0.0	0.0	
14	PQ	-	0.0	0.0	0.0	0.0	
15	PQ	-	320.0	153.0	0.0	0.0	
16	PQ	-	329.0	32.3	0.0	0.0	
17	PQ	-	0.0	0.0	0.0	0.0	
18	PQ	-	158.0	30.0	0.0	0.0	
19	PQ	-	0.0	0.0	0.0	0.0	
20	PQ	-	628.0	103.0	0.0	0.0	
21	PQ	-	274.0	115.0	0.0	0.0	
22	PQ	-	0.0	0.0	0.0	0.0	
23	PQ	-	247.5	84.6	0.0	0.0	
24	PQ	-	308.6	-92.0	0.0	0.0	
25	PQ	-	224.0	47.2	0.0	0.0	
26	PQ	-	139.0	17.0	0.0	0.0	
27	PQ	-	281.0	75.5	0.0	0.0	
28	PQ	-	206.0	27.6	0.0	0.0	
29	PQ	-	283.5	26.9	0.0	0.0	
30	PV	1.0475	0.0	0.0	250.0	-	G10
31	PV	0.9820	9.2	4.6	-	-	G02
32	PV	0.9831	0.0	0.0	650.0	-	G03
33	PV	0.9972	0.0	0.0	632.0	-	G04
34	PV	1.0123	0.0	0.0	508.0	-	G05
35	PV	1.0493	0.0	0.0	650.0	-	G06
36	PV	1.0635	0.0	0.0	560.0	-	G07
37	PV	1.0278	0.0	0.0	540.0	-	G08
38	PV	1.0265	0.0	0.0	830.0	-	G09
39	PV	1.0300	1104.0	250.0	1000.0	-	G01

A.2.3 Generators

The generator dynamic presented is given in Table A.6.

Table A.6 Generator dynamic data in p.u. for the IEEE 39-bus test system [158].

Unit No	*H* (s)	*R*	x'_d	x'_q	x_d	x_q	T'_{do}	T'_{qo}	x_l
1	500.0	0	0.006	0.008	0.02	0.019	7.0	0.7	0.003
2	30.3	0	0.0697	0.170	0.295	0.282	6.56	1.5	0.035
3	35.8	0	0.0531	0.0876	0.2495	0.237	5.7	1.5	0.0304
4	28.6	0	0.0436	0.166	0.262	0.258	5.69	1.5	0.0295
5	26.0	0	0.132	0.166	0.67	0.62	5.4	0.44	0.054
6	34.8	0	0.05	0.0814	0.254	0.241	7.3	0.4	0.0224
7	26.4	0	0.049	0.186	0.295	0.292	5.66	1.5	0.0322
8	24.3	0	0.057	0.0911	0.290	0.280	6.7	0.41	0.028
9	34.5	0	0.057	0.0587	0.2106	0.205	4.79	1.96	0.0298
10	42.0	0	0.031	0.008	0.1	0.069	10.2	0.0	0.0125

Table A.7 Parameters of PSSs for IEEE 39-bus test system.

SGs PSS			
	K	$T_1=T_3$ *(s)*	$T_2=T_4$ *(s)*
G5	18	0.4757	0.1535
G7	38	0.3814	0.1851
G9	22	0.3533	0.0901

A.2.4 Load Flow Results

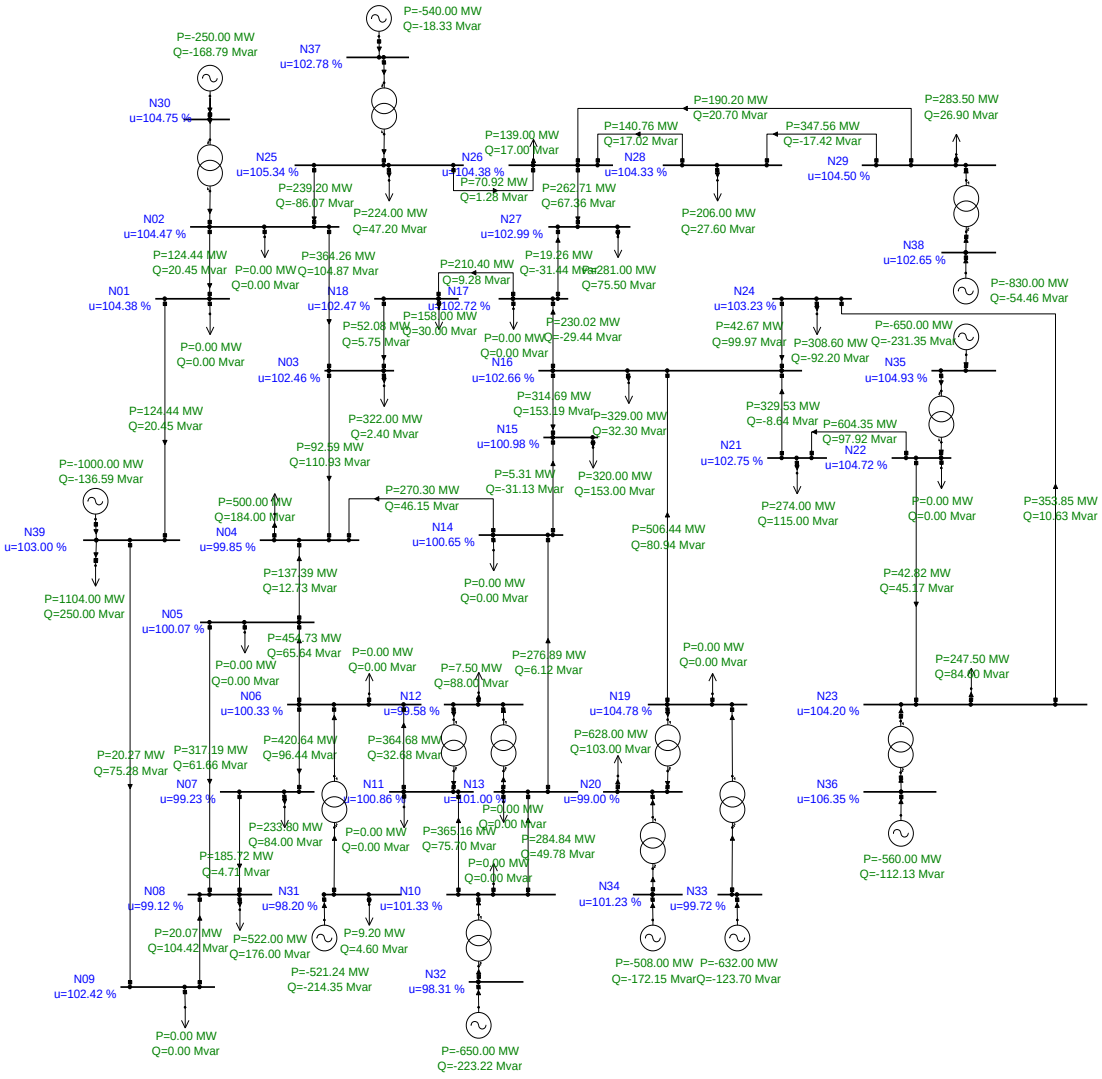

Figure A.2 Load flow results of IEEE 39-bus test system.

A.3 DFIG Wind Turbine Model Parameters

A.3.1 DFIG Machine Parameters

The DFIG machine parameters of the wind turbine used throughout this thesis are presented in Table A.8.

Table A.8 DFIG machine parameters.

Parameter	Value
Rated Power	5 MW
Rated voltage	3.3 kV
Rated frequency	50 Hz
power factor	-0.9 ~ +0.9
Pole pair number	2
Stator winding reactance	0.125 p.u.
Rotor winding reactance	0.05 p.u.
Magnetizing inductance	2.5 p.u.
Stator resistance	0.00299 p.u.
Rotor resistance	0.004 p.u.

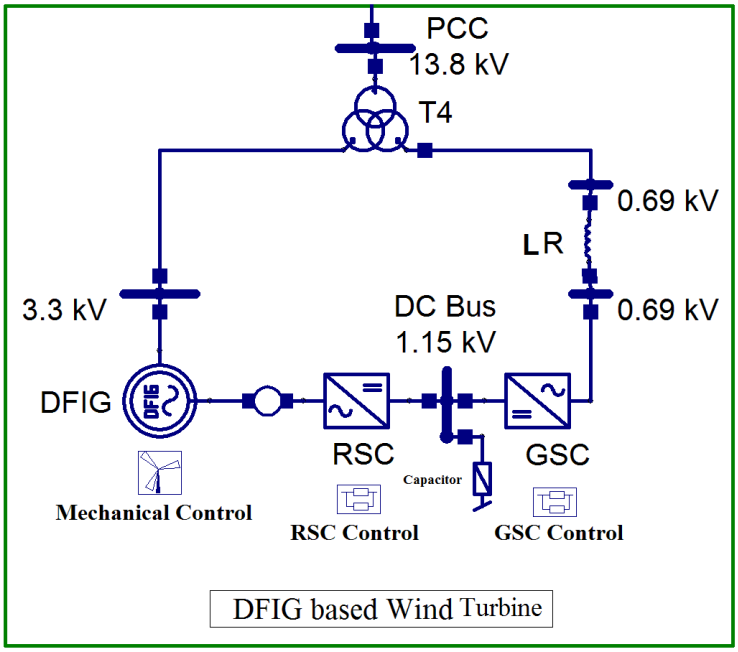

Figure A.3 DFIG based wind turbine.

A.3.2 Mechanical Parameters of the Wind Turbine

The mechanical parameters of the wind turbine are presented in Table A.9.

Table A.9 Mechanical parameters of the wind turbine.

Parameter	Value
Turbine rotor inertia	3.5 s
Generator rotor inertia	0.5 s
Turbine rotor self-damping	0.022 p.u. torgue/(rad/s)
Generator rotor self-damping	0.032 p.u. torgue/(rad/s)
Mutual damping between two mass	1.5 p.u. torgue/(rad/s)

A.3.3 DFIG Controller Parameters

A.3.3.1 DFIG-RSC Controller Parameters

The control parameters of DFIG-RSC is presented in Table A.10.

Table A.10 DFIG-RSC controller parameters.

Parameter	Value
Time Constant of the First-stage Low-Pass Filter	0.001s
Proportional Gain of the d-axis P Controller	1.0 p.u.
Time Constant of the d-axis P Controller	0.1 s
Proportional Gain of the q-axis Q Controller	1.0 p.u.
Time Constant of the q-axis Q Controller	0.1 s
Time Constant of the Second-stage Low-Pass Filter	0.0001s
Proportional Gain of the d-axis Current Controller	0.2 p.u.
Time Constant of the d-axis Current Controller	0.01 s
Proportional Gain of the q-axis Current Controller	0.2 p.u.
Time Constant of the q-axis Current Controller	0.01 s

Table A.11 Parameters of DFIG PSSs for IEEE 9-bus and IEEE 39-bus test systems.

	DFIGs PSS		
	K	*T1=T3*	*T2=T4*
IEEE 9-bus Test System			
DFIG1	170	0.06308	0.26497
IEEE 39-bus Test System			
DFIG1	120	0.1599	0.1325
DFIG2	140	0.3179	0.2106

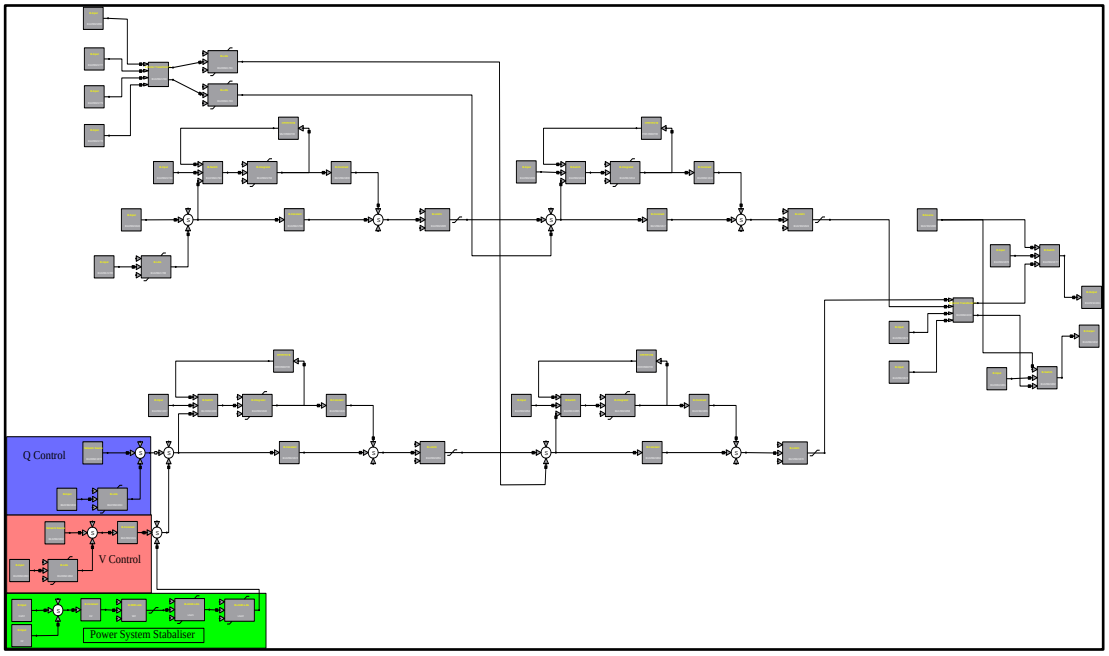

Figure A.4 DFIG-RSC controller including PSS.

A.3.3.2 DFIG-GSC Controller Parameters

The control parameters of DFIG-GSC is presented in Table A.12.

Table A.12 DFIG-GSC controller parameters.

Parameter	Value
Proportional Gain of the d-axis V_{dc} Controller	5.0 p.u.
Time Constant of the d-axis V_{dc} Controller	0.1 s
Proportional Gain of the q-axis Q Controller	1 p.u.
Time Constant of the q-axis Q Controller	0.1s
Time Constant of the Second-stage Low-Pass Filter	0.0001s
Proportional Gain of the d-axis Current Controller	1.0 p.u.

Parameter	Value
Time Constant of the d-axis Current Controller	0.015 s
Proportional Gain of the q-axis Current Controller	3.0 p.u.
Time Constant of the q-axis Current Controller	0.015 s

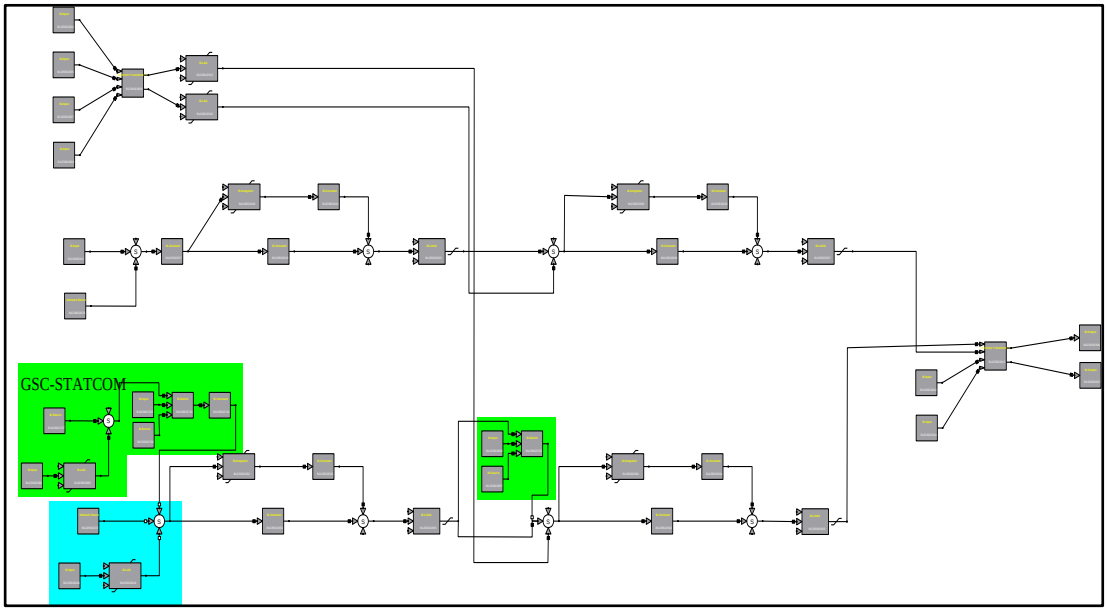

Figure A.5 DFIG-GSC controller including STATCOM mode.

A.3.3.3 Pitch Angle Controller Parameters

The pitch controller parameters of DFIG base wind turbine is presented in Table A.13

Table A.13 Parameters of pitch angle controller.

Parameter	Value
Upper pitch angle rate limit	10
Proportional gain of PI controller	150
Integrator gain of PI controller	25

Parameter	Value
Proportional gain of the compensator	3
Integrator gain of the compensator	30
Blade response time constant	0.3
Lower pitch angle limit	0
Upper pitch angle limit	27

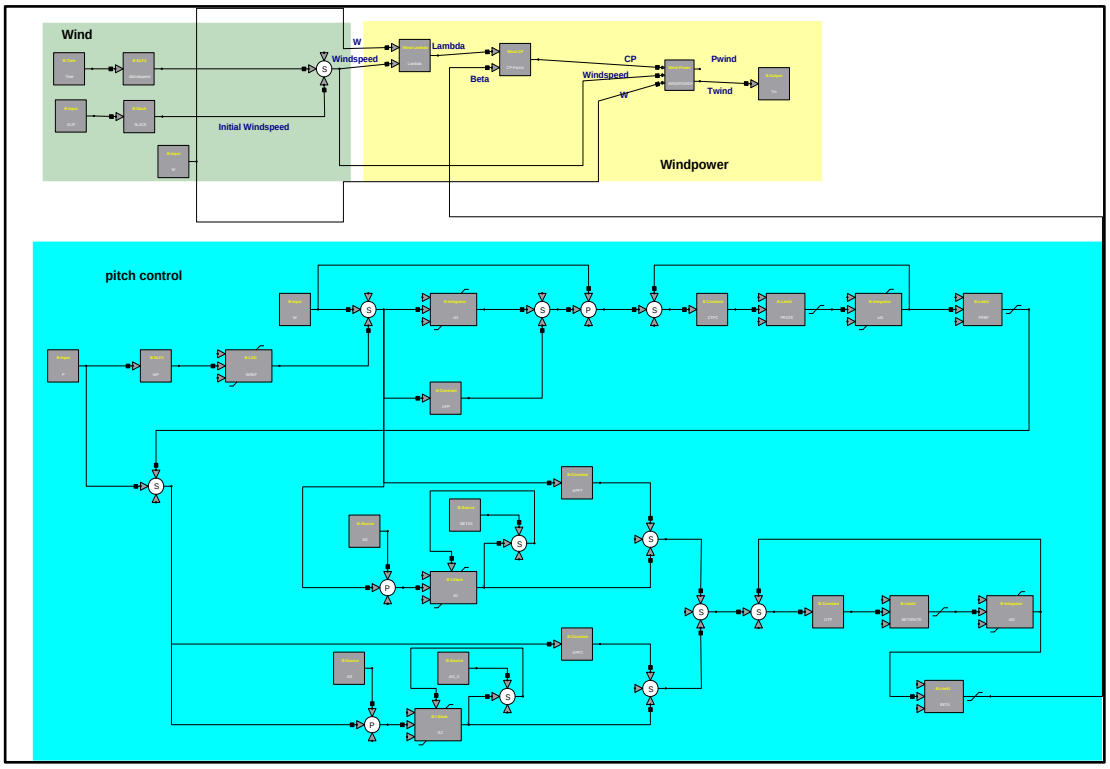

Figure A.6 Pitch angle controller.